A STUDY ON UNCERTAINTY-BASED FLOOD ANALYSIS

A THESIS SUBMITTED TO
THE GRADUATE SCHOOL OF NATURAL AND APPLIED SCIENCES
OF
MIDDLE EAST TECHNICAL UNIVERSITY

BY

MUSTAFA BERKAY AKPINAR

IN PARTIAL FULFILLMENT OF THE REQUIREMENTS
FOR
THE DEGREE OF MASTER OF SCIENCE
IN
CIVIL ENGINEERING

JANUARY 2023

Approval of the thesis:

A STUDY ON UNCERTAINTY-BASED FLOOD ANALYSIS

submitted by **MUSTAFA BERKAY AKPINAR** in partial fulfillment of the requirements for the degree of **Master of Science** i**n Civil Engineering, Middle East Technical University** by,

Prof. Dr. Halil Kalıpçılar
Dean, Graduate School of **Natural and Applied Sciences** _____

Prof. Dr. Erdem Canbay
Head of the Department, **Civil Engineering** _____

Prof. Dr. S. Zuhal Akyürek
Supervisor, **Civil Engineering, METU** _____

Prof. Dr. A. Melih Yanmaz
Co-Supervisor, **Civil Engineering, METU** _____

Examining Committee Members:

Assoc. Prof. Dr. Koray Kamil Yılmaz
Geological Eng, METU _____

Prof. Dr. S. Zuhal Akyürek
Civil Eng, METU _____

Prof. Dr. A. Melih Yanmaz
Civil Eng, METU _____

Assoc. Prof. Dr. Müsteyde Baduna Koçyiğit
Civil Eng, Gazi University _____

Assist. Prof. Dr. Meriç Yılmaz
Civil Eng, Atılım University _____

Date: 27.01.2023

I hereby declare that all information in this document has been obtained and presented in accordance with academic rules and ethical conduct. I also declare that, as required by these rules and conduct, I have fully cited and referenced all material and results that are not original to this work.

Name Last name : Mustafa Berkay, Akpınar

Signature :

ABSTRACT

A STUDY ON UNCERTAINTY-BASED FLOOD ANALYSIS

Akpınar, Mustafa Berkay
Master of Science, Civil Engineering
Supervisor: Prof. Dr. S. Zuhal Akyürek
Co-Supervisor: Prof. Dr. A. Melih Yanmaz

January 2023, 93 pages

A hydraulic model is a collection of mathematical equations that give a simple representation of reality with the inputs obtained from hydrological assessments to estimate flow, flow depth and velocity in channels. Basically, hydraulic models require digital elevation models, Intensity-Duration-Frequency curves, maximum flows from hydrographs, and roughness coefficients from field studies and/or satellite images. Inherently, these major inputs have uncertainties due to the complex nature of the evaluation processes of inputs and boundary conditions. In recent years, researches have shown that roughness coefficients and evaluated maximum flows may have error margins of 5% to 15%; this may result in underestimation for expected flow depths compared to evaluated ones. In this study, convenient probability distributions in the nature of uncertainties in peak discharge of the input hydrograph and Manning's roughness value have been investigated separately and in combined manner in flood modelling. The study was conducted and modelled with an automated Monte Carlo-based method of HEC-RAS and Visual Basic Applications software in the catchment of Yılanlı Dere, in Samsun. 1-D hydraulic model was used. The results show that the maximum flows and roughness values may cause uncertainties in flow depths up to 10% of the total capacity of cros-

sections without overflow in this region. Moreover, distances of the cross-sections to the hydraulic structures existing along the river and topographic conditions can also directly affect these uncertainties. It is obtained that the distributions of the flow depth at the cross-sections were changed.

Keywords: Hydraulic Models, Uncertainties, Probabilistic Flood Modelling

ÖZ

BELİRSİZLİK TABANLI TAŞKIN ANALİZİ ÜZERİNE BİR ÇALIŞMA

Akpınar, Mustafa Berkay
Yüksek Lisans, İnşaat Mühendisliği
Tez Yöneticisi: Prof. Dr. S. Zuhal Akyürek
Ortak Tez Yöneticisi: Prof. Dr. A. Melih Yanmaz

Ocak 2023, 93 sayfa

Hidrolik modeller, nehir kanallarındaki akışı, su seviyesini ve hızı tahmin etmek için hidrolojik hesaplamalar ile elde edilen girdilerle gerçeğin temel bir temsilini veren matematiksel denklemler bütünüdür. Temel olarak, hidrolik modeller, sayısal yükseklik modelleri, hidrograflar, Şiddet-Süre-Dönüş Aralığı eğrileri ile maksimum akımları, saha çalışmalarından ve/veya uydu görüntülerinden elde edilen pürüzlülük katsayılarını gerektirir. Doğası gereği, bu temel girdiler, girdilerin ve sınır koşullarının elde edilme süreçlerinin karmaşık doğasından dolayı belirsizliklere sahiptir. Son yıllarda yapılan araştırmalar, pürüzlülük katsayılarının ve hesaplanan maksimum akışların %5 ile %15'lik bir hata payına sahip olabileceğini göstermiştir; bu da, olması gereken seviyelere kıyasla elde edilen su seviyelerinin olduğundan daha düşük tahmin edilmesine neden olabilmektedir. Bu çalışmada, girdi hidrografın maksimum debisindeki ve Manning pürüzlülük katsayısındaki belirsizliklerin doğadaki uygun istatistiksel dağılımları ayrı ayrı ve birleşik şekillerde ele alınarak modellenmiştir. Çalışma, Samsun ili Yılanlı Dere havzasında Monte Carlo tabanlı otomatize edilmiş bir yöntem kullanılarak HEC-RAS ve Visual Basic Applications yazılımlarının entegrasyonu ile yürütülmüş ve modellenmiştir. Sonuçlar, su seviyelerinin, maksimum akım ve pürüzlülük katsayıları belirsizliklerinden kaynaklı

olarak bu bölgedeki kesitlerin taşkın durumu olmadan taşıyabilecekleri kapasitelerinin %10'unu kadar belirsizlik yaratabildiğini göstermektedir. Ayrıca en kesitlerin nehir boyunca mevcut olan hidrolik yapılara uzaklıkları ve topoğrafik koşullar da bu belirsizlikleri doğrudan etkileyebilmektedir. Bu en kesitlerdeki su seviyesi çıktı dağılımlarının değiştiği belirlenmiştir.

Anahtar Kelimeler: Hidrolik Model, Belirsizlikler, Olasılıksal Taşkın Modellemesi.

To my family and beloved ones

ACKNOWLEDGMENTS

I would like to express my deepest gratitude to my supervisor Prof. Dr. Zuhal Akyürek and co-supervisor Prof. Dr. Melih Yanmaz for sharing their experiences, guidance and encouragement with patience throughout the study. Their contributions and mentorships to my life is invaluable.

I would like to express my sincere thanks to Çağrı Karaman, Kenan Bolat and Semih Kuter for sharing all their help and guidance for the study. They were always elder brothers for me.

I would like to thank my dear friends in my life and Civil Engineering family Gökalp Aksekili, Taylan Utkurak, Berkay Akyol, Ali Agboyraz, İpek Saraçlar, Acarkan Dokuzağaç, Bekir Günnar, Nuri Lale, Zafer Üstün, Burak Gülerce, Sinan Bezirci, Özgür Aydoğmuş, Okan Ok, Zeynep Oral, Emirhan Özgeliş, İpek Şalk, Eren Karanacakoğlu, Mehmet Büyükkeskinli, Alp Bayrak, Emirhan Ünlü, Berkay Karahan, Bersu Çelikkol, Fatih Önder, Pamir Türkoğlu and everyone whose names I could not mention for their presence and valuable moral support for this period.

I would like to give my gratitude to my dear family, Nazmiye, Hayretdin and Yusuf Ege Akpınar for their motivation and patience during the study.

TABLE OF CONTENTS

LIST OF TABLES

TABLES

LIST OF FIGURES

FIGURES

LIST OF SYMBOLS

Ω_y	Coefficient of variation for flow depths
μ_y	Mean values for flow depths
σ_y	Standard deviation for flow depths
n	Manning's roughness coefficient
n_{mean}	Mean values of Manning's roughness coefficients
$\sigma_{manning}$	Standard deviations of Manning's roughness coefficients
1-D	One dimensional
2-D	Two dimensional
3-D	Three dimensional
X_l	Lower limit of roughness coefficients
X_u	Upper limit of roughness coefficients
X_m	Mode of roughness coefficients
Q	Flow (m^3/s)
Q_p	Peak flow (m^3/s)

CHAPTER 1

INTRODUCTION

Floods are defined as overflow of large amount of water submerging the lands beyond its normal limits. Floods are generally induced by heavy flash floods or long-lasting rain. On the other hand, tropical cyclones, monsoon rains and torrential rains also cause flood events (Coon, 1995; Douben, 2006). Floods cause enormous loss of life and property every year. Although, there are many flooding events in developing countries, flooding and consequent problems are also experienced in the developed countries (Douben, 2006). It has been estimated that floods gave rise to 6.8 million deaths throughout 20th century (Kousky, 2014) and billions of people affected by the consequences of the floods (Jonkman et al., 2008).

Generation of river floods are affected by variety of complex atmospheric processes, catchment characteristics, type of precipitation, soil type, topography, land cover, etc. Additionally, the damage factors caused by these complex systems are increased or decreased depending on the population growth, early warning system, indirect impacts like supply chains. The key processes which can give rise to flood or prevent disaster from river floods are depicted in Figure 1.1.

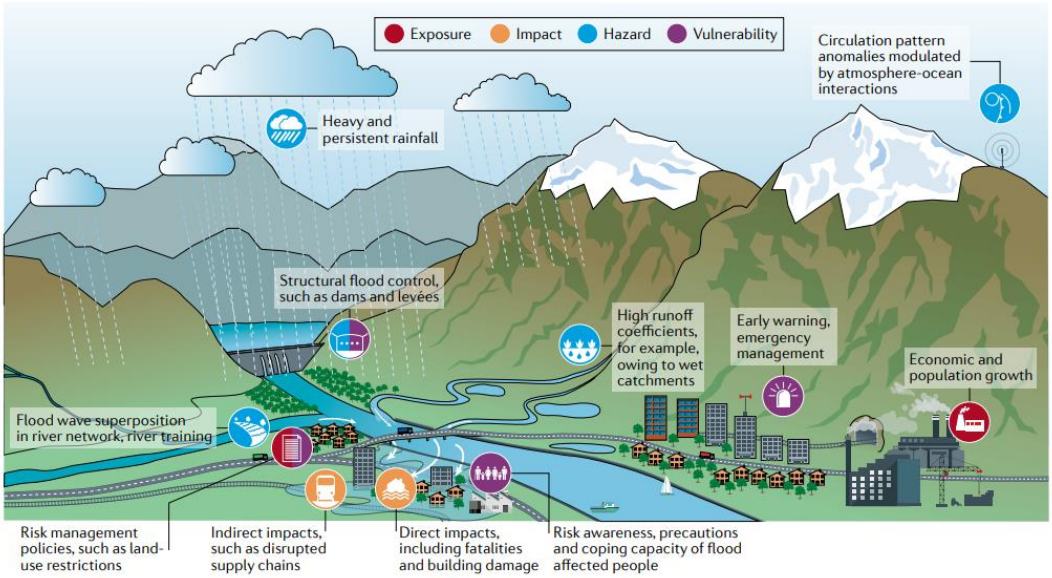

Figure 1.1. Main factors affecting the floods and relevant damages (Merz et al., 2021).

Climate change is also another important issue to consider flood risk and flood mitigation for authorities. Climate change affects factors of flooding, such as duration and intensity of precipitation, soil abstraction due to the extreme temperatures, snow melt, etc. Authorities must observe the outputs of climate models for future projections to take necessary precautions. Recent studies indicate that changes in 100-year flood frequencies for large parts of the world are around plus or minus 20% (Arnell & Gosling, 2016; Tabari, 2020). Therefore, due to consistent outputs of climate models, a decrease is possible in flood magnitude around the central Europe, central America, and southwest Africa. On the contrary, there is a likelihood that flood frequencies could increase across the high latitude Asia and North America, South America, east and south Asia and tropical Africa (Arnell & Gosling, 2016).

Flood risk assessments are carried out by the help of hydrological and hydraulic models. Briefly, a hydraulic model is a collection of mathematical equations to assess the impact of flooding on a river or flood plain. The output observations from

hydraulic models are crucial for planning and designing hydraulic and civil structures.

Since these models have so many inputs and parameters to carry out mathematical process behind the model, uncertainties are inevitable in most of the scenarios for both hydrological (Moges et al., 2021) and hydraulic models (Beven et al., 2018). Although models have uncertainties for flood modelling, there are several techniques to eliminate or decrease the uncertainties with their resources. One of the applicable methods to see all flood extents with determined uncertainty intervals is probabilistic flood modelling approaches. These models allow researchers to observe all different output water surface elevations of simulations across different cross-sections. These observations are crucial especially in the locations where there are contractions in water way due to hydraulic structures, such as bridges. Output water surface distribution types are also important to understand the effect of uncertainty throughout the channels where hydraulic structures and regular cross-sections exist.

In this study, uncertainties in determination and estimation of peak flow and Manning's roughness coefficient for hydraulic models are discussed. A fully probabilistic (Monte Carlo based) 1-D hydraulic model is created in HEC-RAS (Brunner, 2021) to manipulate the hydraulic model via Visual Basic Application codes in fully automated manner. All of the possible flow depths and their relevant fluctuations are then observed with a case study in Samsun/Yılanlıdere sub-basin. The hydraulic model has different type of bridges (i.e., vehicular, pedestrian) and there are many cross-sections to introduce different flow behavior due to slope, length of channel bed, sudden contractions, and flood-prone regions. At the end, all of the probabilistic simulations, which are obtained by the help of the methodology mentioned throughout the study are compiled as tabulated probabilistic results. Therefore, the effects of uncertainties coming from different sources are presented so that it can be seen how flow depths and flood extents are sensitive to the determined uncertainties in hydraulic modelling. The thesis starts with Chapter 1, where the goal of the study is presented. Chapter 2 reviews the recent and relevant literature. The materials and methods those are used in this study are given in detail

in Chapter 3. In Chapter 4 the analyses are represented. The results are given in Chapter 5. Finally, Chapter 5 concludes the thesis, summarizes the work that has been utilized with potential future directions and prospects.

CHAPTER 2

LITERATURE REVIEW

Hydraulic models require some inputs and boundary conditions. Mainly, these requirements are digital elevation models (DEM), hydrographs/peak flows from hydrological studies, soil/land types determined from field studies for hydraulic equation parameters like Manning's roughness coefficient. Briefly, DEMs are used to define topographic information of the study area. They construct the 3-Dimensional shape of hydraulic models. The accuracy of the DEM can affect the flood hydraulics and resultant inundation extent of floods simulated with hydraulic models (Horritt & Bates, 2001) as exemplified in Figure 2.1

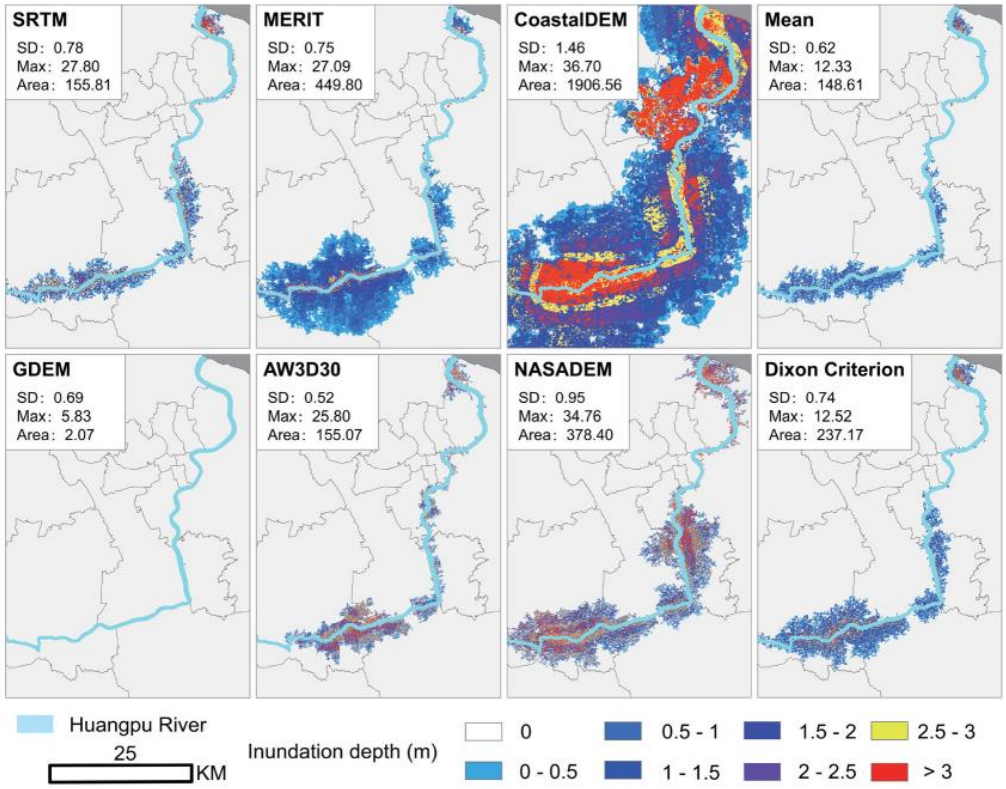

Figure 2.1. Results of flood inundation of different digital elevation models in the same region and same return period (Xu et al., 2021).

Misleading information especially on river floodplains may cause important errors for the outputs of hydraulic models (Bates & De Roo, 2000). Additionally, different topographic information sources including 'Light Detection and Ranging' (LIDAR) and 'Global Positioning System' (GPS) systems with relevant bathymetries directly affect the water surface elevations and discharges (Casas et al., 2006). Hydrographs and relevant peak flows are also very important inputs to simulate flood through a model. Shape of hydrographs of basins are very sensitive to basin characteristics (Li & Sivapalan, 2011). Characteristics of basin like average slope, maximum channel length, the shapes and contribution of subbasins and other hydraulic structures and hydraulic components cause changes in hydrograph shape, time to peak and peak flows. Additionally, duration of precipitation affects the hydrograph shape and behavior of flood, as exemplified in Figure 2.2

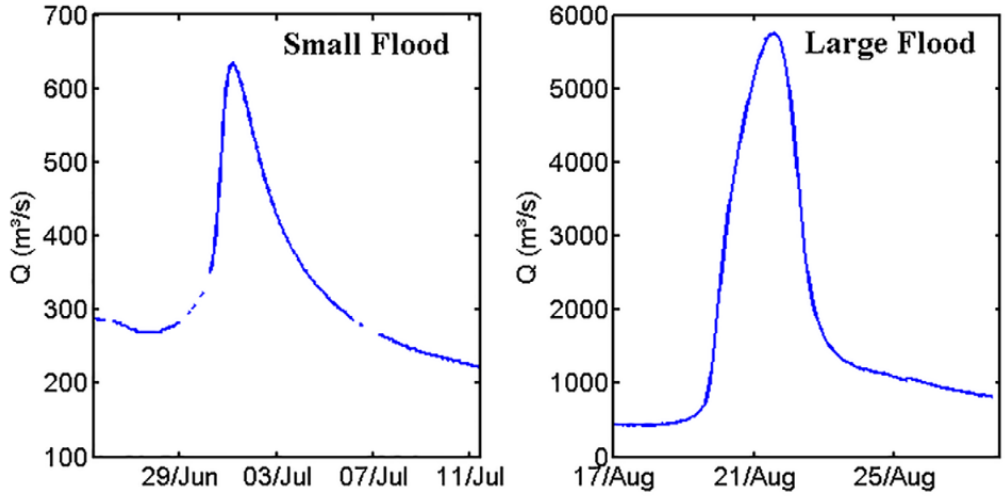

Figure 2.2. Observed hourly discharge data for the Piquiri River (a) a common streamflow hydrograph for a small flood caused faster rising limb and positive skewness. (b) Large flood caused a negative skewness (Fleischmann et al., 2016).

Therefore, determining the hydrographs and resulting peak flows are very complex inherently. Researchers should consider that there are so many factors to construct a design hydrograph. Peak flow estimation and relevant duration have always been an important topic for hydrology. Starting from 20th century, so many methods have been developed like distribution fitting procedures (Gumble, 1941; Singh, 1987) to represent the behavior of rainfall distribution for different return periods, enhanced methods of fitting procedure with convenient unit hydrographs (Aron & White, 1982) and recent artificial intelligence methods for obtaining hydrographs and peak flows (Chen et al., 2013; Güçlü & Şen, 2016; Tayfur et al., 2018).

Manning's roughness coefficient is the other fundamental input to be determined in hydraulic modelling process. Any changes in the value of roughness coefficients cause significant differences in flow depths' elevations. There are so many studies to estimate the Manning's roughness coefficient for natural streams, vegetated banks and floodplains (Azamathulla & Jarrett, 2013; Coon, 1995) and dynamic coefficients for modelling (Ye et al., 2018). However, these values include some uncertainties (Wohl, 1998) and it is inherent to have the uncertainties inevitably for both peak flows and roughness parameters and researchers have to develop methods to eliminate or at least decrease the uncertainties in an acceptable range (Apel et al., 2004; Domeneghetti et al., 2013; Hall & Solomatine, 2008).

The uncertainties coming from different sources are also important problems for flood risk assessments as well. Flood hazard can be defined due to the exceedance probability of flood damages for some period of time and area (Scawthorn et al., 2006). Inevitably, these estimations are affected by the hydrologic and topographic uncertainties resulted from both models and data observations. Although, the source of uncertainties may be caused from empirical methods for peak discharge calculations, unit hydrograph estimations, distribution fittings, etc., and the uncertainties for roughness coefficients like insufficient field studies, inadequate land/soil information and underestimation of hydraulic terms (Bates et al., 2014), the uncertainties also resulted from observation devices like water-level measurements and stream gauges (Bales & Wagner, 2009).

For most of the cases, the inputs and outputs of hydraulic models refer to a deterministic prediction for both flood area and water stages. Although the aforementioned developed and developing methods in literature can estimate required input precisely, these deterministic methods may underestimate or overestimate the water surface levels, flood extent and peak flows (Beven et al., 2018; Papaioannou et al., 2017). In the literature, the roughness-based uncertainties (Aronica et al., 2002; Bates et al., 2014; Bozzi et al., 2015; Papaioannou et al., 2017; Pappenberger et al., 2005; Vatanchi & Maghrebi, 2019) and hydrological uncertainties (Sharafati et al., 2020; Walega & Ksiazek, 2016) have been studied and it is found out that the uncertainties from the hydraulic/hydrologic sources obtained by both empirical and observational ways cannot be neglected for most of the time.

Although most of the current techniques for flood modelling are generally based on the application of deterministic methods, probabilistic methods have started to prevail in the evaluation of flood risks and relevant outputs (Di Baldassarre et al., 2010) and visualization of flood extent maps. In literature, Monte Carlo based probabilistic approaches have been utilizing for different inputs so that all extents of uncertainties can be obtained. These studies include roughness parameters, hydrographs and peak flows, storm duration for design purposes and their frequencies, and some hydraulic model boundary conditions (Cooper, 2010; Garrote et al., 2021; Loveridge et al., 2013; Merwade et al., 2008; Wang et al., 2022) which are quite helpful to see possible extent of water depth and relevant inundation extents in a probabilistic manner. A brief informative table for deterministic and probabilistic method, is presented in Table 2.1.

Table 2.1. Brief information on deterministic and probabilistic models (Oberndorfer et al., 2020)

	Deterministic Method	*Probabilistic Method*
Input	A single numerical value of the result as explanatory statement with conservative assumptions	At least one numerical or full probabilistic modeling using PDF is required for multiple impact values, including probability of occurrence and uncertainty.
Result	A simple mathematical summation gives the aggregate result of all risks and the expected result of the aggregated risk, but it cannot adequately represent the range of results. Calculations can be supplemented with upper and lower bounds indicating sensitivity that are also deterministic calculations.	Simulation methods e.g., Monte Carlo simulation generate a set of aggregated natural hazards as probability distributions based on a large number of random but realistic scenarios. This method allows you to explicitly account for and handle all kinds of reducible uncertainty.
Qualification	Results are displayed as a single sharp number.	Results are displayed using probability distributions which allow interpretation of value-at-risk.

Additionally, inundation maps can also be obtained with both deterministic and probabilistic approaches. Techniques of deterministic inundation mapping have been increasing and advanced methods, such as physically-based fully 2D hydraulic models are used for the process (Di Baldassarre et al., 2010) and results are quite convenient for most of the situations. However, so many complex coefficients, especially for flood extent, may lead to misleading hazard evaluation (Bates et al., 2004). Probabilistic mapping exhibits all possible extents with occurrence probability of flood in consecutive simulations with different confidence interval for peak flows presented by Garrote et al. (2021) and an example is presented in Figure 2.3.

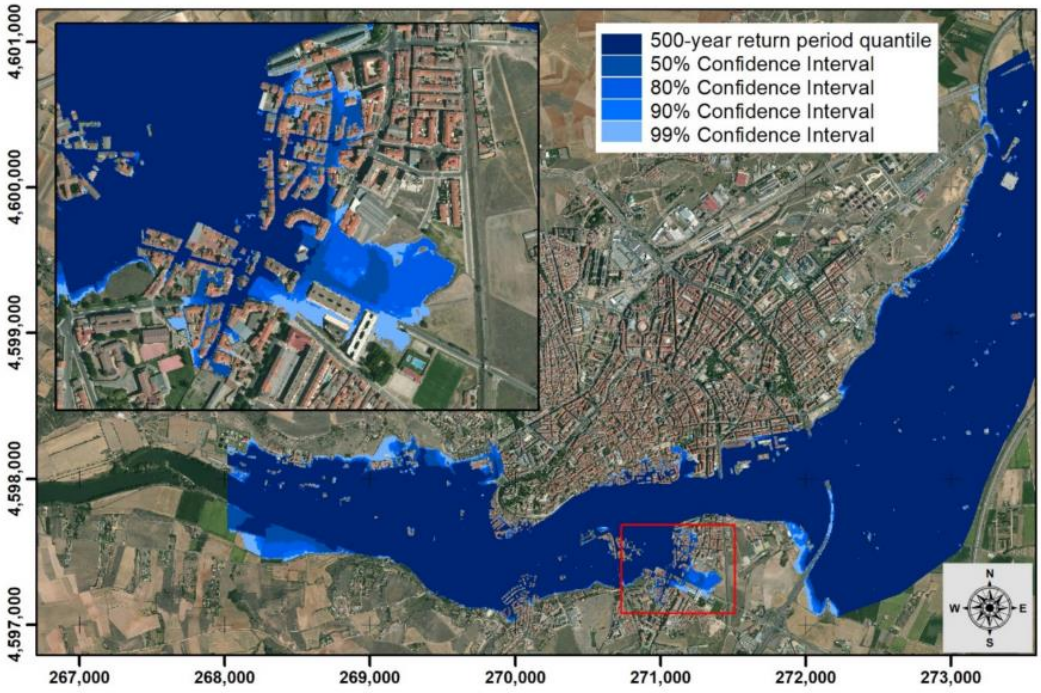

Figure 2.3. An example probabilistic flood mapping with relevant confidence interval (Garrote et al., 2021).

CHAPTER 3

STUDY AREA AND METHODOLOGY

3.1 Study Area

Probabilistic flood modeling and relevant observations are conducted for a sub-basin in Samsun province, Turkey. The city is in the Black Sea region of Turkey. According to the General Directorate of Meteorology, climate is rainy in nearly all seasons with average annual total rainfall amount of 717.9 mm for the period of 1929 – 2021. Although the region is prone to flash floods especially in spring and summer (Bahadır, 2014), the seasonal distribution of precipitation has a pattern of regular distribution. Study area includes the Yılanlıdere River of which outlet is very close to the urbanized city center. Elevations change between 0 – 563 meters with a median value of 177 meters in the region. Location of the study area is presented in Figure 3.1.

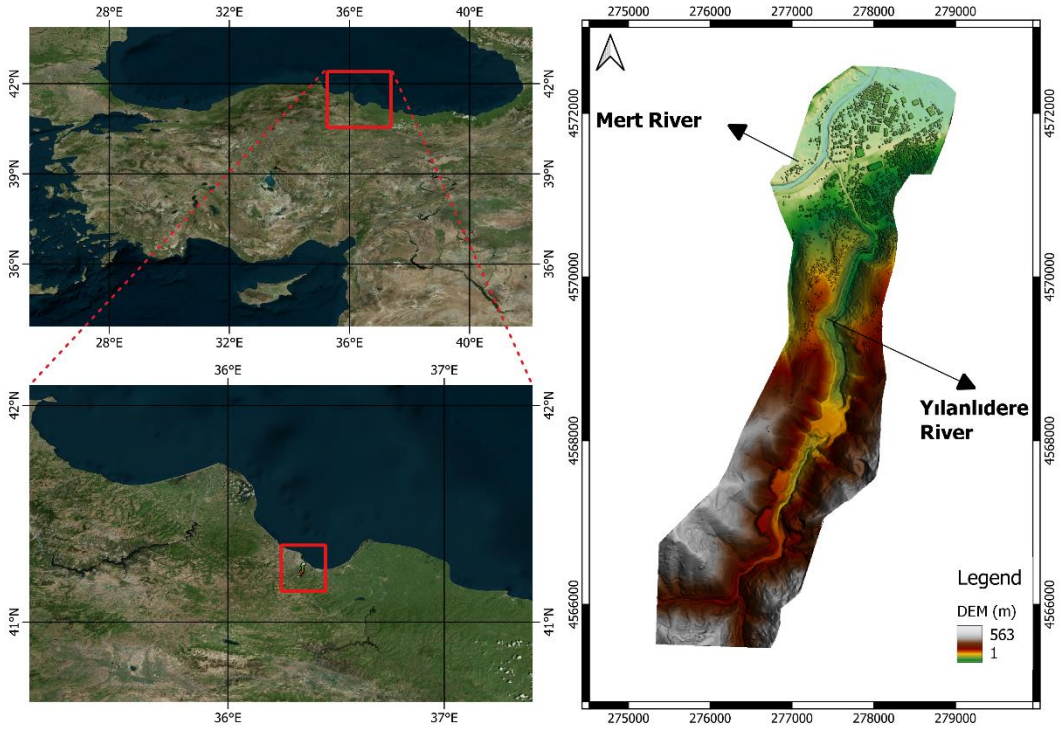

Figure 3.1. Location and digital elevation model of the study area.

Yılanlıdere faced with extreme flood events in the past. Lastly, flood event with casualties was observed in 2012 with the observed average precipitation of 50 mm/day (Akyürek & Karaman, 2021). 12 people lost their lives in this flooding event.

High resolution of Digital Elevation Model is compiled for the region with bathymetric information. When the past flood events were observed in the area, flooding to the urban area is mainly started from the sections of bridges because of the contraction around them. There are 7 bridges along the river (3 pedestrian and 4 vehicular) presented in Figure 3.2. The geometric details of the bridges are obtained from the bridge cross-sectional drawings, and they are inserted into the hydraulic model properly to see flow depths fluctuations around the bridges (1 to 3 meters just after and just before). The locations of the bridges and the drawings of the bridge selected as critical one (it is named as critical because of the flood prone behavior observed in the past flood in 2012) can be seen in Figure 3.3.

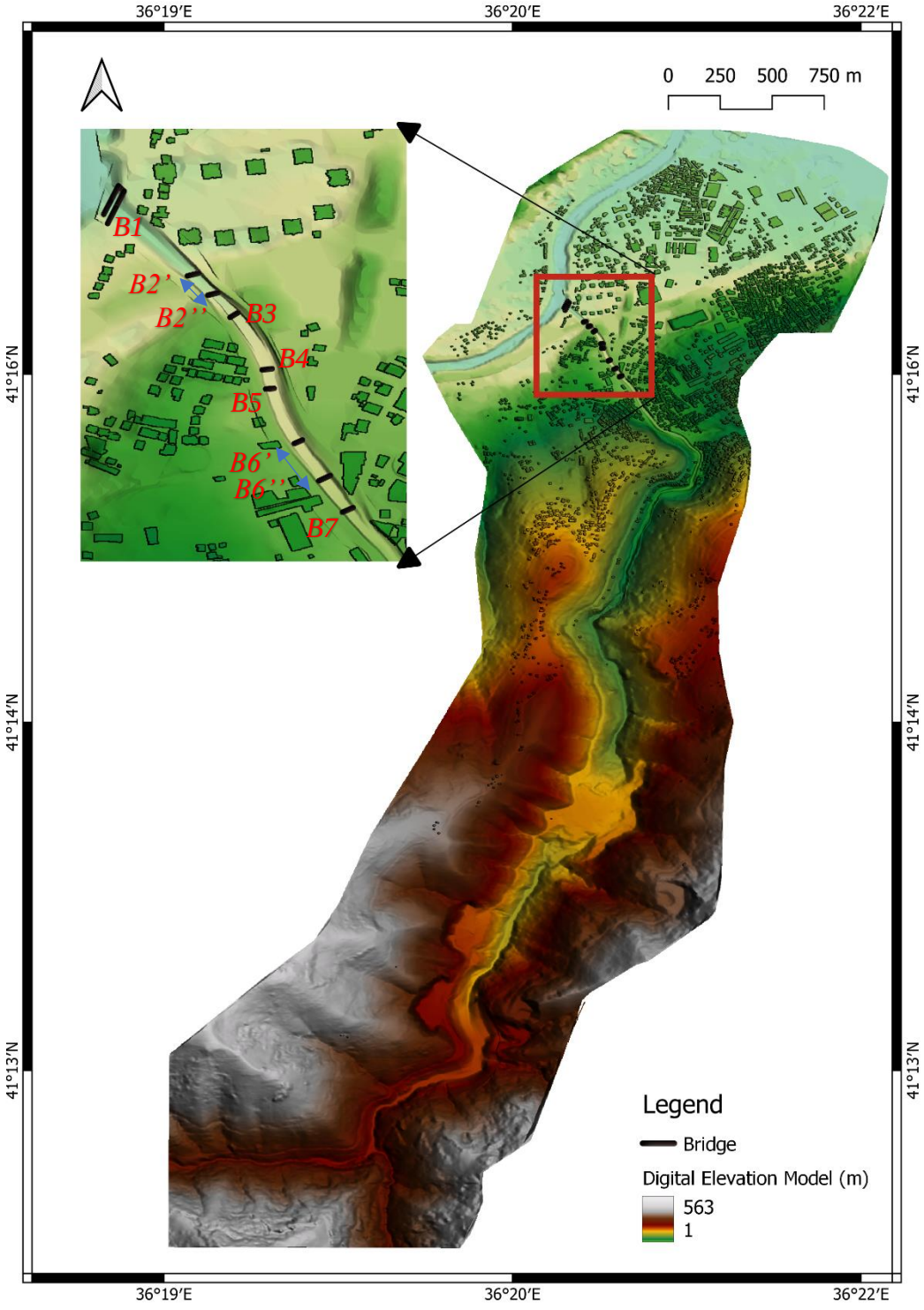

Figure 3.2. Locations of the bridges in the study area (‘ symbol indicates end of bridges for junctions while ‘‘ indicates the start of junctions).

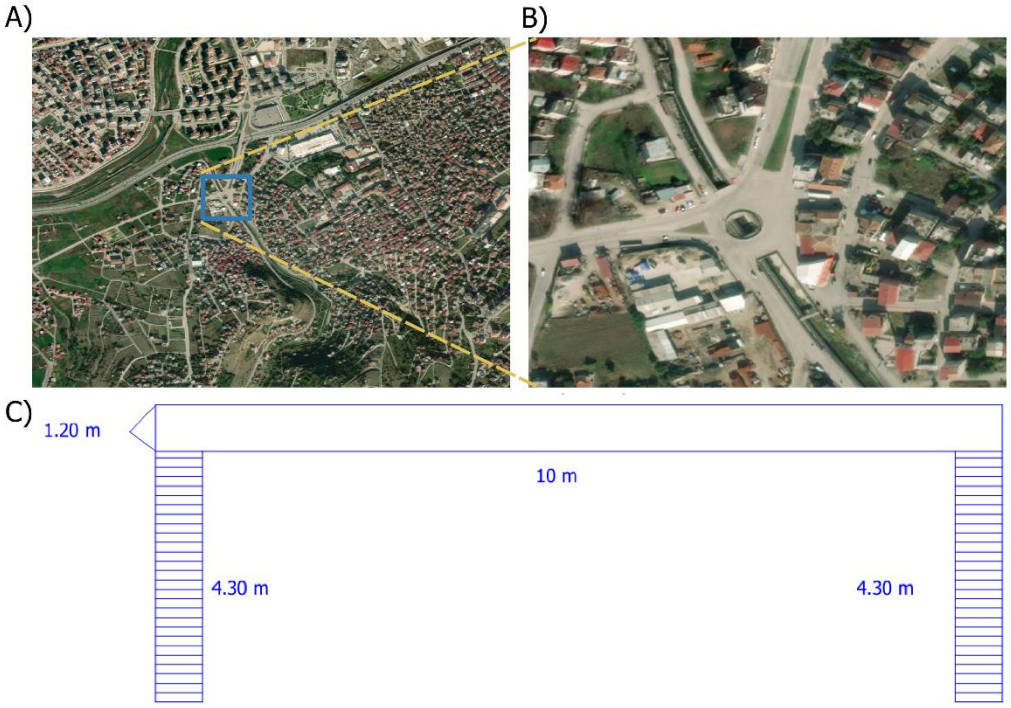

Figure 3.3. Location (A), closer view (B) and the cross-sectional drawing of the bridge (C) picked as critical one (vehicular junction).

Types of the bridges also vary in the region. There are vehicular, pedestrian, vehicular-junction types of bridges in the study area. The length of these bridges and their maximum possible flow depths without flooding is tabulated in Table 3.1

Table 3.1. Types of bridges, lengths and relevant maximum possible flow depths without flooding.

Bridge Type and Code	***Length (m)***	***Maximum Possible Flow Depth Without Flooding (m)***
Vehicular (B2)	11	4.10
Pedestrian (B3)	10	5.20
Vehicular (Junction) (B6)	10	4.30
Pedestrian (B7)	10	4.45

Mainly, bridges are located in the downstream part of the Yılanlıdere River, which discharges to Mert River. Land cover of the study area is obtained from the datasets of European Space Agency (ESA) as shown in Figure 3.4. The land cover is different in downstream compared to upstream parts. While trees and shrublands dominate the upstream parts, built-up regions exit at the downstream parts. Although a complex land information exists in the area, there is no specific field study carried out for the morphology to detect possible extents of roughness coefficients. Commonly used hydraulic roughness values had been used in previous studies.

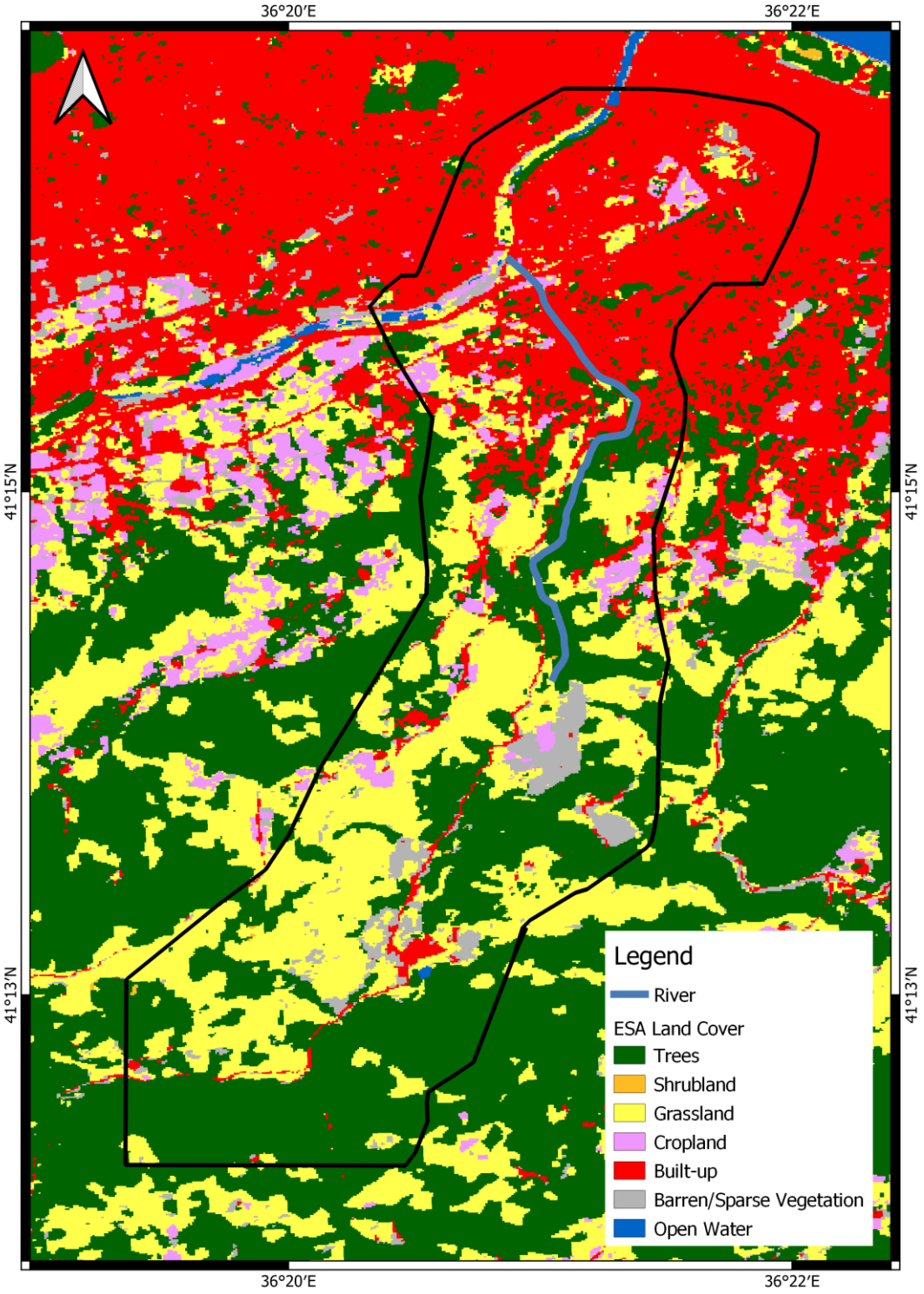

Figure 3.4. Land cover of the region obtained from ESA for 2020

3.2 Methodology

Hydraulic models can be one dimensional (1D), two dimensional (2D) or combined 1D-2D coupled models. These models have advantages and disadvantages (Mino et al., 2006; Vozinaki et al., 2017) depending on the flood area, characteristics of flood plain and the type of floods. Researchers should select the type of model and the software by considering the necessary conditions for a stable output from the model. Common software platforms for hydraulic modeling are given in Table 3.2.

Table 3.2. Common hydraulic software platforms (Teng et al., 2017).

1D Flood Modellers	*2D Flood Modellers*	*1D-2D Flood Modellers*
• ESTRY • HEC-RAS • InfoWorks ICM • MIKE FLOOD • Flood Modeller • SOBEK Suite • SIPSON • FASTER • HYDRO River	• TUFLOW • HEC-RAS • InfoWorks ICM • MIKE FLOOD • JFlow • Flood Modeller Pro • DIVAST • TELEMAC 2D • JFLOW • TRENT • FINEL 2D • UIM • XP2D	• TUFLOW Classic • HEC-RAS • InfoWorks • MIKE FLOOD • JFlow • Flood Modeller Pro • XPSWMM • LISFLOOD-FP • TRENT • XPSTORM

HEC-RAS (Brunner & CEIWR-HEC, 2016) is one of the most popular hydraulic modelling software, which has the capabilities of modelling 1-Dimensional, 2-Dimensional and integration of 1-D and 2-D flood modelling calculations considering all relevant structures and land information, such as

overbank/floodplains, levees, structures, channels, culverts, etc. HEC-RAS software is freely available and updated regularly with new features and relevant documentations. Steady flow, unsteady flow, sediment transport, and water quality modeling options are available for users. It allows user to interact the software through a graphical interface for all options. The data created by user are saved by different extensions so that it can be manipulated separately in different projects or in other softwares.

Main reason to choose HEC-RAS for this study is that the user can manipulate all data with some codes and applications. After the versions of HEC 5.0.x, the owners started to create some libraries through Visual Basic Application, so that users can manipulate the HEC-RAS with some automated processes like editing geometries, editing flows, changing dam breach parameters and implementing different Manning's roughness coefficients (Goodell, 2014).

After some design processes, HEC-RAS comes with installed Visual Basic library called 'HECRASController' in default mode. Now, this library has more than a hundred functions to manipulate hydraulic model with some codes. Additionally, researchers have been trying to adapt these Visual Basic Applications functions to other programming languages, such as MATLAB (Leon & Goodell, 2016) and Python (Dysarz, 2018). A snapshot of the overview of the library can be seen in Figure 3.5.

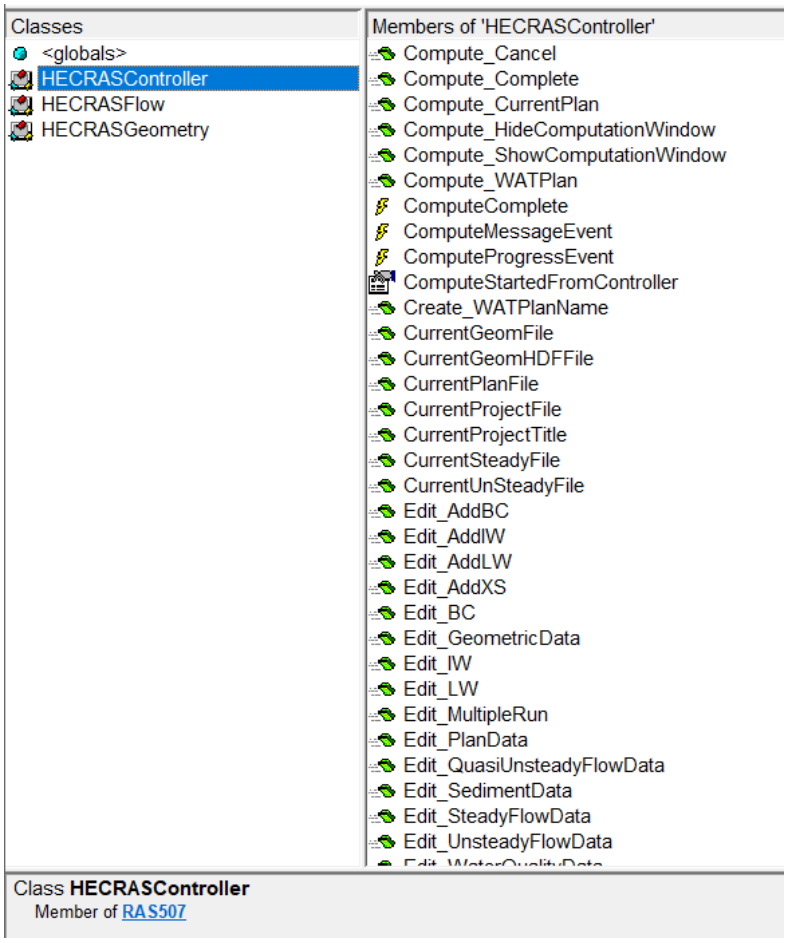

Figure 3.5. Functions of 'HECRASController' library in Visual Basic Application.

Manipulations of HEC-RAS are carried out by the developer panel of Excel Visual Basic Application in this study. All codes are compiled to manipulate flow values and roughness parameters with defined number of simulations. Codes can change the peak flow values and Manning's roughness parameters throughout the simulations and export the results in both tabulated form and/or rasterized tiff extensions. However, R programming language is utilized for statistical operations. Monte Carlo based input generation might lead to inappropriate results in Excel. Especially, different probability distributions like triangular cannot be generated with the help of default functions. R enables users to define upper and lower limits, standard deviations and statistical tests to check whether distributed inputs are properly generated.

Briefly, manipulation of HEC-RAS has following steps:

- Generation of probabilistic inputs with relevant statistical parameters via R programming language.
- Importing these distributions to the Visual Basic Applications.
- Running Visual Basic codes to manipulate HEC-RAS with distributed inputs.
- Saving results of all simulations in a tabulated form (flow depths for cross-sections with their flow and Manning's values at that moment).
- Exporting all individual simulation results as .tiff extensions
- Merging these individual tiff results to obtain a probabilistic flood inundation map

There are so many cross-sections and bridges which are used to create the 1-D hydraulic model, only 9 cross-sections with 4 bridges (Figure 3.7) are chosen to observe the flow depth changes and corresponding statistical quantities (i.e., skewness, coefficient of variation and standard deviation) as output. The reason to use these bridges is that there is little information on some of the drafts for others. However, these 4 bridges have the proper drafts obtained by Water State Hydraulics. Cross-section around bridges (named as just before and just after the bridges throughout the study) are few meters away from the defined bridges (i.e., 1-3 meters). The selection is made out for all possible slopes (i.e., higher slopes in the upstream part and lower slopes in the city center) and cross-section types (i.e., irregular, and wider channels in some parts and regular with narrow channels in other locations) although slopes do not vary in the downstream parts. All cross-sections with zoomed views can be seen in Appendix A. Flow depth differences due to some quantiles, standard deviations, coefficient of variations and skewness values of selected cross-sections are presented in Chapter 4. However, due to the critical overflow behavior of the vehicular junction bridge (B6) (Figure 3.3) in the past flood event, the results are shown separately for the nearby cross-sections of the mentioned bridge.

Schematic overview performed in this study is depicted in .

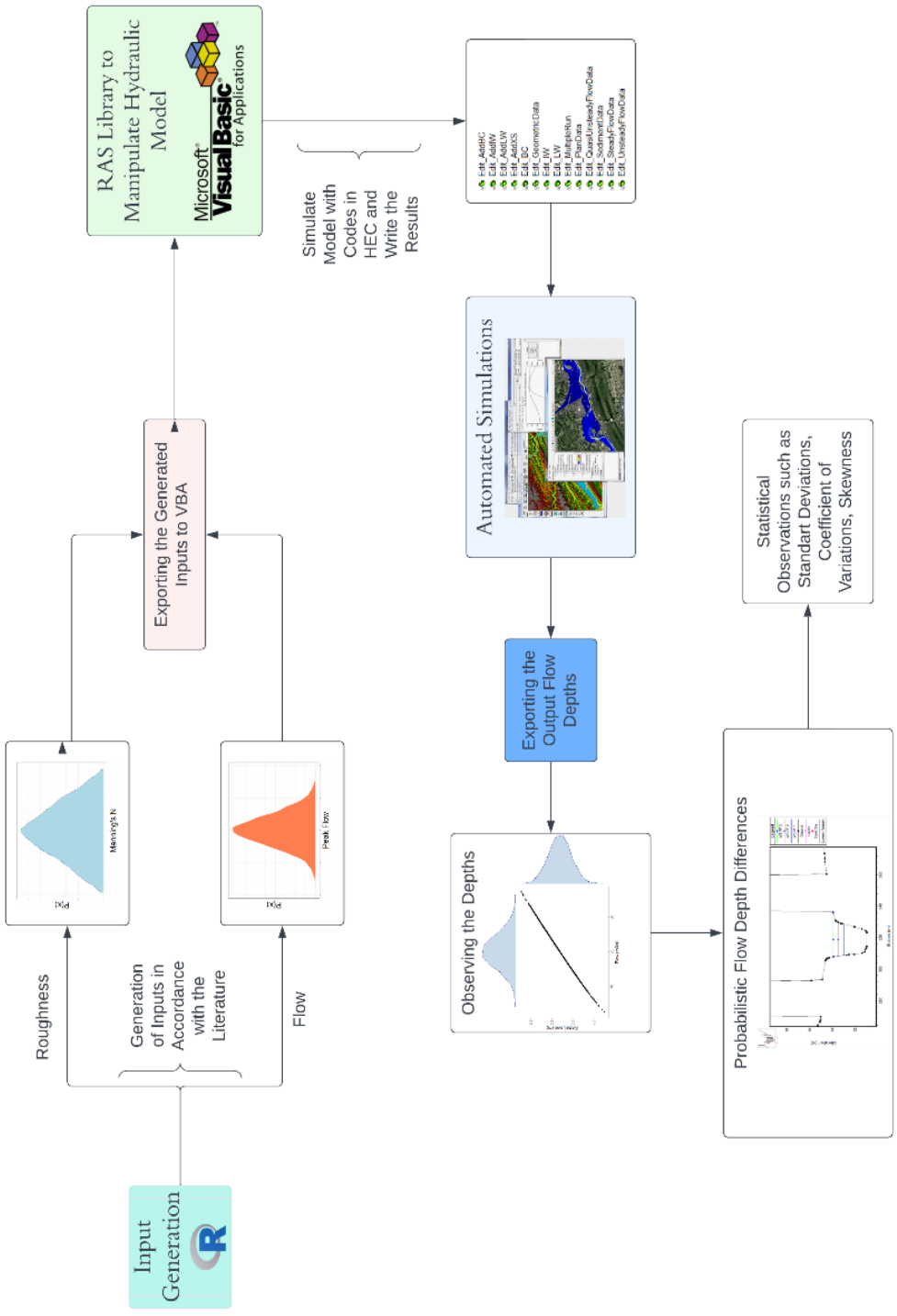

Figure 3.6. Steps of HEC-RAS manipulations and simulations.

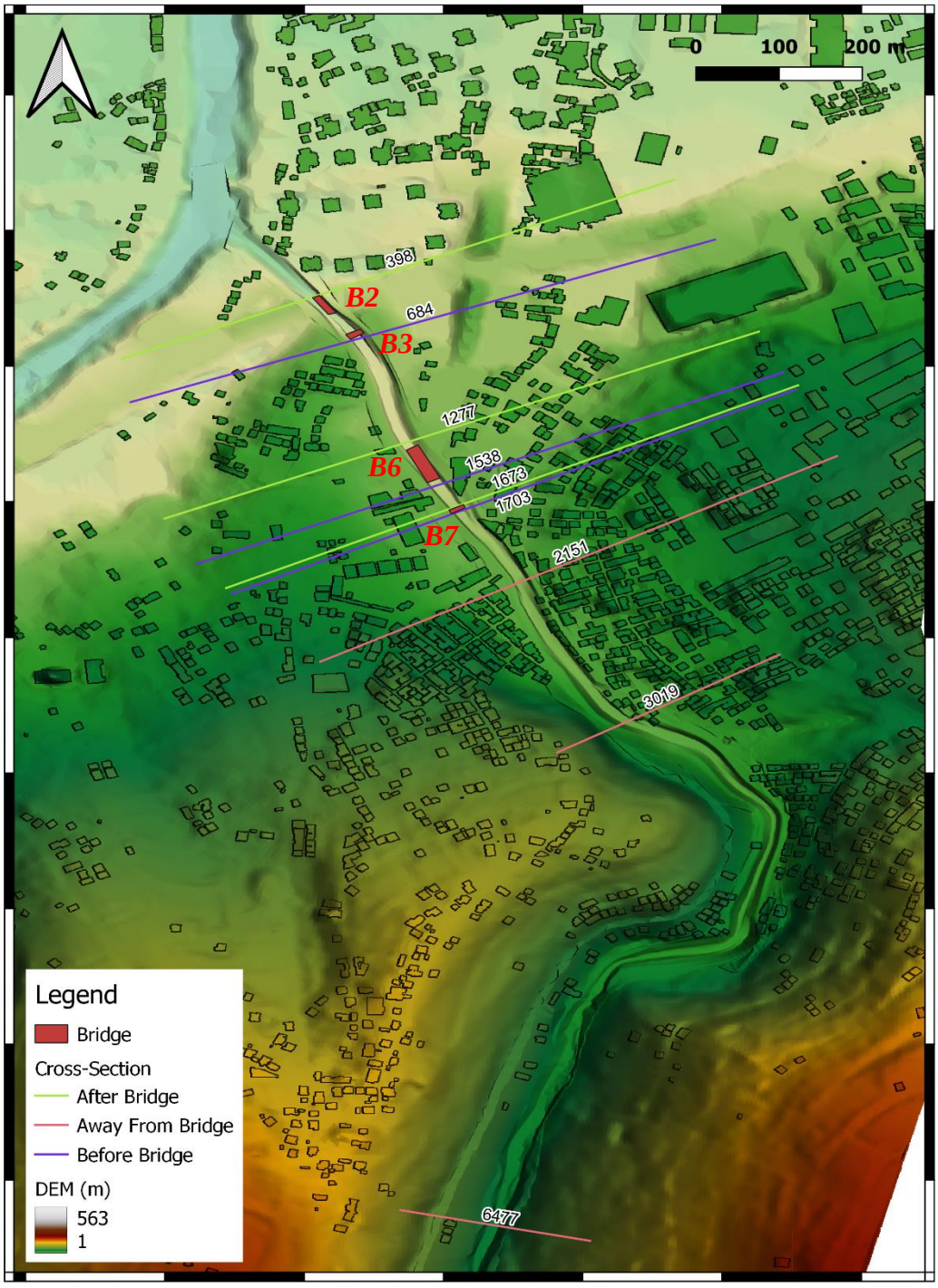

Figure 3.7. Chosen cross-sections and bridges to observe outputs throughout the study (bridge codes and the cross-section names are given automatically in HEC-RAS).

CHAPTER 4

FLOOD MODELLING

4.1 Number of Simulations

Determining the proper number of simulations in Monte Carlo approach is an important concept. It is a worth-stressing situation that what should be the necessary number of simulations so that all statistical parameters can be utilized properly. There are some statistical and mathematical approaches for this determination process. Some researchers (Beard et al., 1984) mentioned empirical methods within the identified confidence intervals. Convergence studies are also quite popular and utilizable by computing the variance of the simulations for different number of trials till the similar errors or relevant coefficient of variances are obtained (Jaeckel, 2002, Sobol, 1975). They help to understand behavior of distributions and find the point which should be the lowest number to obtain properly distributed inputs. The main idea is to obtain nearly the same value of variations of distributions in order to say it is unnecessary to generate new data to fit in defined distributions.

Similarly, some trials are conducted till similar coefficient of variations are seen in order to determine the required number of simulations for Monte Carlo approaches. Normally distributed flows (Q) with a constant Manning's roughness coefficient (n) are utilized for determination of proper number of simulations. The coefficient of variation (Ω_y) is the ratio of the standard deviation (σ_y) to the mean (μ_y). The formula of the coefficient of variation is shown in Equation 4.1.

$$\Omega_y = \frac{\sigma_y}{\mu_y} \qquad (4.1)$$

For this purpose, some random cross-sections (totally random from all cross-sections for both statistical results and hydraulic stability) are chosen carefully such that all behaviors (i.e., contractions around bridges, high slopes that rarely exist and regular channels) and calculations of coefficient of variations are conducted for each section. These cross-sections are presented in Figure 4.1. It is observed that resultant coefficient of variations for flow depths do not change significantly after 5000 number of simulations in this study as shown with logarithmic plots of these observations in Figure 4.2. From these trials, '5000' number of simulations are accepted to be used in all scenarios for the probabilistic flood modelling scenarios of the study including all types of uncertainties with separate observations and combined ones. As seen, there is no significant decrease in coefficient of variation coming from the statistical errors of distributions after 5000 simulations in different cross-sections.

Figure 4.1. Randomly selected cross-sections for determination process of proper number of simulations.

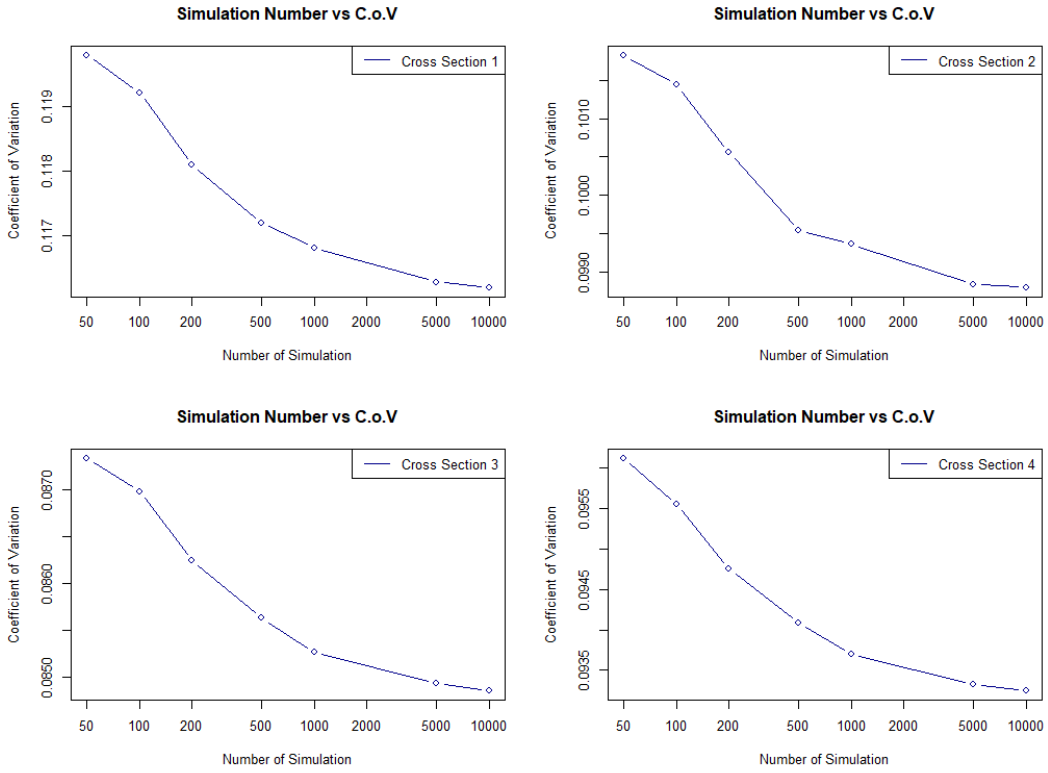

Figure 4.2. Simulation number versus coefficient of variation for randomly selected cross-sections.

4.2 Hydraulic Simulations

After determining the convenient number for simulations, three main types of simulations are carried out to see the ranges of uncertainties for the flow depth of channels. These are ‘simulations of changing flows with constant Manning’s roughness coefficient, ‘simulations of changing Manning’s roughness coefficient with constant flow’ and ‘simulations with both changing flow and changing Manning’s roughness coefficient’. Firstly, simulations are implemented in a separate manner so that effects of defined uncertainties can be seen one by one at different cross-sections. After this, combined simulations that allow hydraulic model to run the coincidences of extreme inputs of defined uncertainties are run.

4.2.1 Simulations with Changing Flows and Constant Manning's Roughness Coefficient

Since the selected distribution types and parameters depict the behavior of variable in nature, statistical properties of defined uncertainties must be built on delicately. There have been numerous developed methods in the literature since early 20th century for rainfall-runoff processes. Starting from distribution fitting examples with local data (Gumble, 1941; Singh, 1987) and derivations of unit hydrographs (Rosso, 1984; Singh et al., 1985), so many developments have been existed in hydrology like derivation of unit hydrographs with distribution fitting application (Aron & White, 1982), very popular and recent artificial intelligent techniques for both hydrograph and their peak flows prediction (Chen et al., 2013; Güçlü & Şen, 2016; Tayfur et al., 2018) are available to use for designers and researchers as well. Although these methods and other techniques in the literature are quite successful, uncertainties are probable and these deterministic methods might lead underestimate and overestimate peak flows especially in the regions where calibration of model is not possible as mentioned. Uncertainties coming from peak flow determination is investigated in this section with constant Manning's roughness coefficient to see the extent of difference in flow depths and their relevant distributions due to the locations like in front of the bridges, just before the bridges and away from the bridges for peak flow uncertainties. There are lots of perspectives affecting the flow uncertainties including the shape of channels, topography, hydrology, etc. (Bessar et al., 2020). Accordingly, the errors and uncertainties are mostly based on empirical approaches for hydrographs which means the behavior of the flow uncertainties are appropriate with a normal distribution. Additionally, considering these mentioned wide ranges on techniques and the literature, it is seen that the uncertainties can vary between 10 -20%. Therefore, the variations in flow values (i.e., peak flows) must be within a convenient range (Di Baldassarre et al., 2010; Xu et al., 2017). For this reason, coefficient of variation of 16.6% is chosen to be implemented for peak flow uncertainties so that proper deterministic peak flow value to distribute can be found

in a probabilistic manner without flooding. Some peak flow values are implemented not to cause overflow in main channel, and it is seen that peak flow of deterministic input can be 60 m^3/s without overflow and representing all of the flow depths which are not affected from overflow case. The peak flow caused the flood in 2012 was around 720 m^3/s. The river can convey 100-110 m^3/s without causing any flooding. Contemplating the extent of normal distribution away from the mean for 99.73%, mean peak flow was selected as 60 m^3/s with a standard deviation of 10 m^3/s with a coefficient of variation of 16.6% throughout Monte Carlo simulations. Manning's roughness coefficient which is constant throughout the simulations is chosen as 0.05 considering the previous studies for the area and all types of possible extents of Manning's roughness coefficient over the study channel with relevant calculations (Arcement & Schneider, 1989). Distributed peak flow values can be seen in Figure 4.3

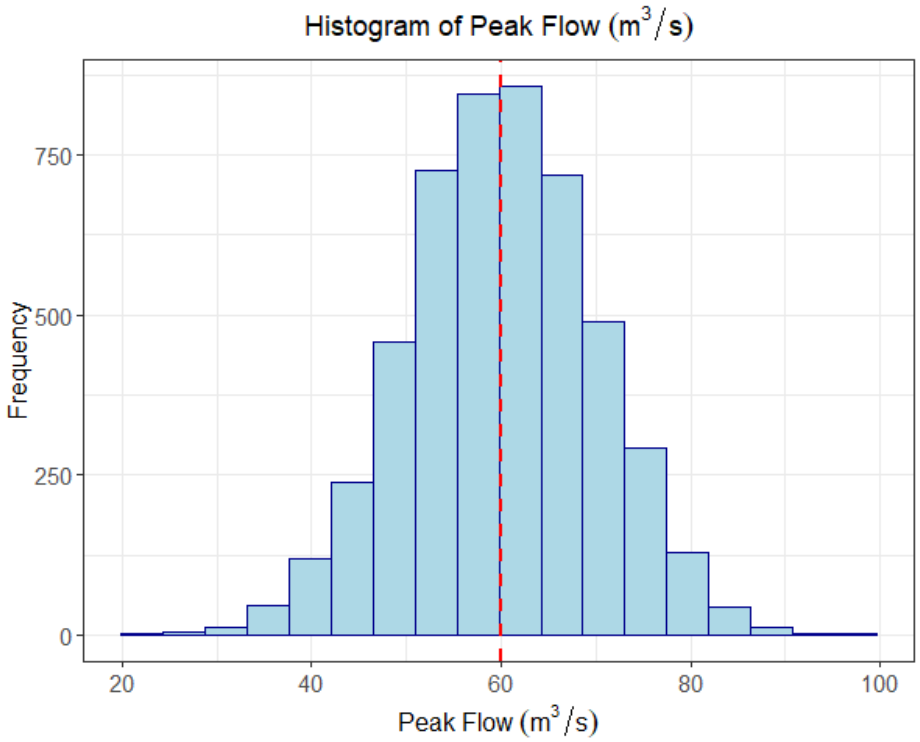

Figure 4.3. Histogram of peak flows obtained with Monte Carlo approach.

4.2.2 Simulations with Changing Manning's Roughness Coefficients and Constant Flow

Determination of the appropriate distribution of Manning's roughness coefficient and relevant statistical parameters are another crucial step to progress studiously since flow depths can be very sensitive for the Manning's roughness coefficient due to the uncertainty (Kim et al., 2010). There are detailed and comprehensive studies to determine an adequate constant Manning's roughness coefficient for channels and flood plains including vegetated banks (Coon, 1995), grass-lined channels (Abood et al., 2006), vegetated furrows for irrigation purposes (Kamali et al., 2018) and even the dynamical coefficients for basin-scaled models (Ye et al., 2018) to determine a proper deterministic roughness parameter. Since roughness parameters have quite complex natures both inside the channels and in the floodplains (Engman, 1986), the randomness is the inherent part of Manning's roughness parameter. Accordingly, triangular distribution is quite suitable to employ in many cases. It can be used in different research areas like character classifications (Yoo, 2019), risk analysis (Joo & Casella, 2001) or uncertainties like Manning's roughness coefficient (Bozzi et al., 2015). For this reason, triangular distribution may result in more logical behaviors when the randomness is especially important (Subirana et al., 2017). Therefore, triangular distribution of Manning's roughness coefficients is used in the Monte Carlo simulations. Some studies proved that roughness parameters may include uncertainty up to 15% (Bozzi et al., 2015; Yanmaz, 2000).

The triangular distribution needs three main parameters to properly fit in a model. They are represented as:

- the lower limit: 'x_l', lowest value of all probable Manning's roughness coefficients.
- the upper limit 'x_u', the highest values of all probable Manning's roughness coefficients.
- the mode 'x_m', the mode (also mean if the distribution is selected as not skewed) of all probable Manning's roughness coefficients.

In accordance with literature, coefficient of variation for the triangular distribution is selected as 12.5% for these simulations. If mode (or mean if there is no skewness) value of triangular distribution and the relevant coefficient of variation are determined, lower limit and upper limit can be obtained by using following equations.

$$x_m = \frac{1}{2}\left(\frac{x_l}{x_u}\right) \tag{4.2}$$

$$C.o.V = \Omega_y = \frac{1}{\sqrt{6}}\frac{(x_u - x_l)}{x_u + x_l} \tag{4.3}$$

$$\mu_{roughness} = \frac{1}{2}(x_l + x_u) \tag{4.4}$$

Using the information of decided parameters as x_m = 0.05 and C.o.V = 12.5%, lower limit of the triangular distribution becomes '0.0354' and upper limit of the distribution becomes '0.0646'. Using these data and relevant functions, the input histogram of triangular distribution for Manning's roughness coefficient is presented in Figure 4.4. An example of these determination process of values is presented in Appendix E.

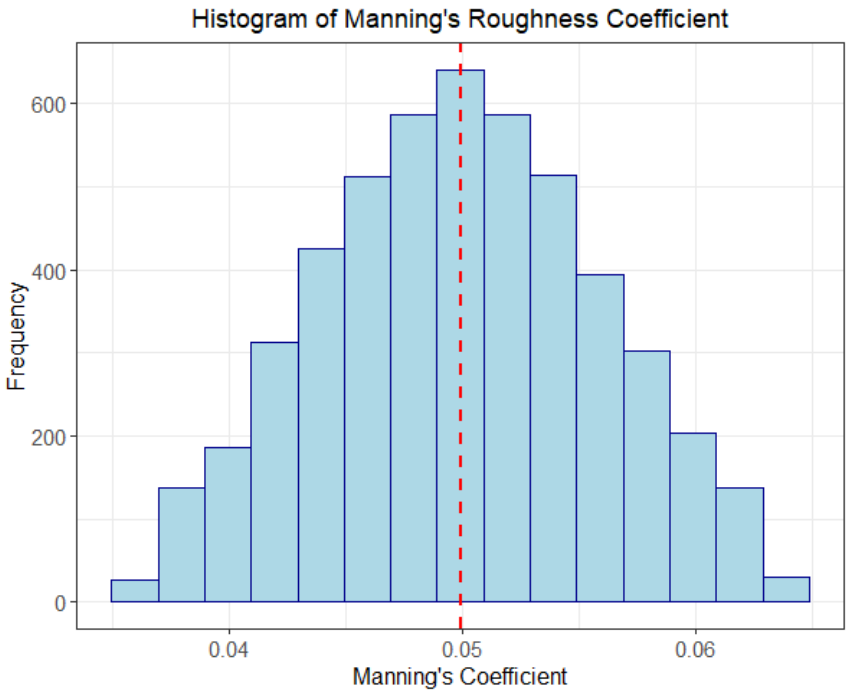

Figure 4.4. Histogram of Manning's roughness coefficient obtained from Monte Carlo approach.

4.2.3 Simulations with Changing Flows and Changing Manning's Roughness Coefficients

In the combined case, peak flows and Manning's roughness coefficients are manipulated via Monte Carlo simulations simultaneously. The relevant parameters and distributions are the same as the cases where the simulations are carried out separately. Triangularly distributed Manning's roughness coefficients with the mean value of 0.05 and lower and upper bounds are selected as 0.0354 and 0.0646. Just like roughness coefficients, peak flows are simulated by using the same distribution and statistical parameters where normal distribution with 60 m^3/s of mean flow and standard deviation of 10 m^3/s is used (Figure 4.5). The values produced from distributions were selected totally randomly, and it is confirmed that all possible

extends (i.e., minimum roughness coefficient with minimum flow or vice versa) are implemented to see the whole extent of output water surface levels in cross-sections and around bridges. Monte Carlo based selections with possible trials are implemented and hydraulic model is simulated.

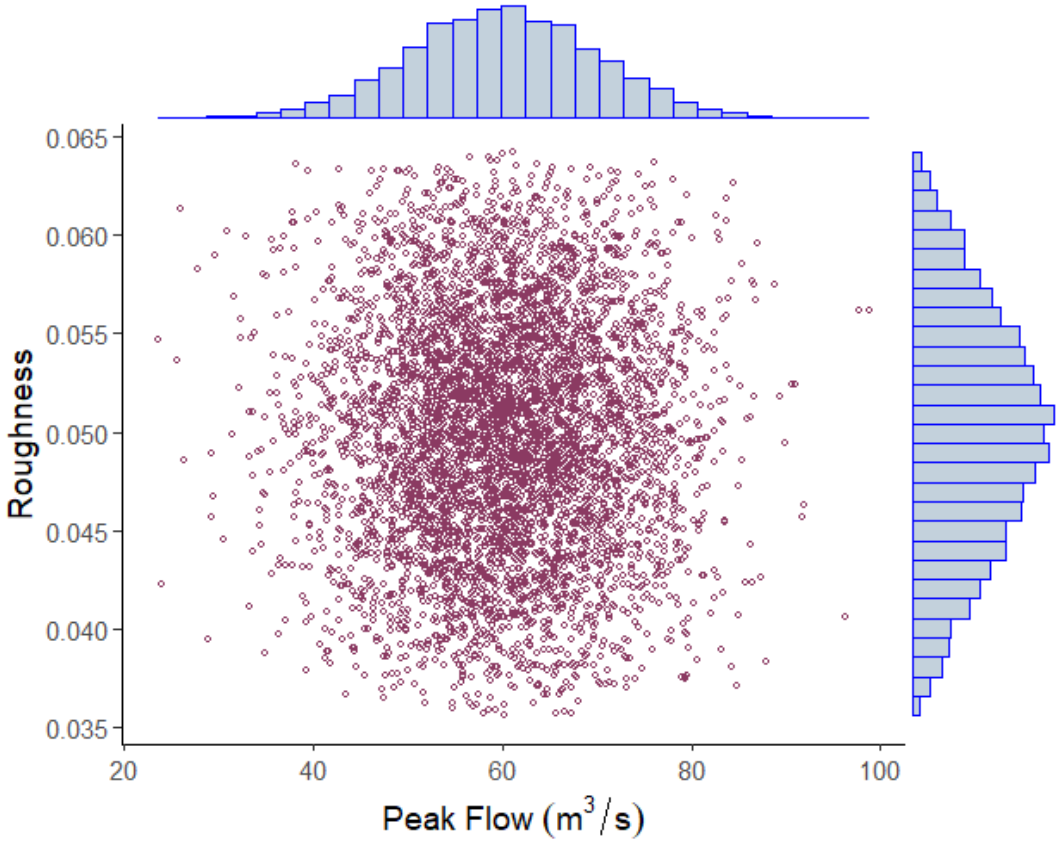

Figure 4.5. Applied combination of Manning's roughness parameters and peak flows.

It is worth to mention that main goal of the combined case is to see what happens when extreme cases of uncertainties (i.e, extreme values of roughness and peak flows) coincide throughout channel and relevant cross-sections.

Since the hydraulic model includes different type of cross-sections including bridges and their sudden contractions, the output flow depths resulted from the merged uncertainties is vital to analyze especially at flood-prone sections. As can be seen in

Figure 4.5, all possibilities within the determined variations of uncertainties are expected to give underestimation and overestimation in flow depths.

CHAPTER 5

RESULTS

5.1 Flow Uncertainties with Constant Manning's Roughness Coefficient

Normally distributed flows (with defined mean value and standard deviation) with a constant Manning's roughness coefficient are observed at different cross-sections around bridges and regular waterways close to both downstream and upstream of the river. It is ensured that all types of sections (including wide, narrow, around the bridge, having high slope, having low slope, etc.) are considered for studies as mentioned. In this scenario, Manning's roughness coefficient is assumed as 0.05 (mean value) throughout the simulations.

Figure 5.1. View of the bridge (B6) selected as critical one due to past flood events with modelled cross-section numbers (i.e, 1277 and 1538 cross-sections after and before the bridge).

Marginal distributions of flow depths and peak flow values for the critical vehicular junction bridge are depicted in Figure 5.2. Output flow depth distributions are convenient with the normal distributions with a wide range. In the extreme cases, fluctuations are quite sensitive due to the capacity of bridge section (maximum flow depth is 4.30 meters as seen in Figure 3.3).

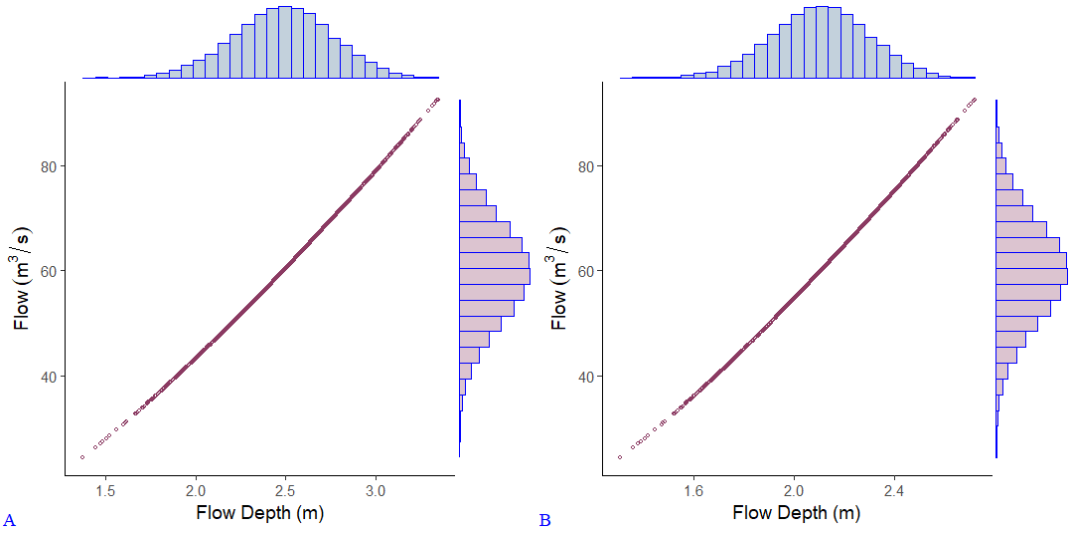

Figure 5.2. Histograms of simulated peak flows and flow depths for a) before the critical bridge (named as 1538) and b) after the critical Bridge (named as 1277).

As it is seen in Figure 5.2, flow depths do not reach the maximum level (i.e, 4 meters (Appendix A)) which means there is no overflow as expected. However, flow depths have quite wide range and they are quite sensitive to the defined uncertainty variations at the cross-section of this bridge. When wider cross-sections on the upstream part is selected (i.e, cross-section number is 3019), range is decreased (Figure 5.3).

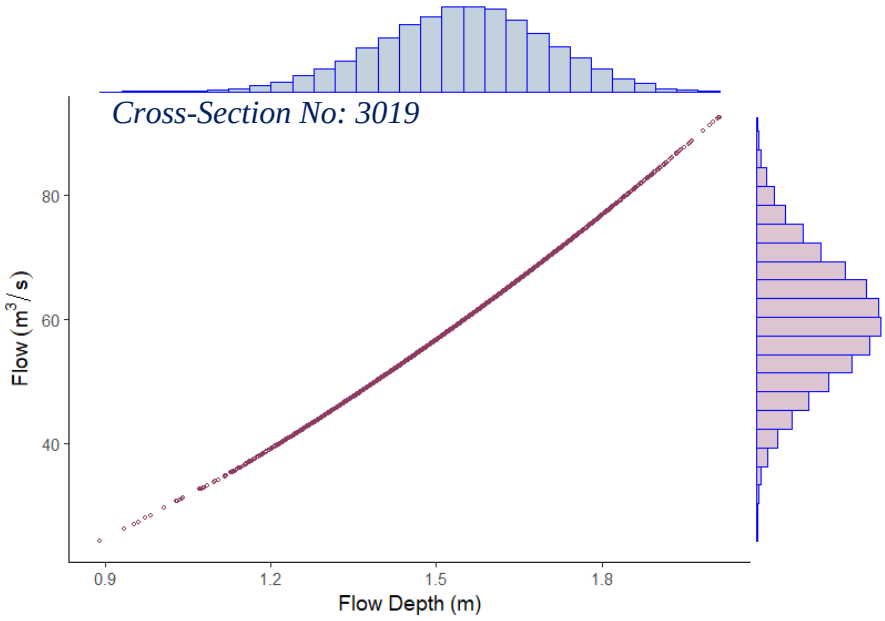

Figure 5.3. Histograms of simulated peak flow and flow depths for cross-section 3019.

Although, slopes are similar at the cross-sections, channel width is quite changeable, which directly affects the flow depth uncertainties at the cross-section. All of the marginal distributions of cross-sections of flow uncertainties are given in Appendix B.

In order to see the effects of flow uncertainties visibly at the critical bridge, quantiles of 5% and 95% for simulated flows are taken and flow depth outputs due to these quantiles are shown at the cross-sections just before and after the bridge (Figure 5.4) which have the flow depth differences of 93 cm and 75 cm, respectively.

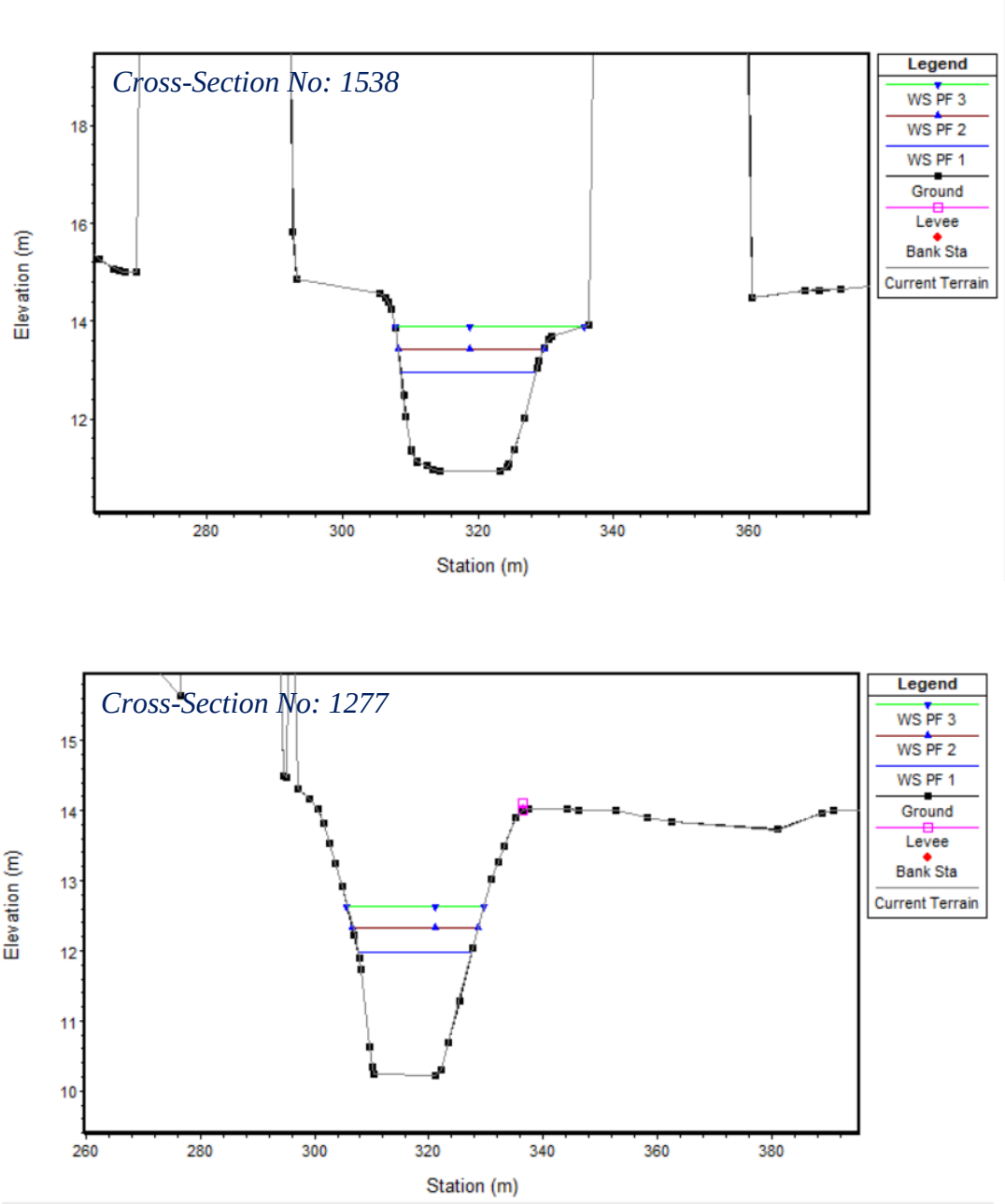

Figure 5.4. Flow depths due to 5% and 95% quantiles of simulated flows 1 meter (section 1538) and 1.5 meters after (section 1277) the most critical bridges.

In order to see all extent of results, standard deviations, coefficient of variations and skewness values of cross-sections are observed for all selected bridges. First

observations are about the standard deviations which are considerably high around bridges compared to the other cross-sections. They reach around 0.28 meters in the contraction parts of the bridges (Figure 5.5).

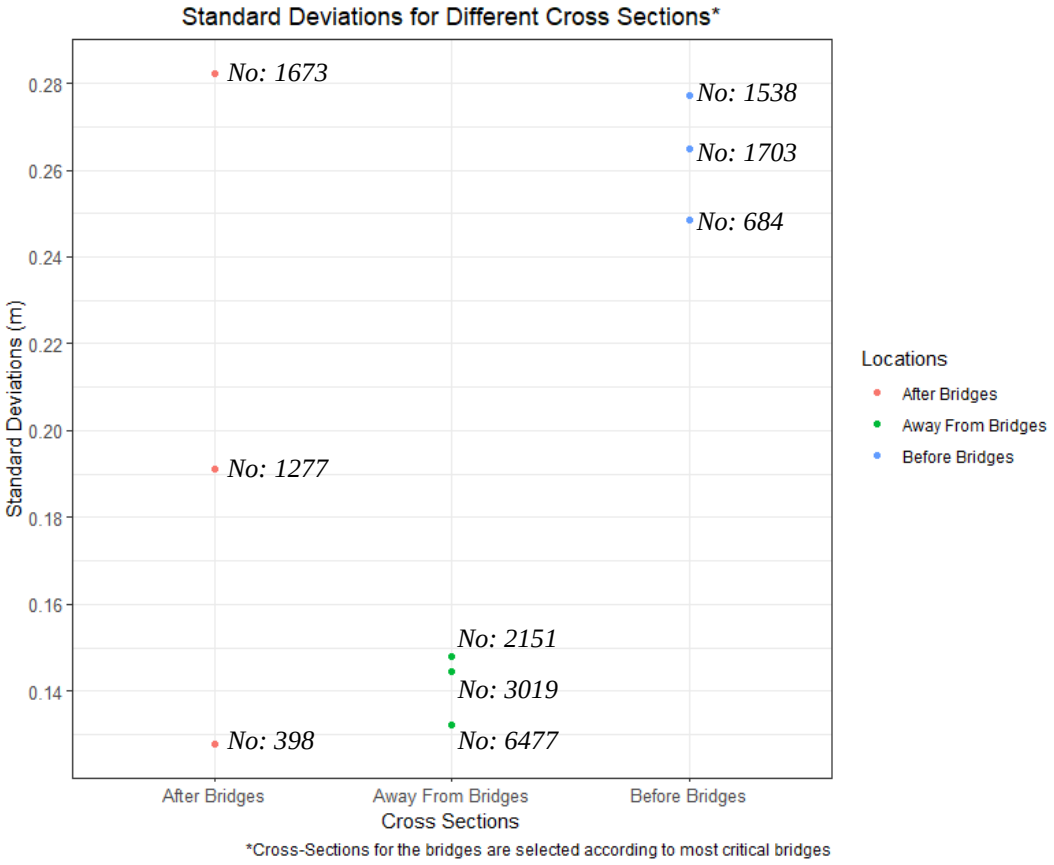

Figure 5.5. Standard deviations for flow uncertainties at different cross-sections.

As seen in Figure 5.5, standard deviations are consistently higher just before the bridges. These higher results are directly affected by the sudden contraction of the flow path due to bridges. Although standard deviations are lower for the cross-sections away from bridges, they have still valued around 0.15 meters which can be risky for a flood warning system in this region where floodplain is considerably limited.

When the coefficient of variation (C.o.V) values are observed, flow depths have tendencies to behave similarly without depending on locations, which concludes that differences in standard deviations were indicators of the effects for flow uncertainties on contraction parts in the main channels. Since the possible wetted perimeters decrease because of the contraction and the discharge directly affects the flow depth in subcritical flow, output flow depth distributions had wider intervals with negligible change in coefficient of variation (Figure 5.6). The contraction and decrease in wetted perimeter changes due to the type of bridges, i.e., characteristics of bridge infrastructural elements and utilization factors (pedestrian, vehicular) increased the flow uncertainties.

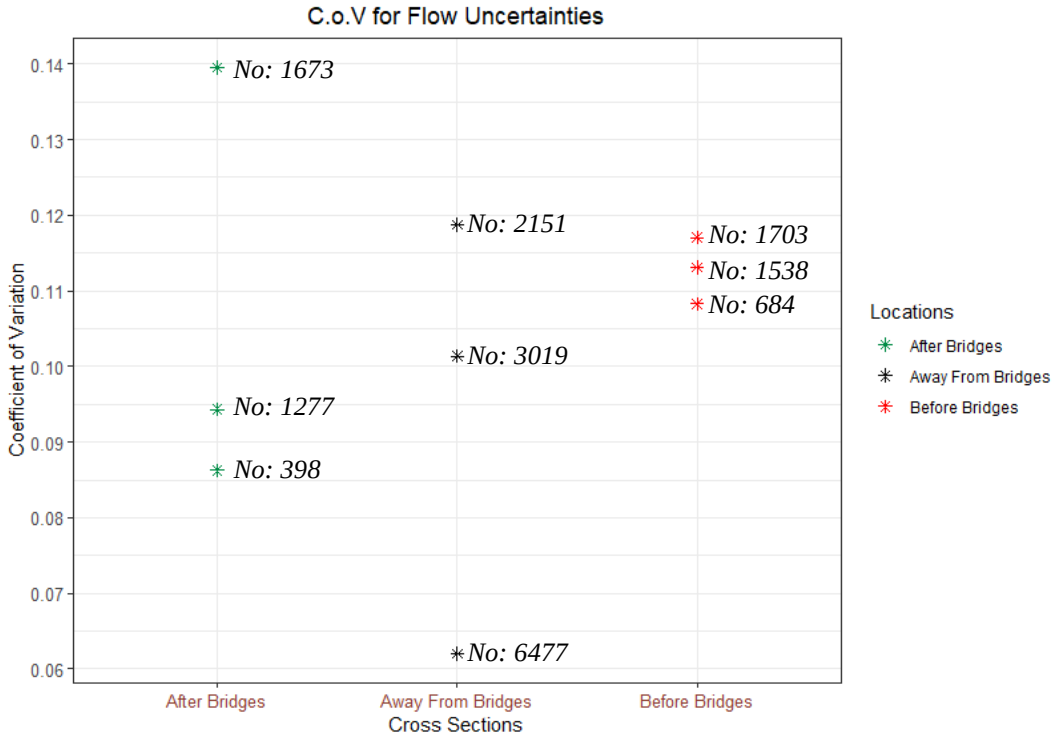

Figure 5.6. Coefficient of variation for flow uncertainties at different cross-sections.

Additionally, distributions of output flow depths and their corresponding skewness are another important statistical parameters for uncertainty estimation (Bozzi et al.,

2015). Throughout the simulations for flow uncertainties with constant Manning's roughness value, it is observed that output flow depths are mostly normally distributed with slightly negative skewness values up to -0.30 (Figure 5.7) occurred at all cross-sections regardless of location, structures and channel width differences, especially in downstream parts. When the average differences for average flow depth and 75%-95% quantiles of output flow depths are observed, values have the interval starting from 0.09 meters to 0.43 meters for flow uncertainties.

Table 5.1. Average differences (m) between mean flow depth (m) and quantiles (75% and 95%) for flow uncertainties.

Uncertainty	***Location***	***Differences(m) (75% -95%)***
Only Flow	Before Bridges	0.18 – 0.43
Only Flow	After Bridges	0.14 – 0.33
Only Flow	Away From Bridges	0.09 – 0.23

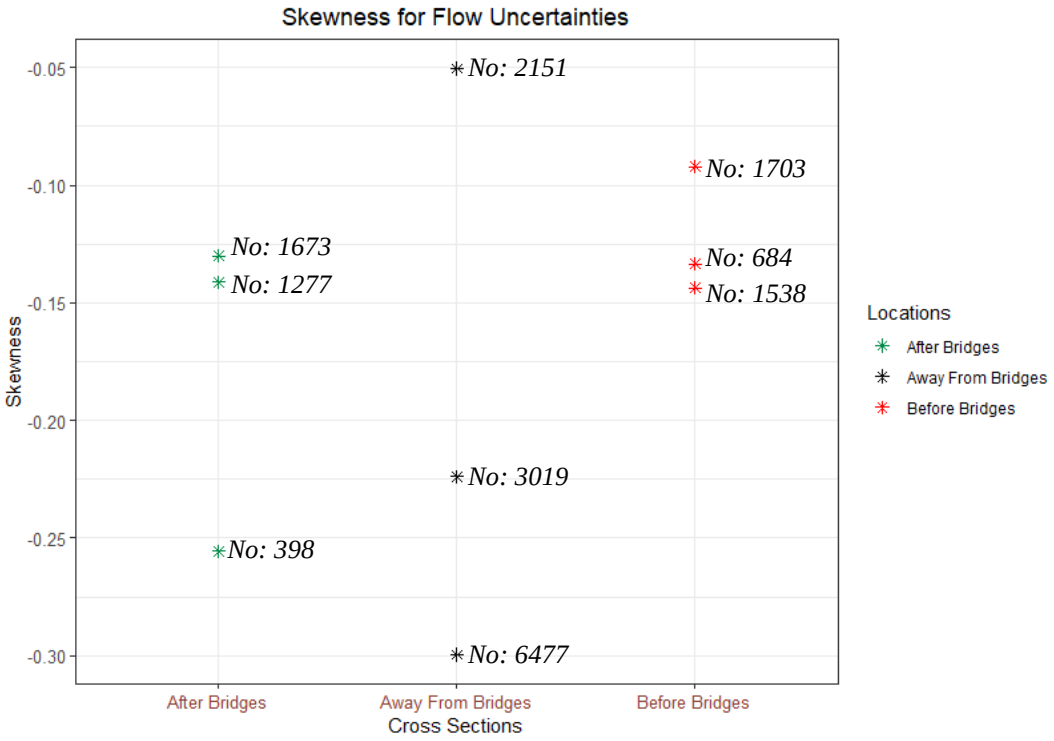

Figure 5.7. Skewness values for flow uncertainties at different cross-sections.

5.2 Manning's Roughness Uncertainties with Constant Flow

Pre-defined triangularly distributed Manning's roughness coefficients are simulated with constant flow value to see all flow depth fluctuations for different cross-sections by questioning whether the uncertainties behave the same as in the normally distributed flow values. Constant flow value (which is Q = 60 m^3/s) is selected so that there cannot be overflow that directly affects the output distribution types and fluctuations. The most critical bridge is observed again for the Manning's roughness uncertainty in detail (Figure 5.8) for the output flow depth distributions.

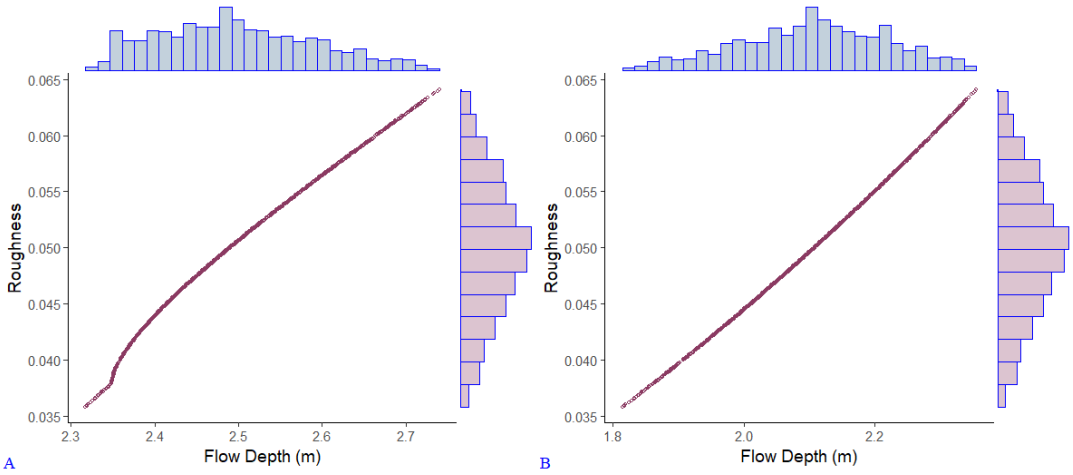

Figure 5.8. Histograms of simulated Manning's roughness parameter and flow depths for A) before the critical bridge (as named 1538) and B) after the critical bridge (as named 1277).

As seen, uncertainty in Manning's roughness coefficient tends to have smaller results compared to flow uncertainties. However, the ranges are still important especially for flood warning system in the critical bridge. Flow depth differences can reach up to 50 cm which is quite important for this kind of bridge that have contractions. Additionally, effects of flow depth change due to Manning's roughness coefficient do have non-linearities. Another example is presented for output flow depth of wider and irregular cross-section (i.e., named as 3019) is shown in Figure 5.9.

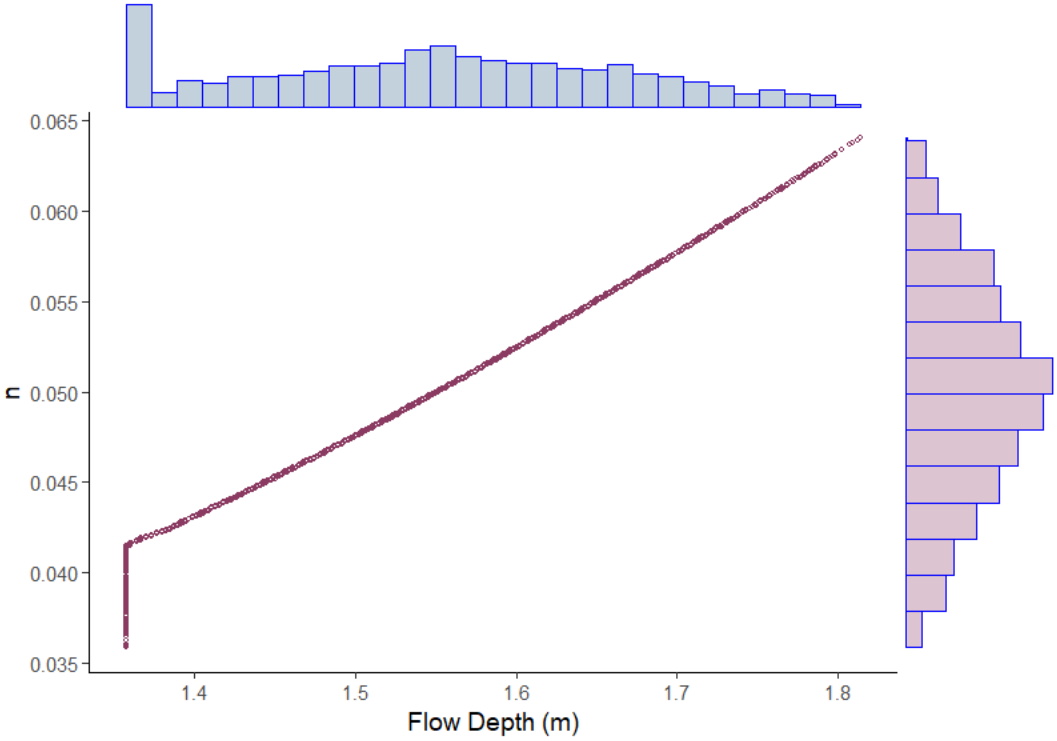

Figure 5.9. Histograms of simulated manning's roughness coefficient and output flow depths for cross-section 3019.

Interestingly, flow depths are not affected up to a certain low limit of Manning's roughness coefficient for this wider upstream channel (see Figure 3.7 for the location of cross-section). This is important to mention that Manning roughness uncertainties for lower thresholds (i.e., smaller than 0.042 for this case) do not affect these cross-sections. However, it still has 40 cm flow depth uncertainties although it is a wide cross-section. All output flow depth distributions for cross-sections are given in Appendix C.

When all cross-sections are observed, in this scenario, standard deviations decreased considerably up to 75% (Figure 5.10) due to the characteristics of roughness parameters on flow depths and due to the lower coefficient of variations in inputs of Manning's roughness values. As seen, standard deviations are higher in the locations of regular cross-sections which are quite away from bridges and hydraulic structures. Values vary between 0.02 to 0.13 meters throughout the simulations. Due to the

structural behavior of roughness parameters at the bridge sections, it is seen that flow depth fluctuations are not affected from Manning's roughness uncertainties as much as flow uncertainties in most of the cross-sections.

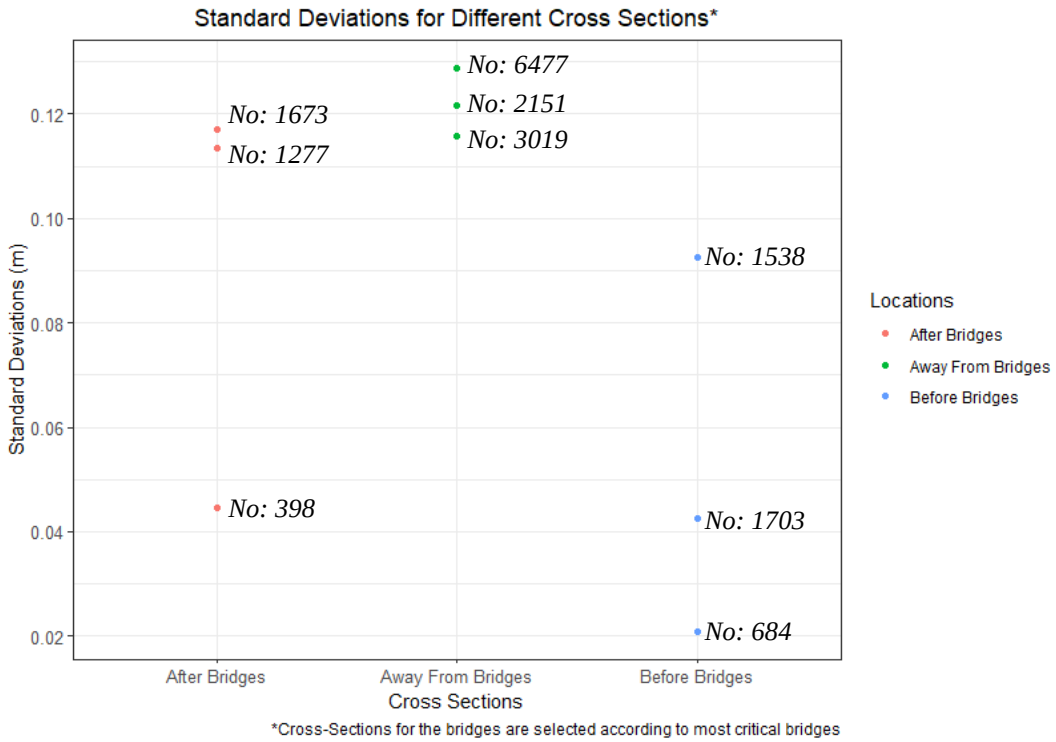

Figure 5.10. Standard deviations for Manning's roughness uncertainties at different cross-sections.

On the other hand, except some of the cross-sections, heavily positive skewness values are observed due to the convergence in the lower percentiles of output flow depths. Output flow depths tend to not to change till extreme Manning's roughness values are simulated (Figure 5.11). Therefore, standard deviations are affected due to these results. Although standard deviations are not high in critical sections, regular cross-sections away from bridges have important fluctuations compared to their quantiles (Table 5.2). Flow depths reach to 0.21 meters away from the bridges and 0.16 meters after the bridges when 95% quantile input is simulated.

Table 5.2. Average differences (m) between mean flow depths and quantiles (75% and 95%) for roughness uncertainties.

Uncertainty	*Location*	*Differences(m) (75% -95%)*
Only N	Before Bridges	0.03 – 0.09
Only N	After Bridges	0.06 – 0.16
Only N	Away From Bridges	0.09 – 0.21

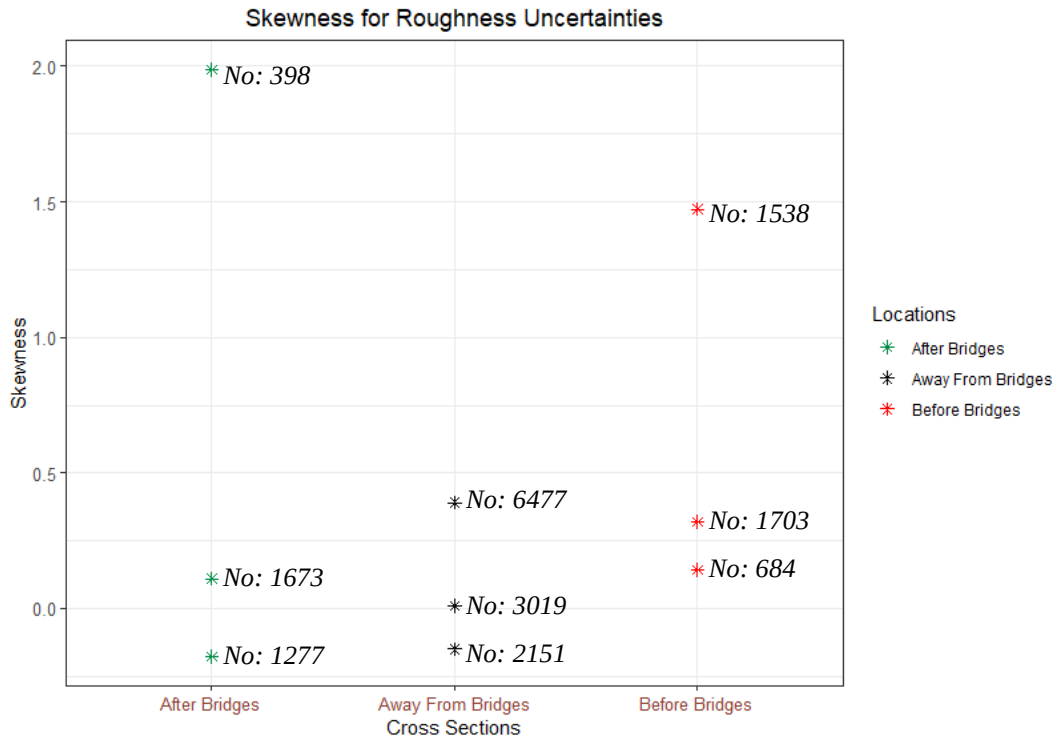

Figure 5.11. Skewness values for Manning's roughness uncertainties at different cross-sections.

Coefficient of variations tend to result in smaller values compared to flow uncertainties (Figure 5.12). Variations have values between 0.01 to 0.09 meters. However, the cross-sections away from bridges ended up with higher results which is caused by the distribution types of output flow depths and relevant skewness values. Skewness intervals of the cross-sections away from the bridges are more

stabilized and smaller which means the uncertainties of roughness coefficients around the contraction parts of the main channels gave output flow depths changing slowly at first but after a threshold, flow depths change considerably. This is not the case at all times. In some cross-sections just before and just after the bridges, roughness values have even negatively skewness values. This might be explained by the topography and relevant sudden changes, velocity of water, changes in channel sizes, and the sudden contraction of flow due to bridges.

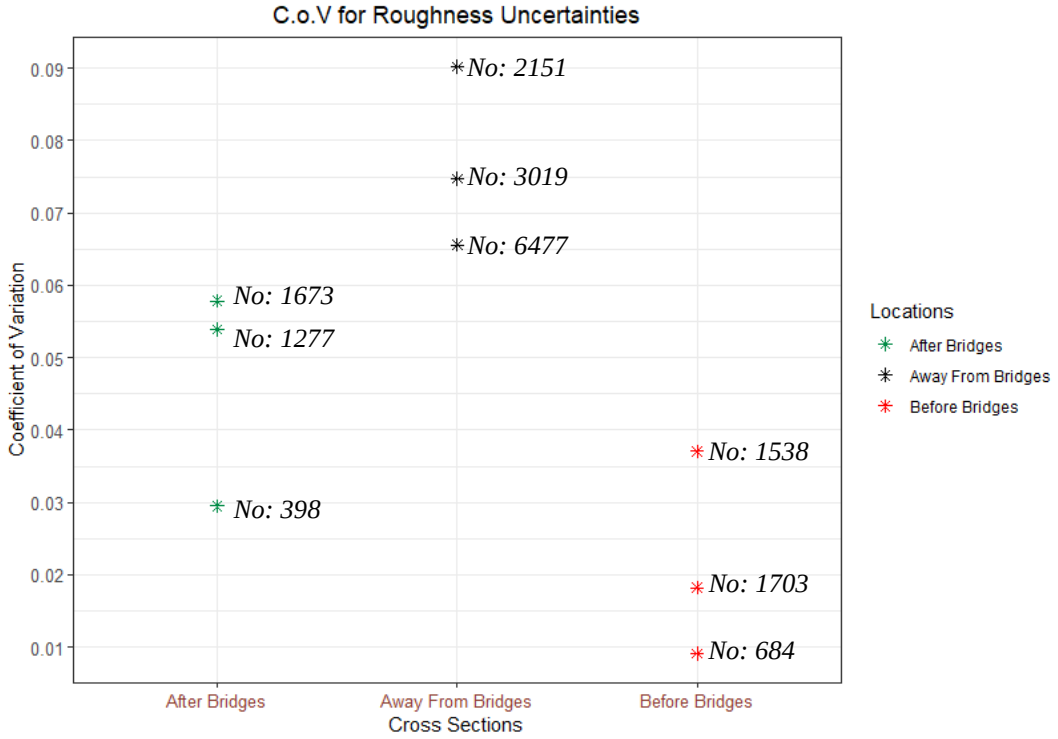

Figure 5.12. Coefficient of variation for Manning's roughness uncertainties at different cross-sections

5.3 Combined Flow and Manning's Roughness Uncertainties

5.3.1 Combined Flow and Manning's Roughness Uncertainties Without Overflow

Combined case is considered to cover all possible uncertainties caused by flow and roughness coefficients. All probable extreme cases also simulated by taking into consideration that there are no overflows from the main channel and neighboring structures so that the effects of overtopping can be eliminated and observed with the Monte Carlo simulations. In this scenario, codes automatically integrate the distributed peak flow values with distributed roughness coefficients randomly. Therefore, all combinations like maximum peak flow with minimum roughness value or maximum roughness value with maximum flow are utilized.

Firstly, the critical cross-sections before and after the critical bridge (Figure 5.1) are observed separately. One of the most important observations to check is that whether all simulated peak flows and Manning's roughness coefficients are utilized or not. In order to achieve this, 3-Dimensional perspective plot is obtained as in Figure 5.13. It is seen that HEC-RAS and Visual Basic codes combined all possible uncertainties for Manning's roughness coefficient and peak flows for cross-sections. This is quite important to mention for dependable results.

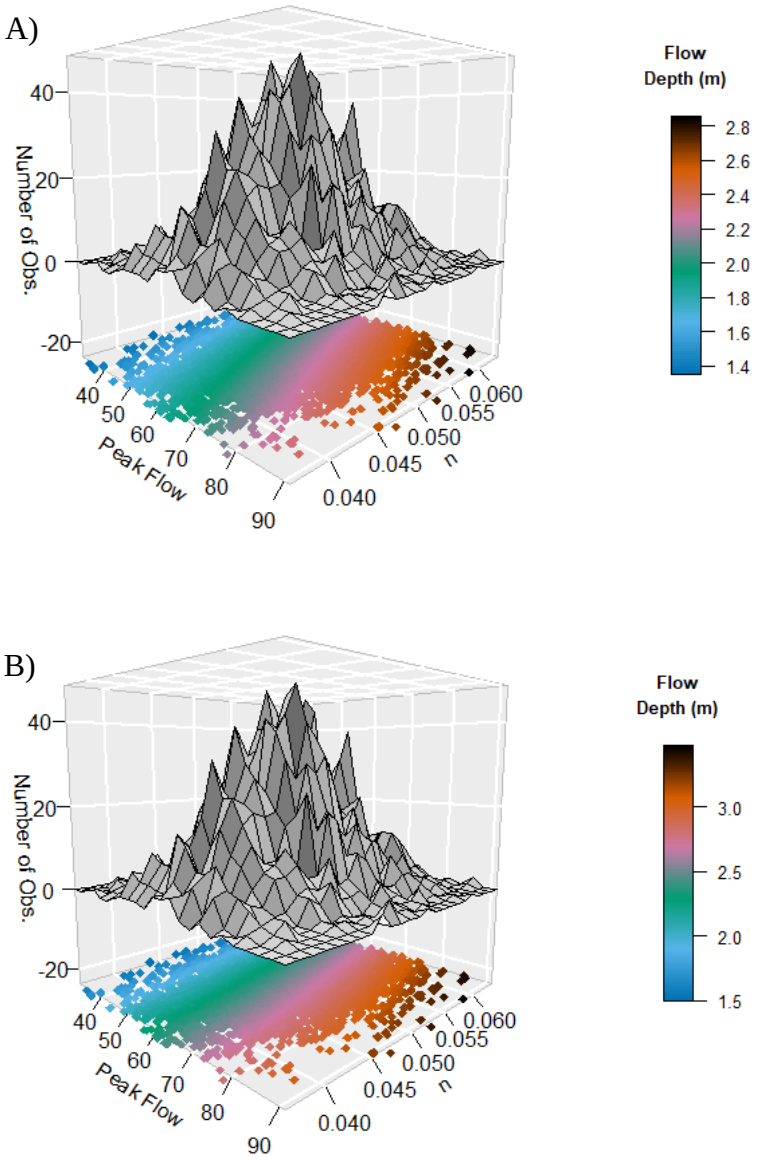

Figure 5.13. Number of observations (simulated values) for peak flows (m^3/s) and Manning's roughness coefficient with flow depth (m) values for cross-section A) after the critical bridge - 1277 and B) before the critical bridge - 1538.

When output flow depths of cross-section 1277 and cross-section 1538 are observed, it is seen that flow depths change up to 1 meter due to 5% and 95% quantiles (Figure 5.14) which is quite important for this bridge opening since it has a maximum

capacity of 4.3 meters (Figure 3.3). Additionally, the output flow depths tend to have normal distribution although Manning's uncertainties are triangularly distributed. All output flow depth histograms are given in Appendix D with 5% and 95% quantiles.

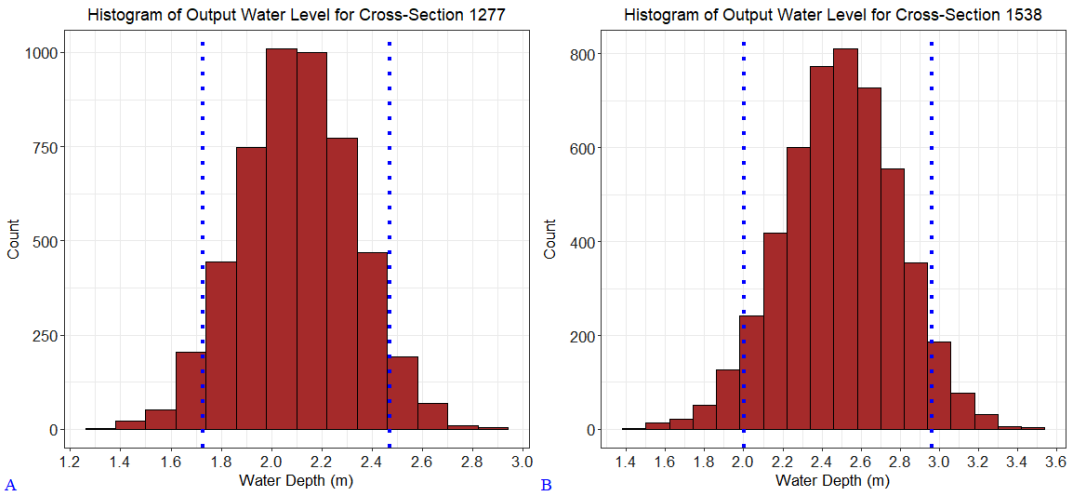

Figure 5.14. Histogram of output flow depths with 5% and 95% quantiles (blue lines) for cross-sections of combined uncertainties 1277 (after the critical bridge) (A) and 1538 (before the critical bridge) (B).

Briefly, if all cross-sections are observed in this combined uncertainties, standard deviations before and after the bridges do not increase significantly as expected. Results estimate that standard deviations vary between 0.13 meters to 0.31 meters after the bridges and 0.25 meters to 0.29 meters before the bridges. However, cross-sections away from the bridges gave significant increase although the sections are quite wide. Flow depths reach to 0.20 meters away from the bridges (Figure 5.15). So, their flow depth values are changed up to 40% compared to the only peak flow and only Manning's roughness uncertainties cases.

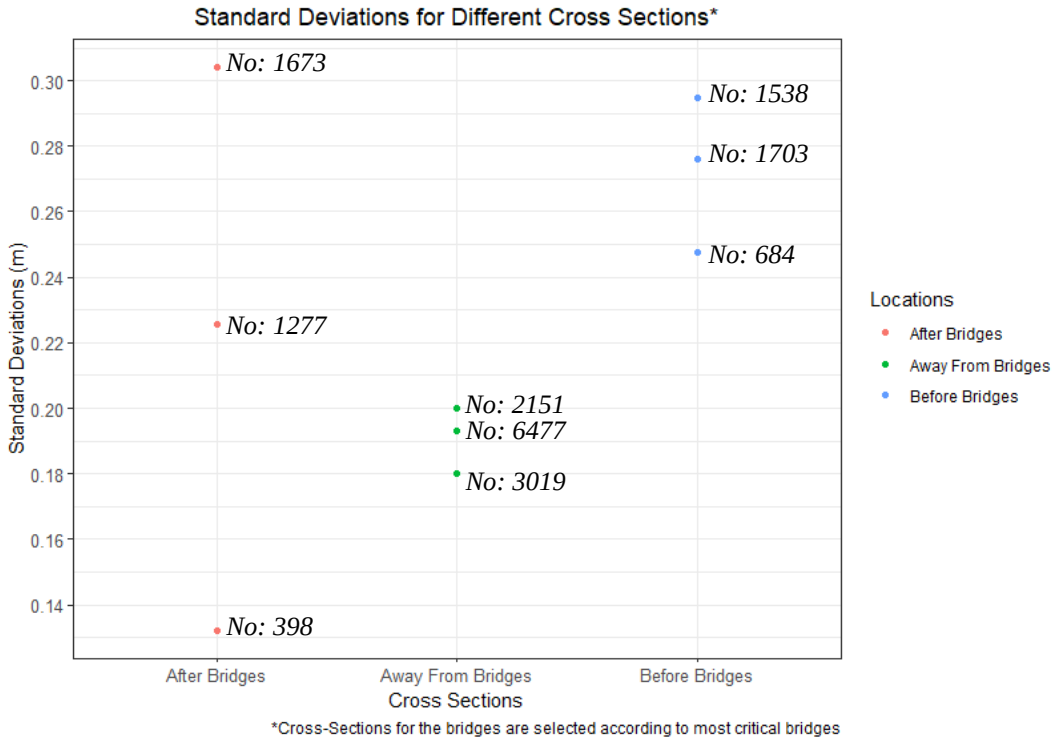

Figure 5.15. Standard deviations for combined uncertainties at different cross-sections.

Additionally, some of the output flow depth distributions end up with normal distribution (for 90% of confidence interval), even though input roughness uncertainties are distributed triangularly. When the skewness values are observed, it's seen that there are no extremes in values which vary between -0.2 to 0.2. The skewness values around bridges (both before and after) are slightly negative. Vice versa, values are slightly positive in the cross-sections away from the bridges (Figure 5.16).

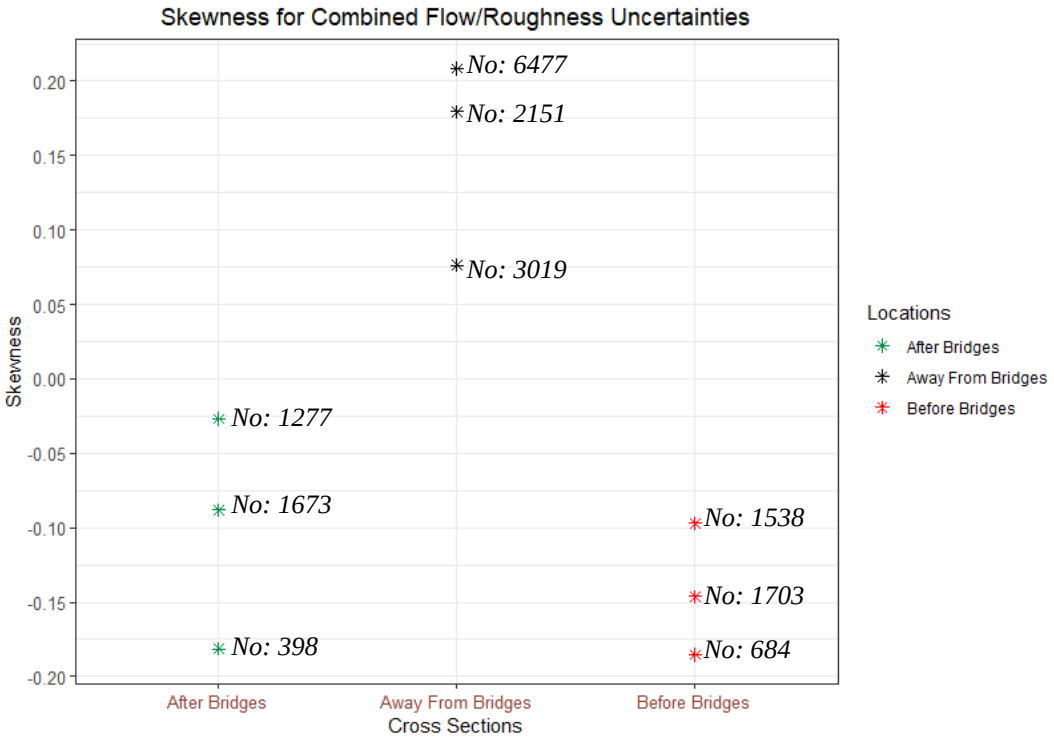

Figure 5.16. Skewness values for combined uncertainties at different cross-sections.

Coefficient of variations for output flow depths increase in this scenario up to 0.15 meters. Again, main increases are observed away from the bridges (up to 30% compared to other scenarios). Values vary between 0.09 m to 0.15 m after bridges and 0.10 m to 0.12 m before bridges and 0.09 m to 0.15 m away from the bridges (Figure 5.17), which show the importance of the combined uncertainties in the regular cross-sections.

Lastly, average differences (m) between mean flow depths and quantiles (75% and 95%) for combined uncertainties are shown in Table 5.3. The results reveal that combined uncertainties with predefined inputs may lead to differences in flow depths up to 0.45 meters around bridges. This can be considered as quite crucial difference especially for flood warning system in the main channel. Additionally, cross-sections away from the bridges become most sensitive sections in flow depths when uncertainties are combined.

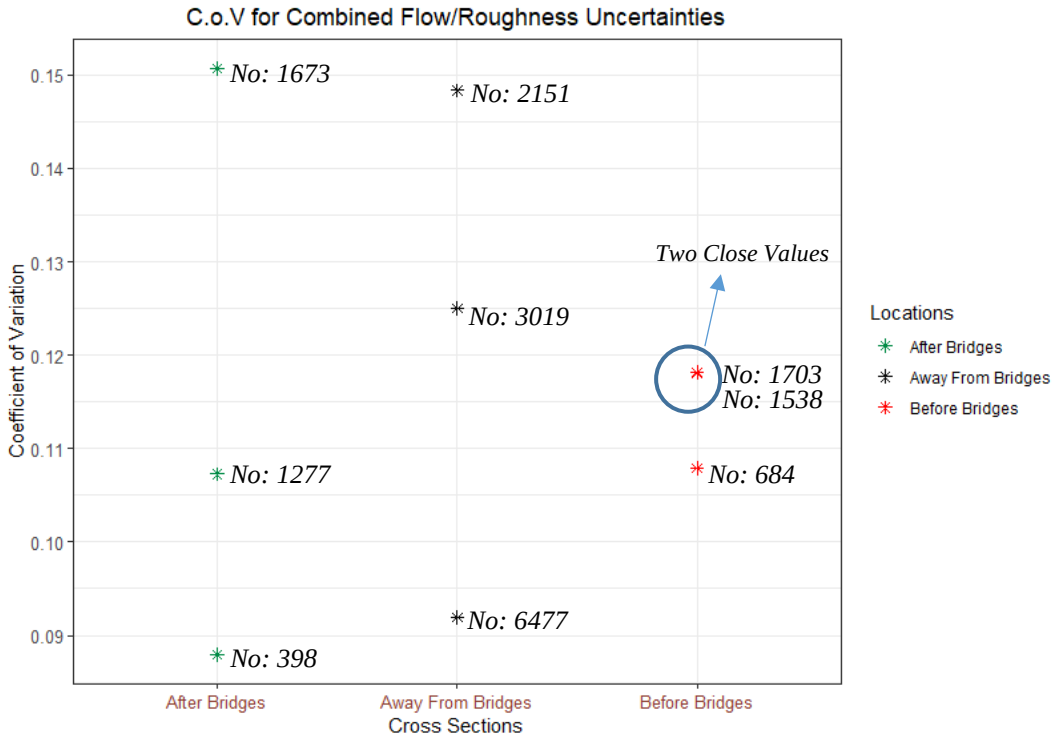

Figure 5.17. Coefficient of variation for combined uncertainties at different cross-sections.

Table 5.3. Average differences (m) between mean flow depths and quantiles (75% and 95%) for combined uncertainties.

Uncertainty	***Location***	***Differences(m) (75% -95%)***
Combined Flow and N	Before Bridges	0.19 – 0.45
Combined Flow and N	After Bridges	0.15 – 0.36
Combined Flow and N	Away From Bridges	0.13 – 0.33

CHAPTER 6

DISCUSSIONS AND CONCLUSIONS

6.1 Discussion of the results

Briefly, it is inevitable not to have uncertainties for the simulated hydraulic models with convenient inputs especially in the regions where calibration is not possible due to the lack of historical data. Different sources of uncertainties and different types of inputs have their own statistical distribution to present their natural behaviors. Peak flow uncertainties come from empirical reasons which mean normal distribution is quite successful to represent their variations. Vice versa, Manning's roughness coefficients' uncertainties arise from very complex behavior of this parameter in both main channel and flood areas. It is so dynamic and depends on so many complex parameters including flow depth, flood extent, type of flow, land cover, and moisture content of soil.

Results have shown that uncertainties and differences in flow depths due to these uncertainties are quite important and cannot be underestimated in hydraulic models. The capacity of main channels may not be sufficient if these uncertainties are not considered carefully. Especially in the contraction regions due to bridges, flow depths can change up to 10% in the extreme scenarios of the inputs. For flow uncertainties with constant Manning's roughness coefficient, normally distributed 5000 peak flows with 16.6% coefficient of variation caused standard deviations up to 0.28 meters. The output flow depths of cross-sections around bridges show the higher standard deviations especially before the bridges. Skewness values are slightly negative for the output flow depth distributions. Their distributions are quite convenient with normal distributions as well. Maximum of 0.43 meter of flow depth difference is observed with simulated mean (deterministic) input and extreme quantile (95%) of peak flows. Coefficient of variations reach up to 0.14 meters.

Although it is expected to have greater coefficient of variations around bridges, the regular cross-sections away from the structures have also important values of variations for flow uncertainties.

In the second scenario, Manning's roughness coefficients are simulated with constant peak flow. Since the main uncertainty source of Manning's roughness coefficients are randomness and complexity, triangular distribution is accepted as appropriate distribution. Triangularly distributed 5000 Manning's roughness coefficient is distributed with lower limit of 0.0354 and upper limit of 0.0646. Mean (and median in this case also) of the roughness coefficient becomes 0.05. These inputs resulted to obtain standard deviations up to 0.13 meters. Unexpectedly, cross-sections away from the bridges tend to have more sensitive behavior for Manning's uncertainties. Same as standard deviations, coefficient of variations for the sections away from the bridges have the highest values. The variations reach up to 0.09 meters due to roughness uncertainties. The skewness values are heavily positive. Output flow depths caused by roughness uncertainties tend to accumulate in a closer region.

In the last scenario, all possible peak flow and Manning's roughness coefficient values are simulated simultaneously, and it has been ensured that all extremities (i.e, coinciding the maximums and minimums of both uncertainties) are simulated. Flow depth differences reach up to 0.45 meters (which is 10% percent of maximum capacity of critical bridge section) due to mean (deterministic) input and extreme coincides (95% quantiles) of both uncertainties. Output flow depth distributions tend to behave as normally distributed. Skewness values are around or close to the zero for most of the cross-sections. Coefficient of variations reach up to 0.15 meters including the cross-sections away from the bridges. For the probabilistic mapping, mean peak flow is increased (Q_p = 90 m^3/s) so that extreme scenarios can initiate overflow. This is a quite important reminder to consider the uncertainties for flood risk maps.

Additionally, the characteristics of the cross-sections and relevant flow characteristics (i.e., velocities) affect the flow depth distributions. It is observed that

cross-sectional capacities are one of the most fundamental differences affecting flow depth differences. Although they take place both just before or just after any bridges (i.e, sections 684 and 1538), they may have quite different skewness intervals and standard deviations.

These flow depth differences, standard deviations and variations are crucially hazardous for the design purposes and long-term residential plannings. Additionally, design parameters of early warning systems for floods may also be affected from these flow depth differences.

Lastly, it is seen that after setting the 1D hydraulic model, this methodology quite easy to be implemented for various study area. After compiling the codes once, user requires to change some small variables in the scripts such as project name, total number of simulations, river/reach names and total number of cross-sections from the HECRAS software. All the procedure can be repeated automatically using the codes.

6.2 Conclusions

This study assesses the uncertainties in 1-D hydraulic modelling for peak flow estimations and Manning's roughness coefficients. Distributions of convenient inputs and relevant uncertainties for peak flows and Manning roughness coefficients are observed with respect to inherent sources of uncertainties. The required number of simulations to represent natural behavior of these inputs are determined. Relevant softwares are integrated and codes are compiled to obtain a fully automated probabilistic 1-D hydraulic model. All combinations of uncertainties are modelled separately and at a time properly. Hydraulic model is set up in Yılanlıdere River in Samsun Province. Model includes high resolution digital elevation model with bathymetric information of main channel. HEC-RAS software is utilized for the hydraulic model. Study area has been facing with flood events for a long time. There are bridges for different purposes along the main channel, which are integrated to the

model. The bridges cause some flood problems in the downstream part of the river due to their contraction parts. A fully probabilistic model that can simulate and manipulate hydraulic model automatically with Visual Basic Application and Python codes is created so that the effects of all ranges of inputs due to uncertainties in peak discharge and roughness value can be represented in separate and combined way.

Normal distribution is used for peak discharge and triangular distribution is used for roughness value. The maximum number of simulations in Monte Carlo runs is determined by considering the significant decrease in coefficient of variation coming from the statistical errors of distributions in different cross-sections. 5000 number of simulations are accepted to be used in all scenarios for the probabilistic flood modelling scenarios of the study including all types of uncertainties with separate observations and combined ones. The results show that the maximum flows and roughness values may cause uncertainties in flow depths up to 50 cm at the cross-sections close to the bridges. In addition to the conveyance property of the cross-sections' the contraction at the cross-sections due to the bridges increases the uncertainty in the flow depth. The steady state results suggest that the probability of underestimating flow depths (up to 50 cm) is far from being negligible, especially when both discharge and roughness are subject to uncertainty. These results are undoubtedly associated with the study site.

It should be mentioned that due to the natural concept of HEC-RAS and the relevant library in the Visual Basic Applications, it is not possible to manipulate a 2-D hydraulic model for Monte Carlo approaches with existing functions which is one of the main limitations. Since HEC-RAS stores the 2-D model data as '.hdf5' format, another library or functions must be compiled to propagate Monte Carlo simulations.

Lastly, Uncertainties are integral parts of hydraulic models. Although their degrees of effects are different, their sources and types are numerous. Therefore, recommended future studies may include:

- Effects of other uncertainties like digital elevation models, boundary conditions, rating curves etc. can be considered.
- Trying different uncertainties in 2-D hydraulic models including different mesh sizes and mesh types can be used.
- Merging mentioned other uncertainties attentively so that all possible flow depth extents can be seen.
- Unsteady flow uncertainties with different durations, i.e., time to peaks and base time probabilistically can be utilized.
- Effect of uncertainties on damage to bridges, such as bridge scouring must be studied.

REFERENCES

Abood, M. M., Yusuf, B., Mohammed, T. A., & Ghazali, A. H. (2006). Manning Roughness Coefficient for Grass-Lined Channel. *Suranaree J. Sci. Technol.*, *13*(4), 317–330.

Akyürek, Z., & Karaman, Ç. (2021). *Samsun Merkez Yılanlıdere Sel Kapanı Yıkılma Analizi ve Taşkın Tehlike Alanlarının Belirlenmesi*.

Apel, H., Thieken, A. H., Merz, B., & Blöschl, G. (2004). Natural Hazards and Earth System Sciences Flood risk assessment and associated uncertainty. *Natural Hazards and Earth System Sciences*, *4*, 295–308. https://www.nat-hazards-earth-syst-sci.net/4/295/2004/nhess-4-295-2004.pdf

Arcement, G., & Schneider, V. (1989). Guide for Selecting Manning ' s Roughness Coefficients for Natural Channels and Flood Plains United States Geological Survey Water. In *Area*. http://www.fhwa.dot.gov/BRIDGE/wsp2339.pdf

Arnell, N. W., & Gosling, S. N. (2016). The impacts of climate change on river flood risk at the global scale. *Climatic Change*, *134*(3), 387–401. https://doi.org/10.1007/s10584-014-1084-5

Aron, G., & White, E. L. (1982). Fitting a Gamma Distribution Over a Synthetic Unit Hydrograph. *JAWRA Journal of the American Water Resources Association*, *18*(1), 95–98. https://doi.org/10.1111/j.1752-1688.1982.tb04533.x

Aronica, G., Bates, P. D., & Horritt, M. S. (2002). Assessing the uncertainty in distributed model predictions using observed binary pattern information within GLUE. *Hydrological Processes*, *16*(10), 2001–2016. https://doi.org/10.1002/hyp.398

Azamathulla, H. M., & Jarrett, R. D. (2013). Use of Gene-Expression Programming to Estimate Manning's Roughness Coefficient for High Gradient Streams. *Water Resources Management*, *27*(3), 715–729. https://doi.org/10.1007/s11269-012-0211-1

Bahadır, M. (2014). A climatic Analysis Of The Floods Of 4th July And 6th August 2012 In Samsun. *Coğrafya Dergisi - Journal of Geography*, 28–50.

Bales, J. D., & Wagner, C. R. (2009). Sources of uncertainty in flood inundation maps. *Journal of Flood Risk Management*, *2*(2), 139–147. https://doi.org/10.1111/j.1753-318X.2009.01029.x

Bates, P. D., & De Roo, A. P. J. (2000). A simple raster-based model for flood inundation simulation. *Journal of Hydrology*, *236*(1–2), 54–77. https://doi.org/10.1016/S0022-1694(00)00278-X

Bates, P.D., Pappenberger, F., & Romanowicz, R. J. (2014). Uncertainty in flood inundation modelling. In *Applied Uncertainty Analysis for Flood Risk Management* (Issue March). https://doi.org/10.1142/9781848162716_0010

Bates, Paul D., Horritt, M. S., Aronica, G., & Beven, K. (2004). Bayesian updating of flood inundation likelihoods conditioned on flood extent data. *Hydrological Processes*, *18*(17), 3347–3370. https://doi.org/10.1002/hyp.1499

Beard, R. ., Pentikainen, T., & Pesonen, E. (1984). *Risk Theory: Stochastic Basis of Insurance (Monographs on Applied Probability & Statistics)*.

Bessar, M. A., Matte, P., & Anctil, F. (2020). Uncertainty analysis of a 1D river hydraulic model with adaptive calibration. *Water (Switzerland)*, *12*(2). https://doi.org/10.3390/w12020561

Beven, K. J., Almeida, S., Aspinall, W. P., Bates, P. D., Blazkova, S., Borgomeo, E., Freer, J., Goda, K., Hall, J. W., Phillips, J. C., Simpson, M., Smith, P. J., Stephenson, D. B., Wagener, T., Watson, M., & Wilkins, K. L. (2018). Epistemic uncertainties and natural hazard risk assessment - Part 1: A review of different natural hazard areas. *Natural Hazards and Earth System Sciences*, *18*(10), 2741–2768. https://doi.org/10.5194/nhess-18-2741-2018

Bozzi, S., Passoni, G., Bernardara, P., Goutal, N., & Arnaud, A. (2015). Roughness and Discharge Uncertainty in 1D Water Level Calculations. *Environmental Modeling and Assessment*, *20*(4), 343–353. https://doi.org/10.1007/s10666-014-9430-6

Brunner, G. W. (2021). *HEC-RAS, River Analysis System User's Manual, Version 6.0*. US Army Corps of Engineers, Institute for Water Resources, Hydrologic Engineering Center (HEC).

Brunner, G. W., & CEIWR-HEC. (2016). HEC-RAS River Analysis System: User Manual 1D and 2D Version 5.0. *US Army Corps of Engineers*, *February*, 1–790. www.hec.usace.army.mil

Casas, A., Benito, G., Thorndycraft, V. R., & Rico, M. (2006). The topographic data source of digital terrain models as a key element in the accuracy of hydraulic flood modelling. *Earth Surface Processes and Landforms*, *31*(4), 444–456. https://doi.org/10.1002/esp.1278

Chen, C. S., Jhong, Y. Da, Wu, T. Y., & Chen, S. T. (2013). Typhoon event-based evolutionary fuzzy inference model for flood stage forecasting. *Journal of Hydrology*, *490*, 134–143. https://doi.org/10.1016/j.jhydrol.2013.03.033

Coon, W. F. (1995). Estimates of Roughness Coefficients for Selected Natural Stream Channels with Vegetated Banks in New York. *Pubs.Usgs.Gov*, 93–161. https://pubs.usgs.gov/of/1993/0161/report.pdf

Cooper, M. (2010). Advanced Bash-Scripting Guide An in-depth exploration of the art of shell scripting Table of Contents. *Okt 2005 Abrufbar Uber Httpwww Tldp OrgLDPabsabsguide Pdf Zugriff 1112 2005*, *2274*(November 2008), 2267–2274. https://doi.org/10.1002/hyp

Di Baldassarre, G., Schumann, G., Bates, P. D., Freer, J. E., & Beven, K. J. (2010). Cartographie de zone inondable: Un examen critique d'approches déterministe et probabiliste. *Hydrological Sciences Journal*, *55*(3), 364–376. https://doi.org/10.1080/02626661003683389

Domeneghetti, A., Vorogushyn, S., Castellarin, A., Merz, B., & Brath, A. (2013). Probabilistic flood hazard mapping: Effects of uncertain boundary conditions. *Hydrology and Earth System Sciences*, *17*(8), 3127–3140. https://doi.org/10.5194/hess-17-3127-2013

Douben, K. J. (2006). Characteristics of river floods and flooding: A global overview, 1985-2003. *Irrigation and Drainage*, *55*(SUPPL. 1). https://doi.org/10.1002/ird.239

Dysarz, T. (2018). Application of python scripting techniques for control and automation of HEC-RAS simulations. *Water (Switzerland)*, *10*(10). https://doi.org/10.3390/w10101382

Engman, E. T. (1986). Roughness coefficients for routing surface runoff. *Journal of Irrigation and Drainage Engineering*, *112*(1), 39–53.

Fleischmann, A., Paiva, R. C. ., Collischonn, W., Sorribas, M., & Pontes, P. R. (2016). On river-floodplain interaction and hydrograph skewness. *Journal of the American Water Resources Association*, *5*. https://doi.org/10.1111/j.1752-1688.1969.tb04897.x

Garrote, J., Peña, E., & Díez-herrero, A. (2021). Probabilistic flood hazard maps from monte carlo derived peak flow values—an application to flood risk management in zamora city (Spain). *Applied Sciences (Switzerland)*, *11*(14). https://doi.org/10.3390/app11146629

Goodell, C. (2014). *Breaking the HEC-RAS code : a user's guide to automating HEC-RAS*. 264.

Güçlü, Y. S., & Şen, Z. (2016). Hydrograph estimation with fuzzy chain model. *Journal of Hydrology*, *538*, 587–597. https://doi.org/10.1016/j.jhydrol.2016.04.057

Gumble, E. J. (1941). The Return Period of Flood Flows. *The Annals of Mathematical Statistics*, *12*(2), 163–190.

Hall, J., & Solomatine, D. (2008). A framework for uncertainty analysis in flood risk management decisions. *International Journal of River Basin Management*, *6*(2), 85–98. https://doi.org/10.1080/15715124.2008.9635339

Horritt, M. S., & Bates, P. D. (2001). Predicting floodplain inundation: Raster-based modelling versus the finite-element approach. *Hydrological Processes*, *15*(5), 825–842. https://doi.org/10.1002/hyp.188

Jaeckel, P. (2002). *Monte Carlo Methods in Finance*. Wiley.

Jonkman, S. N., Vrijling, J. K., & Vrouwenvelder, A. C. W. M. (2008). Methods for the estimation of loss of life due to floods: A literature review and a proposal for a new method. *Natural Hazards*, *46*(3), 353–389. https://doi.org/10.1007/s11069-008-9227-5

Joo, Y., & Casella, G. (2001). Predictive distributions in risk analysis and estimation for the triangular distribution. *Environmetrics*, *12*(7), 647–658. https://doi.org/10.1002/env.489

Kamali, P., Ebrahimian, H., & Parsinejad, M. (2018). Estimation of Manning roughness coefficient for vegetated furrows. *Irrigation Science, 36*(6), 339–348. https://doi.org/10.1007/s00271-018-0593-9

Kim, J. S., Lee, C. J., Kim, W., & Kim, Y. J. (2010). Roughness coefficient and its uncertainty in gravel-bed river. *Water Science and Engineering*, *3*(2), 217–232. https://doi.org/10.3882/j.issn.1674-2370.2010.02.010

Kousky, C. (2014). Informing climate adaptation: A review of the economic costs of natural disasters. *Energy Economics*, *46*, 576–592. https://doi.org/10.1016/j.eneco.2013.09.029

Leon, A. S., & Goodell, C. (2016). Controlling HEC-RAS using MATLAB. *Environmental Modelling and Software*, *84*, 339–348. https://doi.org/10.1016/j.envsoft.2016.06.026

Li, H., & Sivapalan, M. (2011). Effect of spatial heterogeneity of runoff generation mechanisms on the scaling behavior of event runoff responses in a natural river basin. *Water Resources Research*, *47*(5), 1–20. https://doi.org/10.1029/2010WR009712

Loveridge, M., Rahman, A., & Babister, M. (2013). Probabilistic flood hydrographs using Monte Carlo simulation: Potential impact to flood inundation mapping. *Proceedings - 20th International Congress on Modelling and Simulation, MODSIM 2013*, *December*, 2660–2666. https://doi.org/10.36334/modsim.2013.l8.loveridge

Merwade, V., Olivera, F., Arabi, M., & Edleman, S. (2008). Uncertainty in Flood Inundation Mapping: Current Issues and Future Directions. *Journal of Hydrologic Engineering*, *13*(7), 608–620. https://doi.org/10.1061/(asce)1084-0699(2008)13:7(608)

Merz, B., Blöschl, G., Vorogushyn, S., Dottori, F., Aerts, J. C. J. H., Bates, P., Bertola, M., Kemter, M., Kreibich, H., Lall, U., & Macdonald, E. (2021). Causes, impacts and patterns of disastrous river floods. *Nature Reviews Earth and Environment*, *2*(9), 592–609. https://doi.org/10.1038/s43017-021-00195-3

Mino, T., Tanaka, Y., Sakamoto, M., & Fujita, T. (2006). Development of praline derived chiral aminophosphine ligands for palladium -catalyzed asymmetric allylic alkylation. *Yuki Gosei Kagaku Kyokaishi/Journal of Synthetic Organic Chemistry*, *64*(6), 628–638. https://doi.org/10.5059/yukigoseikyokaishi.64.628

Moges, E., Demissie, Y., Larsen, L., & Yassin, F. (2021). Review: Sources of hydrological model uncertainties and advances in their analysis. *Water (Switzerland)*, *13*(1), 1–23. https://doi.org/10.3390/w13010028

Oberndorfer, S., Sander, P., & Fuchs, S. (2020). Multi-hazard risk assessment for roads: Probabilistic versus deterministic approaches. *Natural Hazards and Earth System Sciences*, *20*(11), 3135–3160. https://doi.org/10.5194/nhess-20-3135-2020

Papaioannou, G., Vasiliades, L., Loukas, A., & Aronica, G. T. (2017). Probabilistic flood inundation mapping at ungauged streams due to roughness coefficient uncertainty in hydraulic modelling. *Advances in Geosciences*, *44*, 23–34. https://doi.org/10.5194/adgeo-44-23-2017

Pappenberger, F., Beven, K., Horritt, M., & Blazkova, S. (2005). Uncertainty in the calibration of effective roughness parameters in HEC-RAS using inundation and downstream level observations. *Journal of Hydrology*, *302*(1–4), 46–69. https://doi.org/10.1016/j.jhydrol.2004.06.036

Rosso, R. (1984). Nash Model Relation to Horton Order Ratios. *Water Resources Research*, *20*(7), 914–920.

Scawthorn, C., Blais, N., Seligson, H., Tate, E., Mifflin, E., Thomas, W., Murphy, J., & Jones, C. (2006). HAZUS-MH Flood Loss Estimation Methodology. I: Overview and Flood Hazard Characterization. *Natural Hazards Review*, *7*(2), 60–71. https://doi.org/10.1061/(asce)1527-6988(2006)7:2(60)

Sharafati, A., Khazaei, M. R., Nashwan, M. S., Al-Ansari, N., Yaseen, Z. M., & Shahid, S. (2020). Assessing the uncertainty associated with flood features due to variability of rainfall and hydrological parameters. *Advances in Civil Engineering*, *2020*. https://doi.org/10.1155/2020/7948902

Singh, V. P., Corradini, C., & Melone, F. (1985). A comparison of some methods of deriving the instantaneous unit hydrograph. *Nordic Hydrology*, *16*(1), 1–10. https://doi.org/10.2166/nh.1985.0001

Singh, Vijay P. (1987). On application of the Weibull distribution in hydrology. *Water Resources Management*, *1*(1), 33–43. https://doi.org/10.1007/BF00421796

Sobol, I. . (1975). *Monte Carlo Method (Popular Lectures in Mathematics)*. University of Chicago Press;

Subirana, B., Perez-Sanchis, M., & Sarma, S. (2017). Randomness in Transportation Utility Models. *2017 IEEE 20th International Conference on Intelligent Transportation Systems (ITSC)*, 1426–1431.

Tabari, H. (2020). Climate change impact on flood and extreme precipitation increases with water availability. *Scientific Reports*, *10*(1), 1–10. https://doi.org/10.1038/s41598-020-70816-2

Tayfur, G., Singh, V. P., Moramarco, T., & Barbetta, S. (2018). Flood hydrograph prediction using machine learning methods. *Water (Switzerland)*, *10*(8), 1–13. https://doi.org/10.3390/w10080968

Teng, J., Jakeman, A. J., Vaze, J., Croke, B. F. W., Dutta, D., & Kim, S. (2017). Flood inundation modelling: A review of methods, recent advances and uncertainty analysis. *Environmental Modelling and Software*, *90*, 201–216. https://doi.org/10.1016/j.envsoft.2017.01.006

Vatanchi, S. M., & Maghrebi, M. F. (2019). Uncertainty in Rating-Curves Due to Manning Roughness Coefficient. *Water Resources Management*, *33*(15), 5153–5167. https://doi.org/10.1007/s11269-019-02421-6

Vozinaki, A. E. K., Morianou, G. G., Alexakis, D. D., & Tsanis, I. K. (2017). Comparing 1D and combined 1D/2D hydraulic simulations using high-resolution topographic data: a case study of the Koiliaris basin, Greece. *Hydrological Sciences Journal*, *62*(4), 642–656. https://doi.org/10.1080/02626667.2016.1255746

Walega, A., & Ksiazek, L. (2016). Influence of rainfall data on the uncertainty of flood simulation. *Soil and Water Research*, *11*(4), 277–284. https://doi.org/10.17221/156/2015-SWR

Wang, J., Zhao, J., Zhao, T., & Wang, H. (2022). Partition of one-dimensional river flood routing uncertainty due to boundary conditions and riverbed roughness. *Journal of Hydrology*, *608*(February), 127660. https://doi.org/10.1016/j.jhydrol.2022.127660

Wohl, E. E. (1998). Uncertainty in Flood Estimates Associated with Roughness Coefficient. *Journal of Hydraulic Engineering*, *124*(2), 219–223. https://doi.org/10.1061/(asce)0733-9429(1998)124:2(219)

Xu, K., Fang, J., Fang, Y., Sun, Q., Wu, C., & Liu, M. (2021). The Importance of Digital Elevation Model Selection in Flood Simulation and a Proposed Method to Reduce DEM Errors: A Case Study in Shanghai. *International Journal of Disaster Risk Science*, *12*(6), 890–902. https://doi.org/10.1007/s13753-021-00377-z

Xu, X., Zhang, X., Fang, H., Lai, R., Zhang, Y., Huang, L., & Liu, X. (2017). A real-time probabilistic channel flood-forecasting model based on the Bayesian particle filter approach. *Environmental Modelling and Software*, *88*, 151–167. https://doi.org/10.1016/j.envsoft.2016.11.010

Yanmaz, A. M. (2000). Overtopping risk assessment in river diversion facility design. *Canadian Journal of Civil Engineering*, *27*(2), 319–326. https://doi.org/10.1139/L99-074

Ye, A., Zhou, Z., You, J., Ma, F., & Duan, Q. (2018). Dynamic Manning's roughness coefficients for hydrological modelling in basins. *Hydrology Research*, *49*(5), 1379–1395. https://doi.org/10.2166/nh.2018.175

Yoo, S. W. (2019). *Character Classification with Triangular Distribution*. *7*(2), 209–217. https://doi.org/10.17703/IJACT.2019.7.2.209

APPENDICES

A. CROSS-SECTIONS IN HYDRAULIC MODEL.

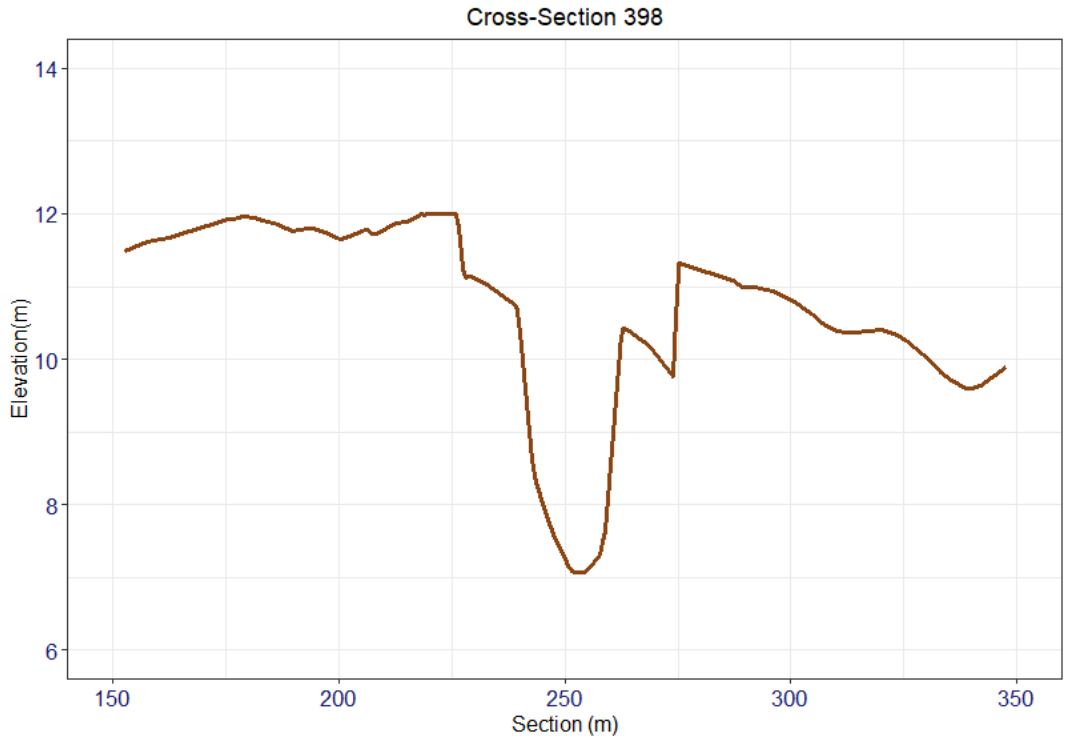

Figure A.1. Cross-Section 398.

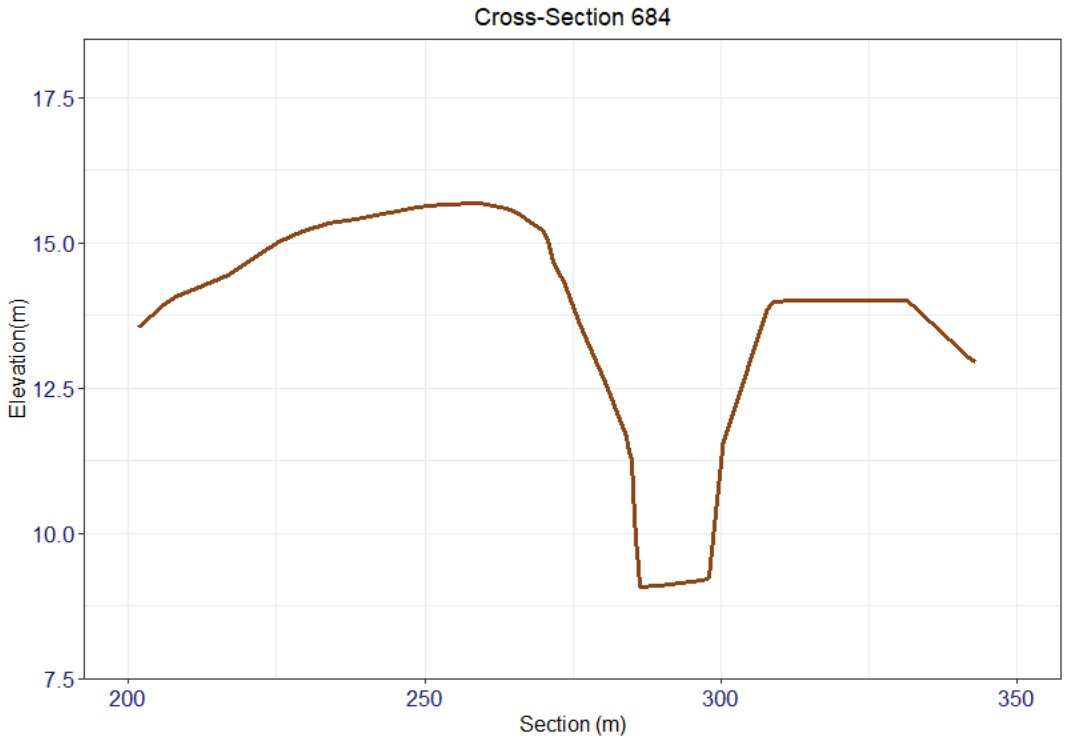

Figure A.2. Cross-Section 684.

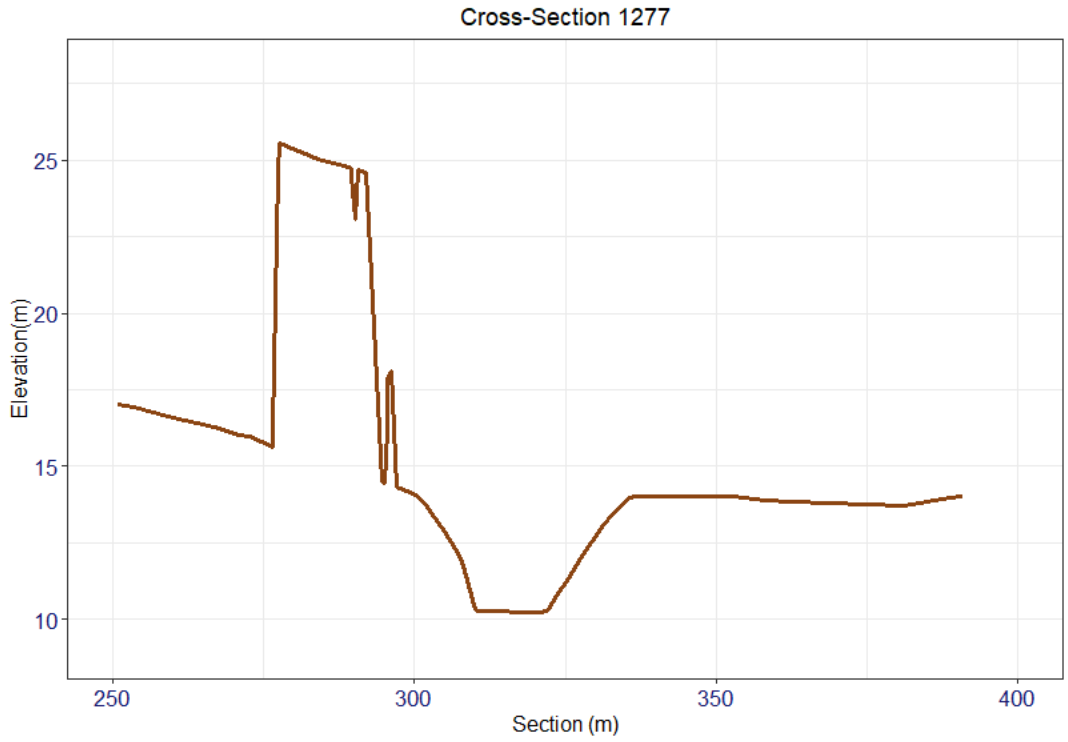

Figure A.3. Cross-Section 1277.

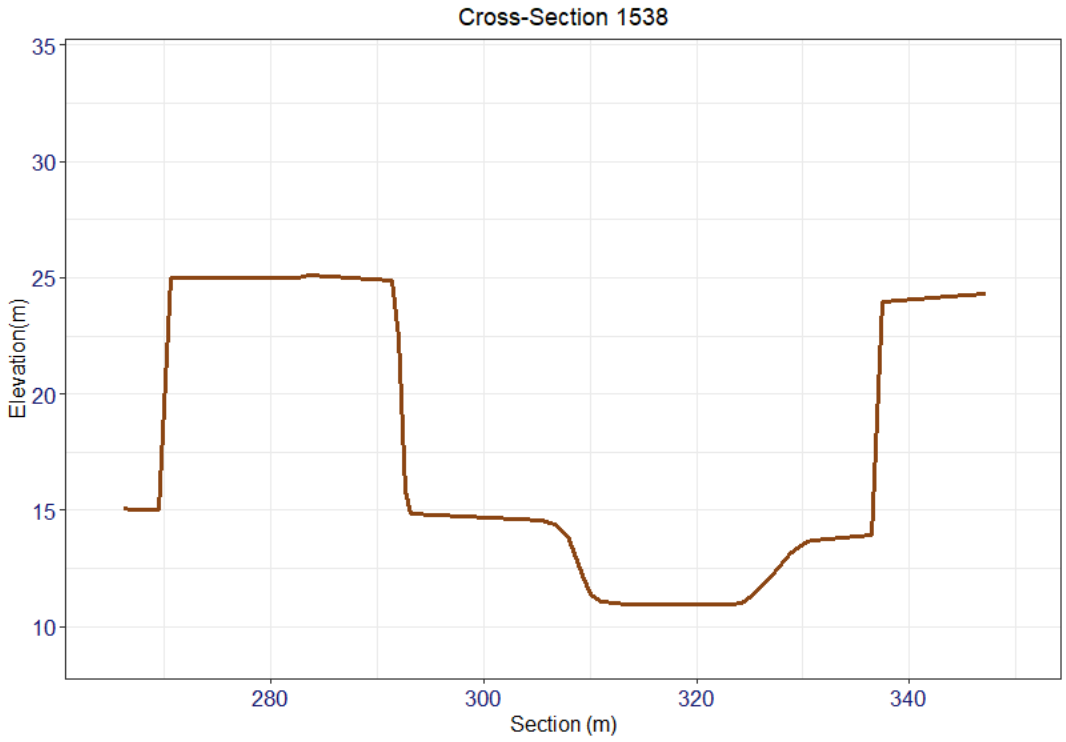

Figure A.4. Cross-Section 1538.

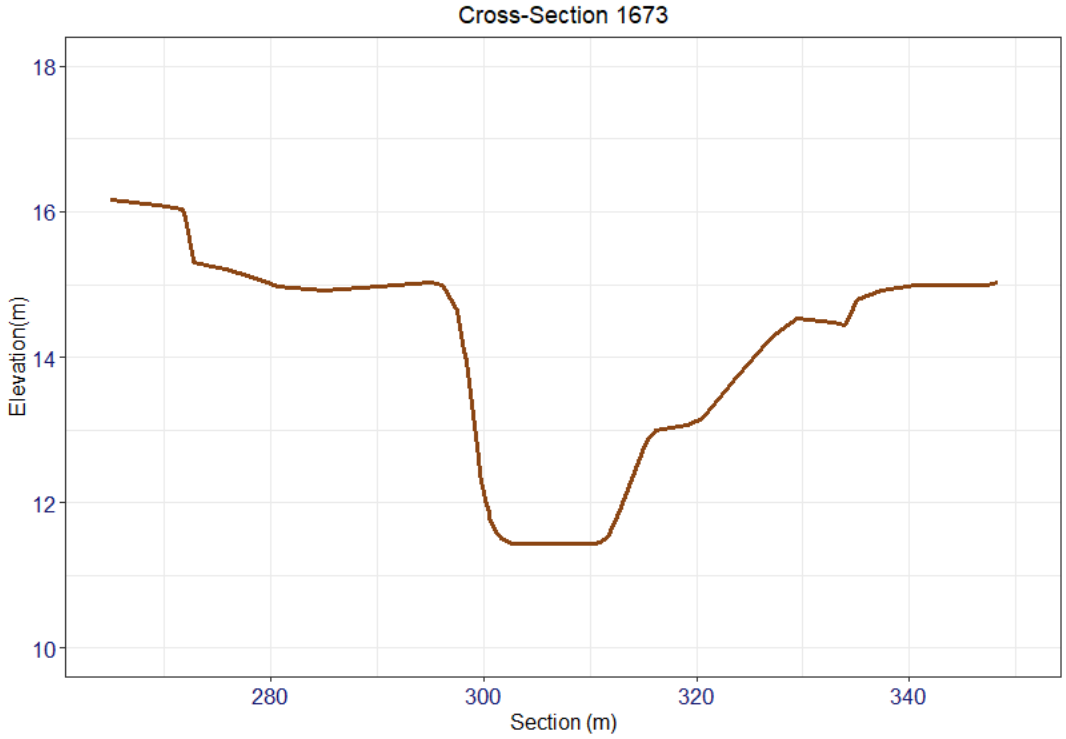

Figure A.5. Cross-Section 1673.

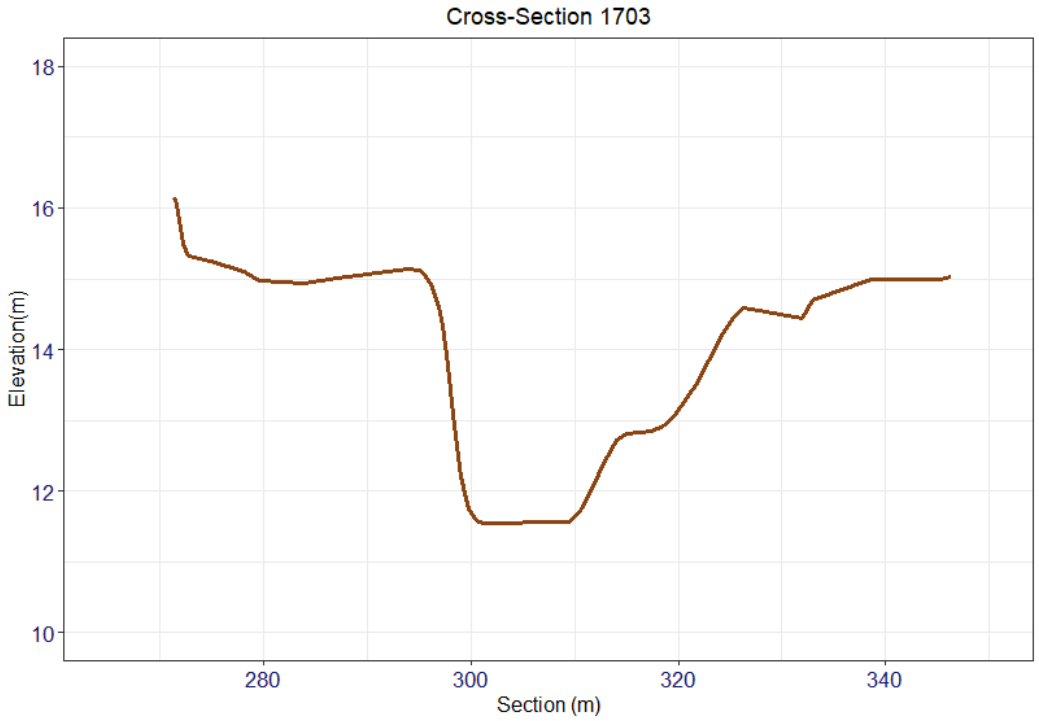

Figure A.6. Cross-Section 1703.

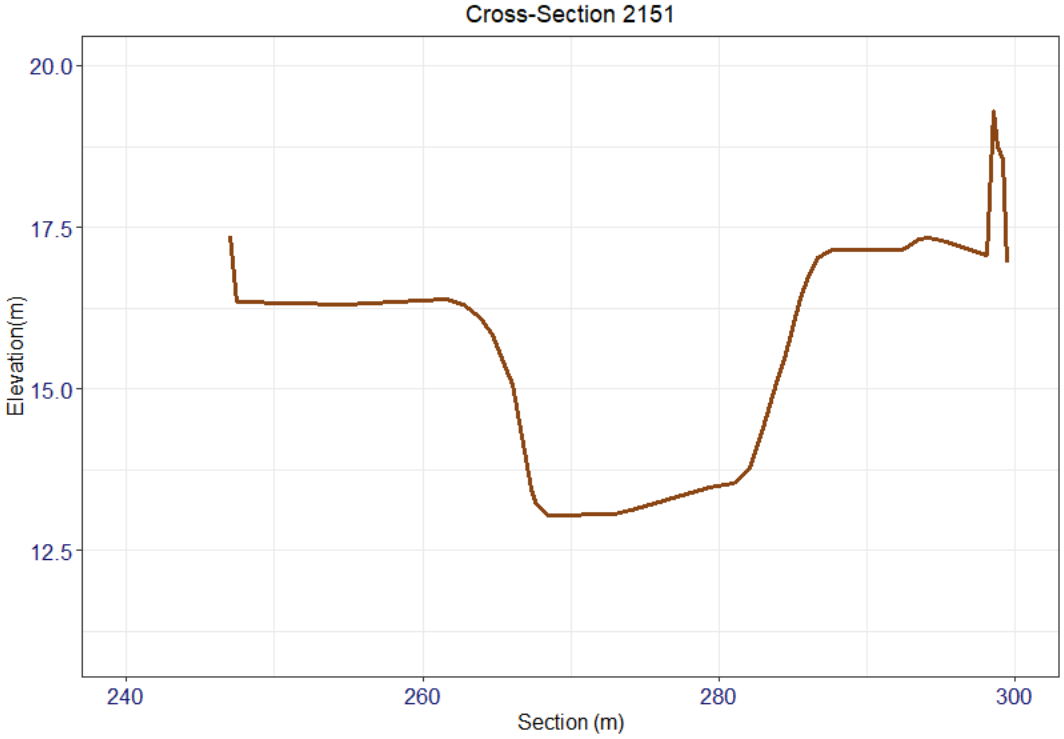

Figure A.7. Cross-Section 2151.

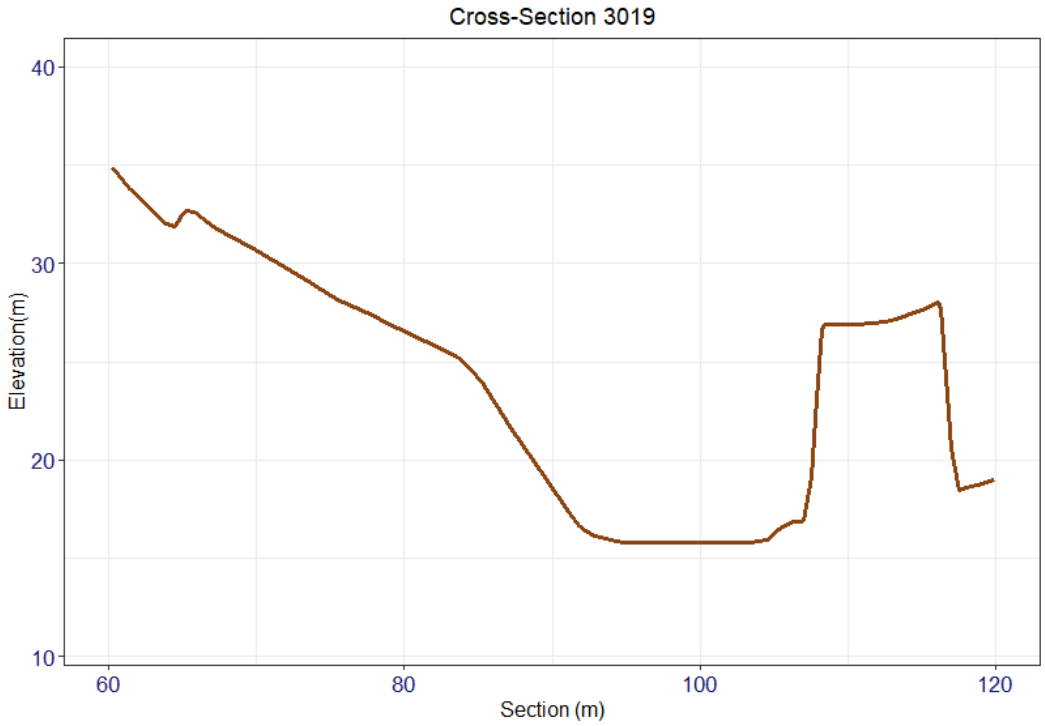

Figure A.8. Cross-Section 3019.

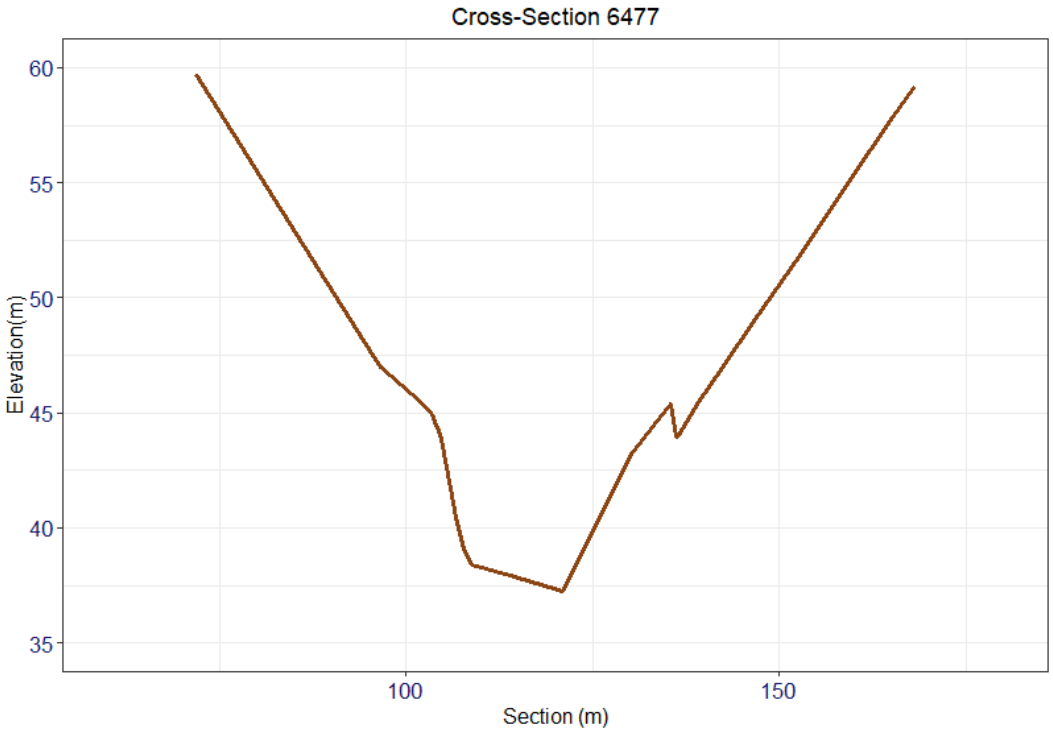

Figure A.9. Cross-Section 6477.

B. MARGINAL DISTRIBUTIONS OF OUTPUT FLOW DEPTHS FOR FLOW UNCERTAINTIES

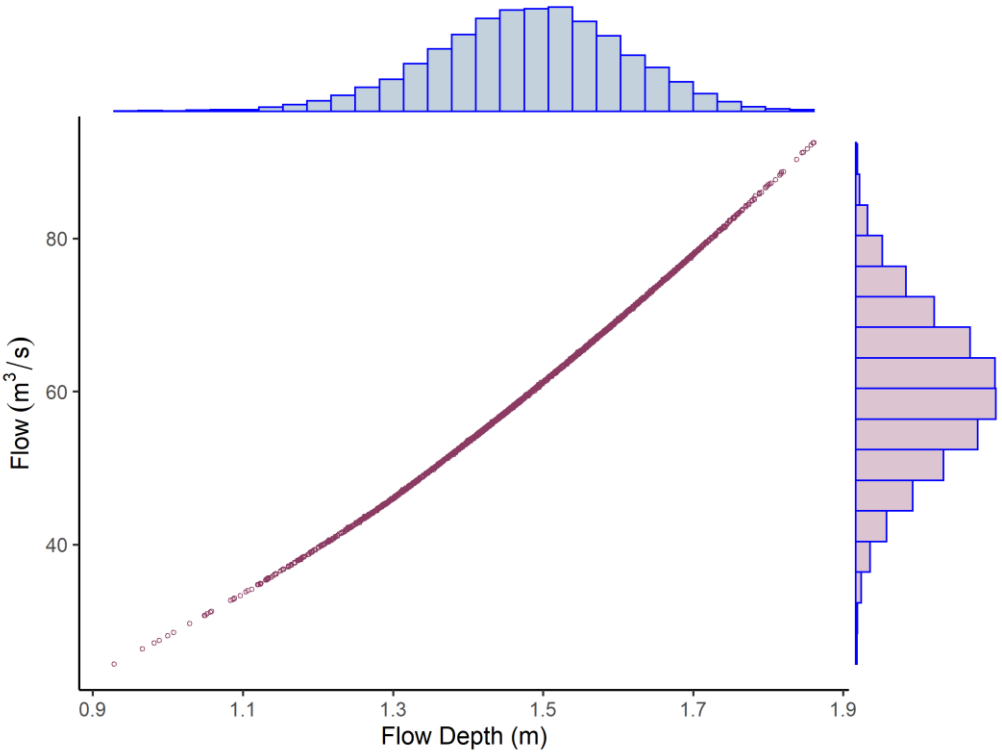

Figure B.1. Marginal Distribution of Output Flow Depth (m) vs Peak Flows (m^3/s) for Cross-Section 398.

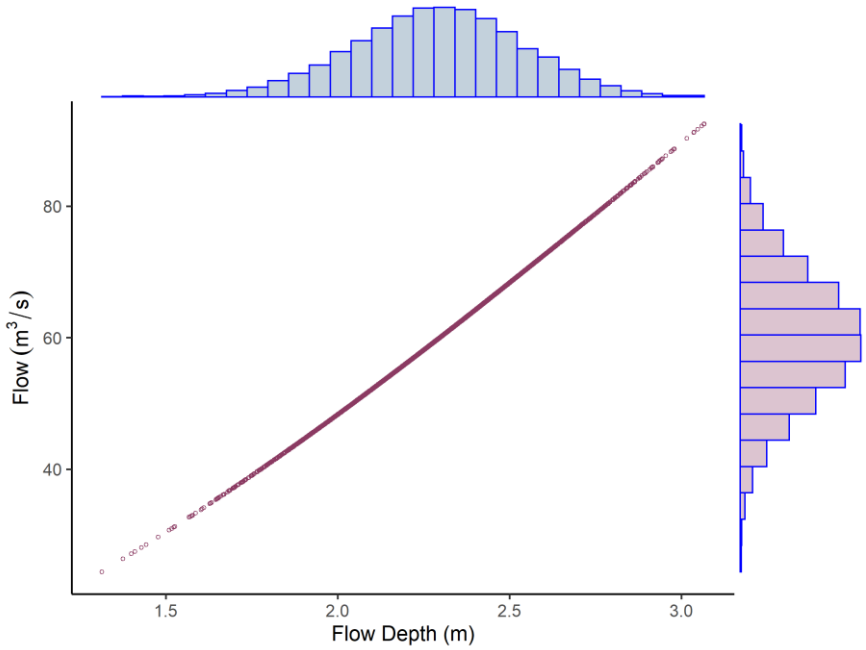

Figure B.2. Marginal Distribution of Output Flow Depth (m) vs Peak Flows (m^3/s) for Cross-Section 684.

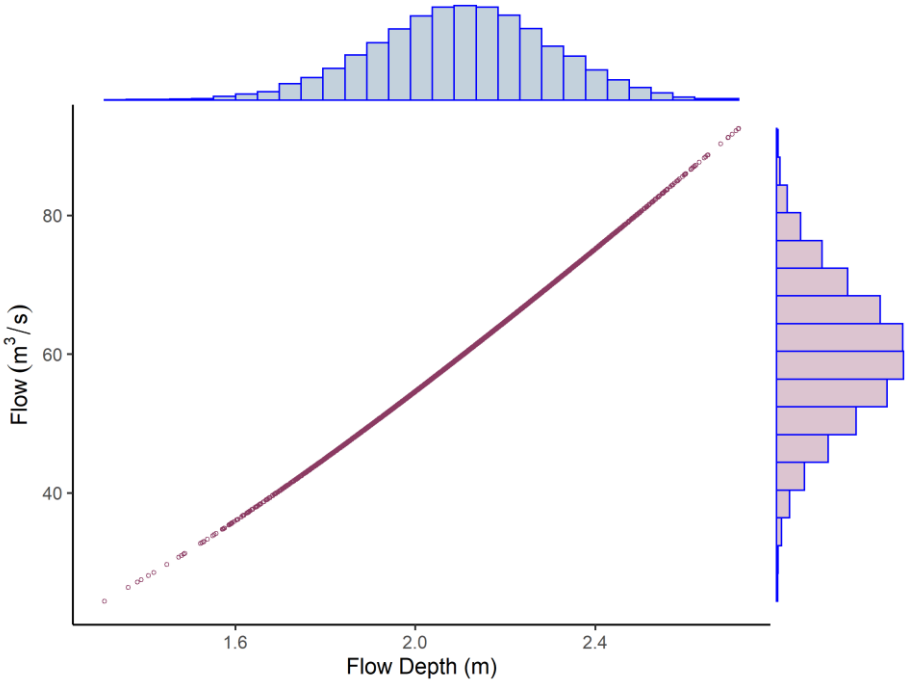

Figure B.3. Marginal Distribution of Output Flow Depth (m) vs Peak Flows (m^3/s) for Cross-Section 1277.

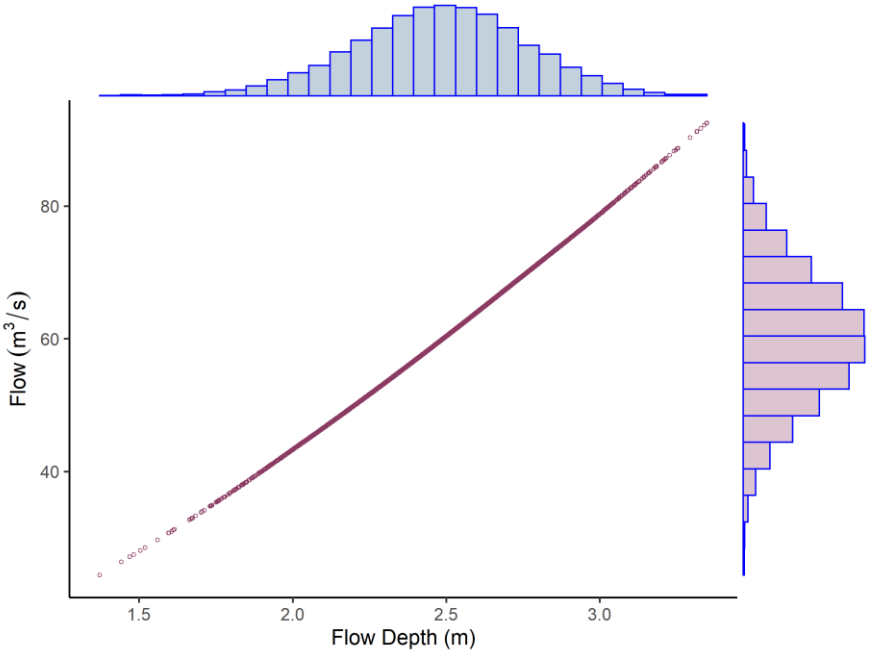

Figure B.4. Marginal Distribution of Output Flow Depth (m) vs Peak Flows (m^3/s) for Cross-Section 1538.

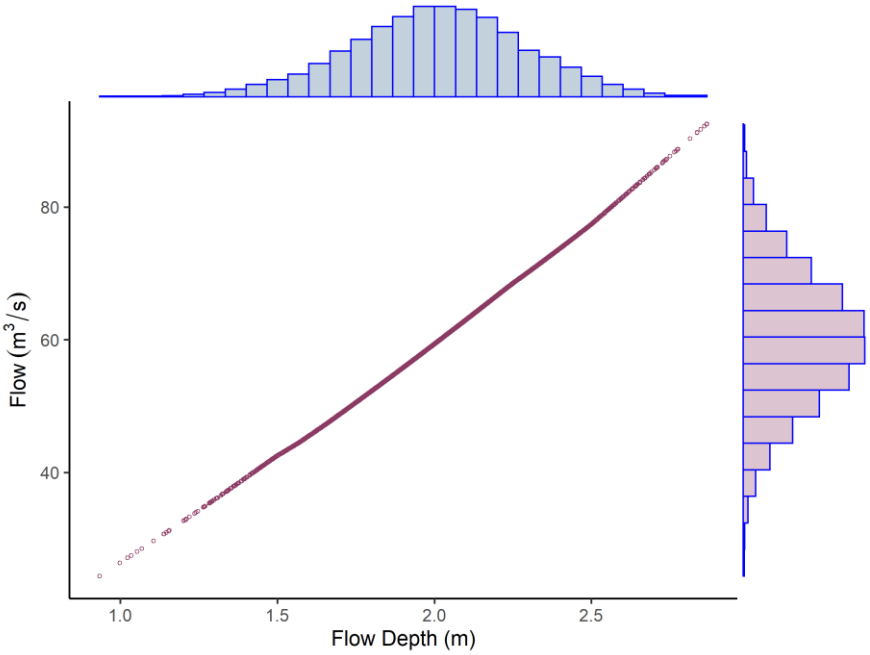

Figure B.5. Marginal Distribution of Output Flow Depth (m) vs Peak Flows (m^3/s) for Cross-Section 1673.

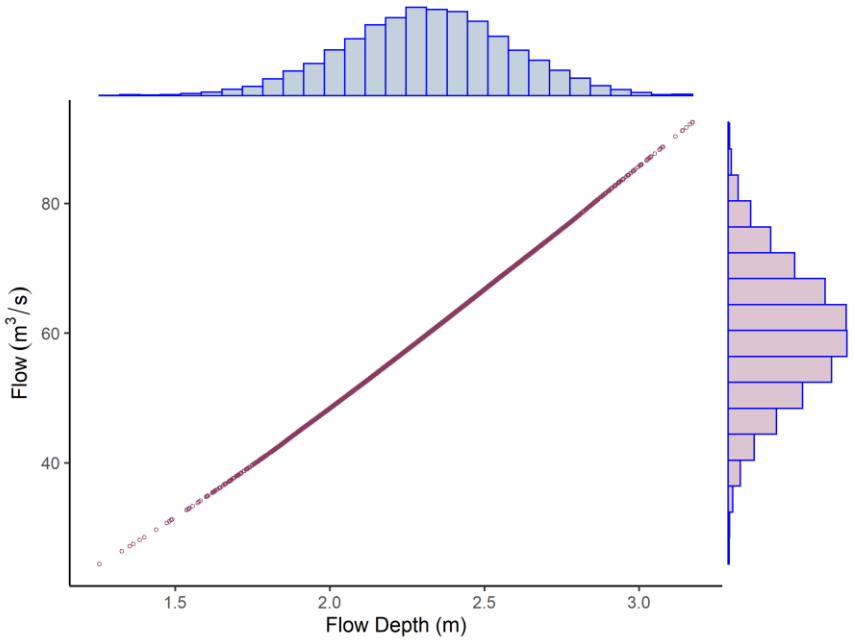

Figure B.6. Marginal Distribution of Output Flow Depth (m) vs Peak Flows (m^3/s) for Cross-Section 1703.

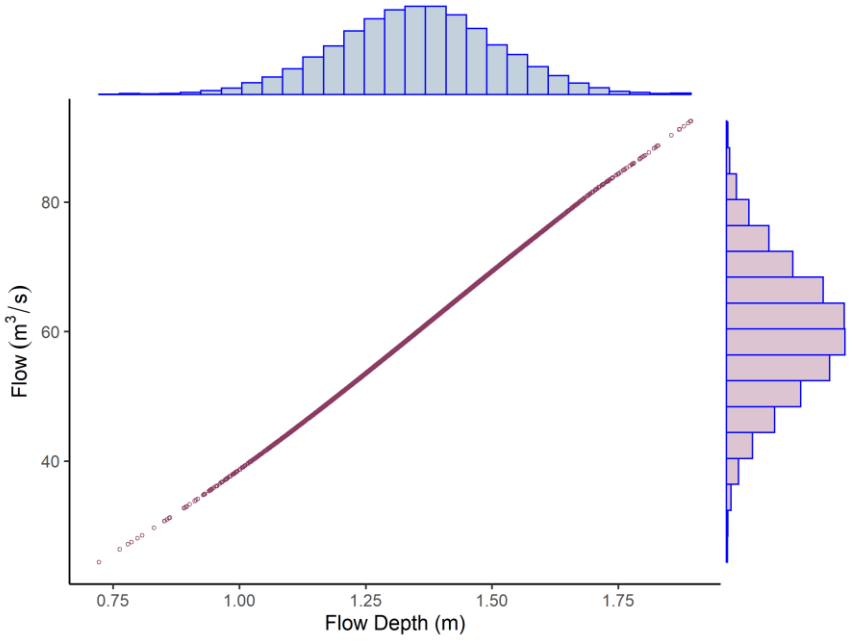

Figure B.7. Marginal Distribution of Output Flow Depth (m) vs Peak Flows (m^3/s) for Cross-Section 2151.

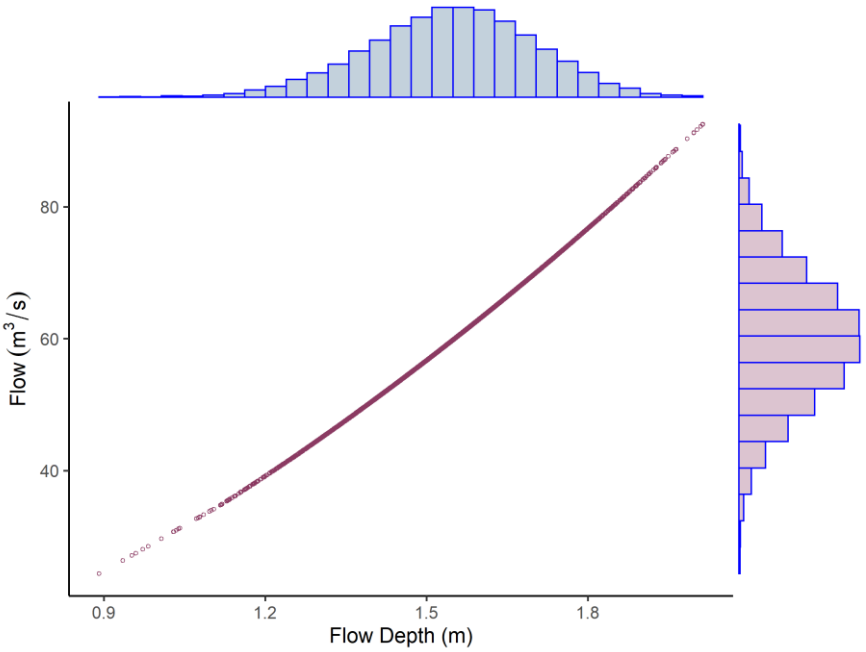

Figure B.8. Marginal Distribution of Output Flow Depth (m) vs Peak Flows (m^3/s) for Cross-Section 3019.

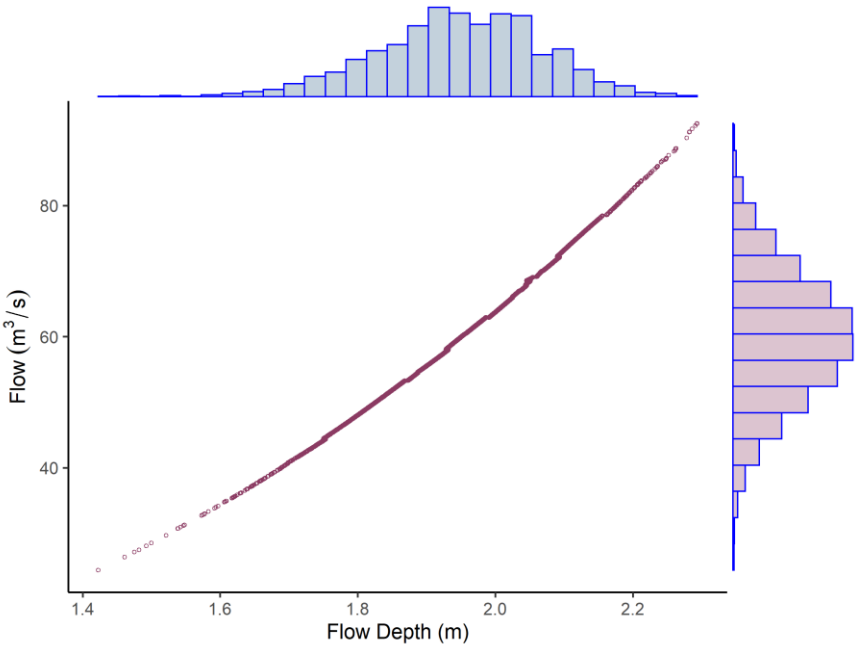

Figure B.9. Marginal Distribution of Output Flow Depth (m) vs Peak Flows (m^3/s) for Cross-Section 6477.

C. MARGINAL DISTRIBUTIONS OF OUTPUT FLOW DEPTHS FOR MANNING'S ROUGHNESS COEFFICIENT UNCERTAINTIES

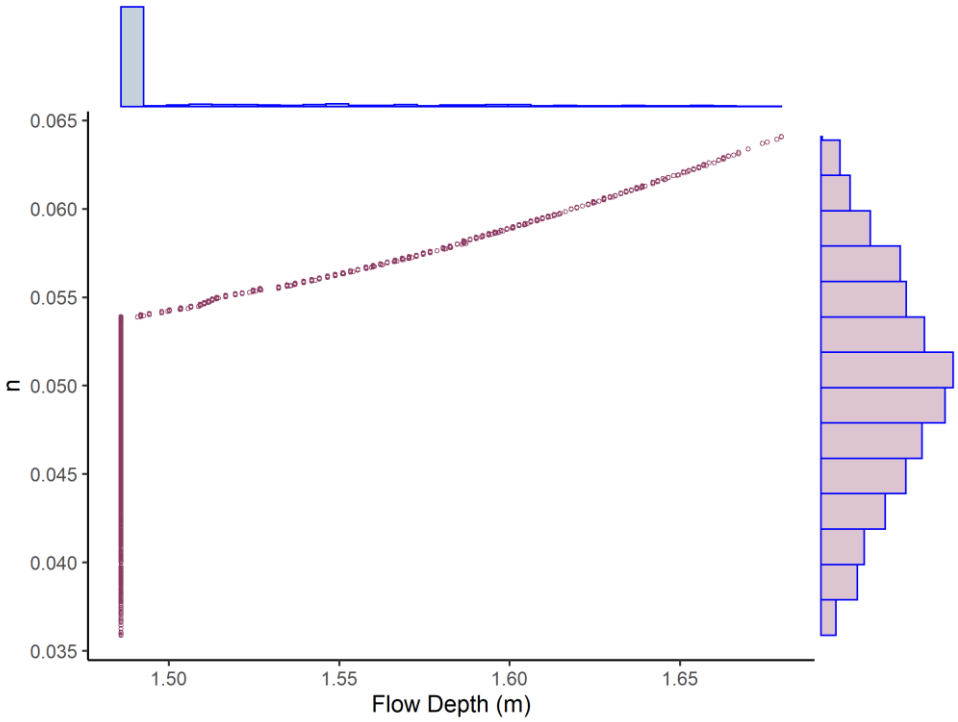

Figure C.1. Marginal Distribution of Output Flow Depth (m) vs Manning's Roughness Coefficient for Cross-Section 398.

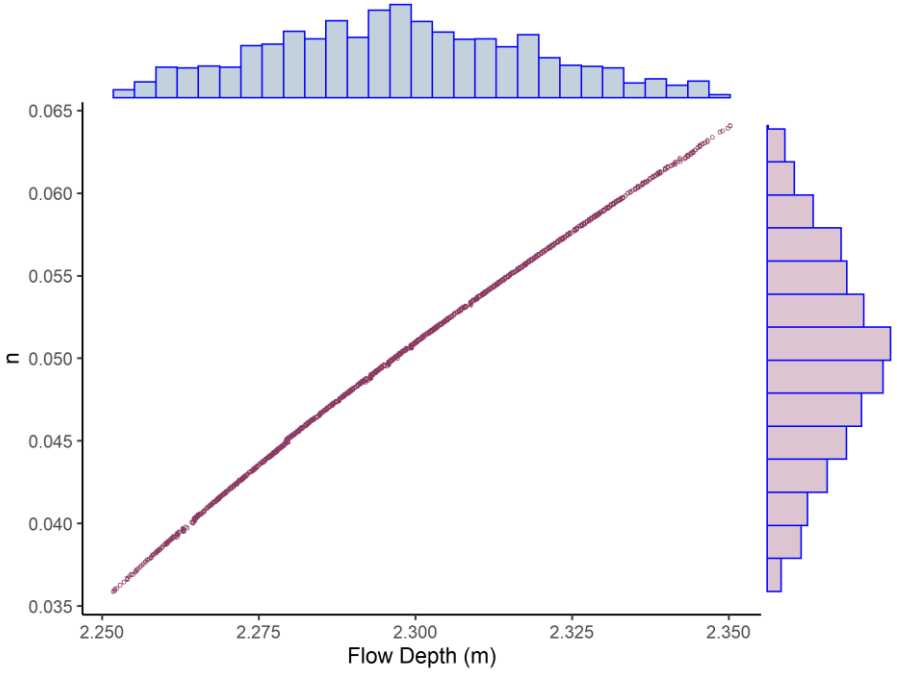

Figure C.2. Marginal Distribution of Output Flow Depth (m) vs Manning's Roughness Coefficient for Cross-Section 684.

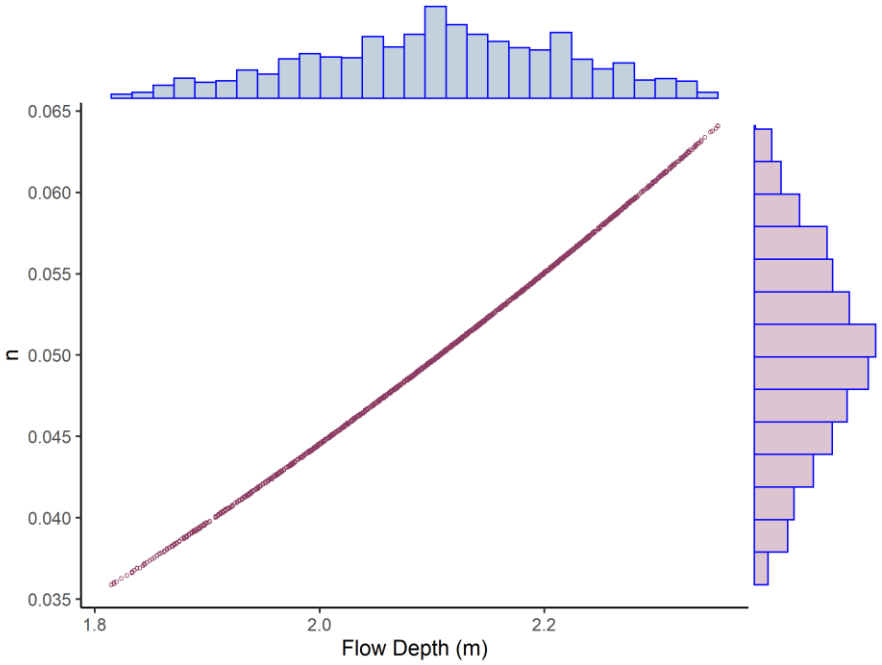

Figure C.3. Marginal Distribution of Output Flow Depth (m) vs Manning's Roughness Coefficient for Cross-Section 1277.

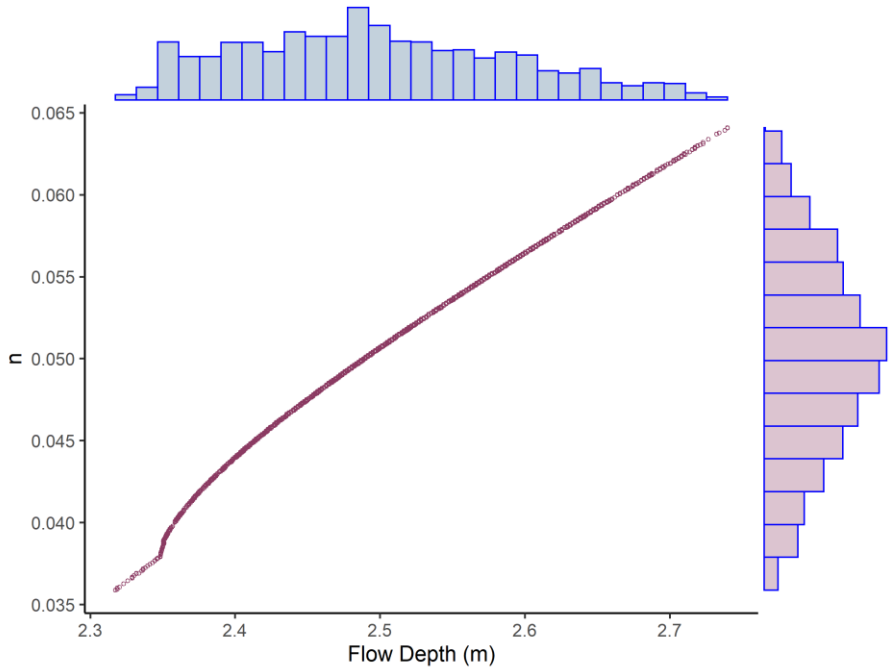

Figure C.4. Marginal Distribution of Output Flow Depth (m) vs Manning's Roughness Coefficient for Cross-Section 1538.

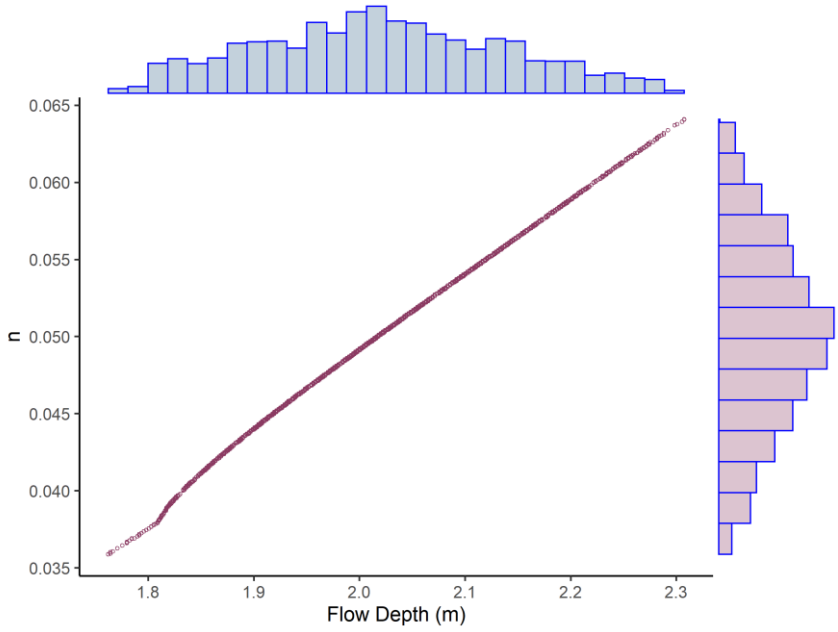

Figure C.5. Marginal Distribution of Output Flow Depth (m) vs Manning's Roughness Coefficient for Cross-Section 1673.

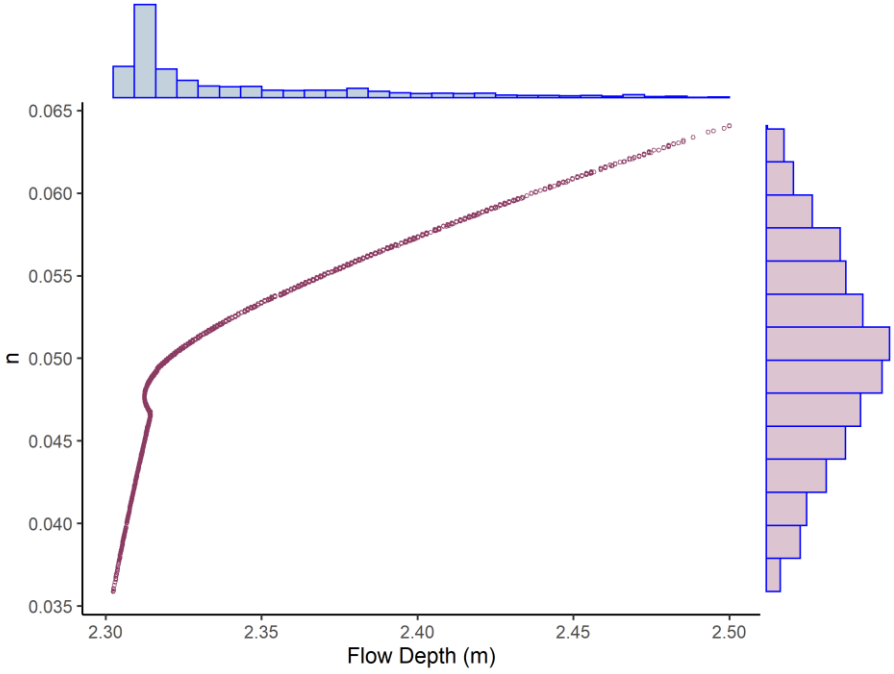

Figure C.6. Marginal Distribution of Output Flow Depth (m) vs Manning's Roughness Coefficient for Cross-Section 1703.

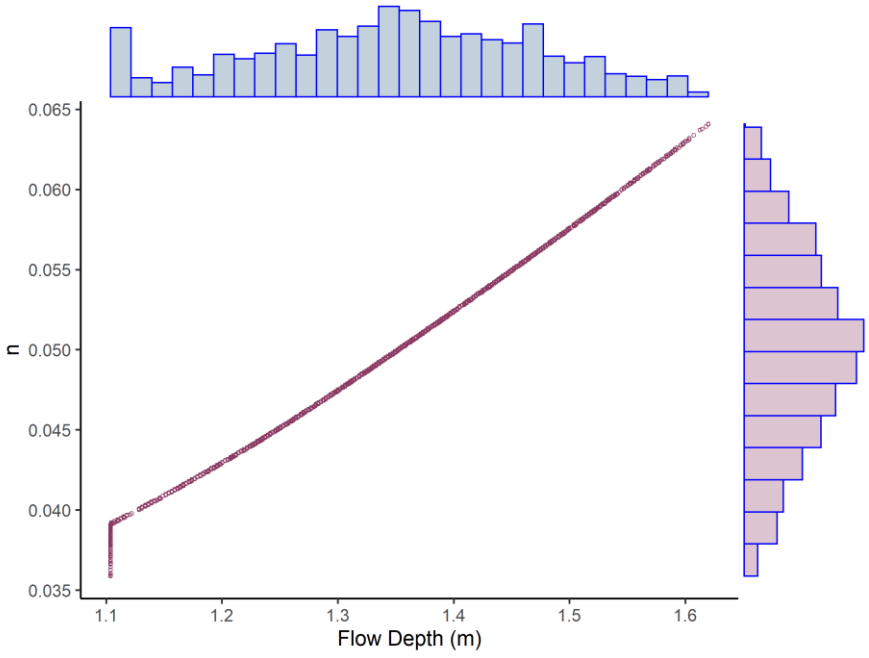

Figure C.7. Marginal Distribution of Output Flow Depth (m) vs Manning's Roughness Coefficient for Cross-Section 2151.

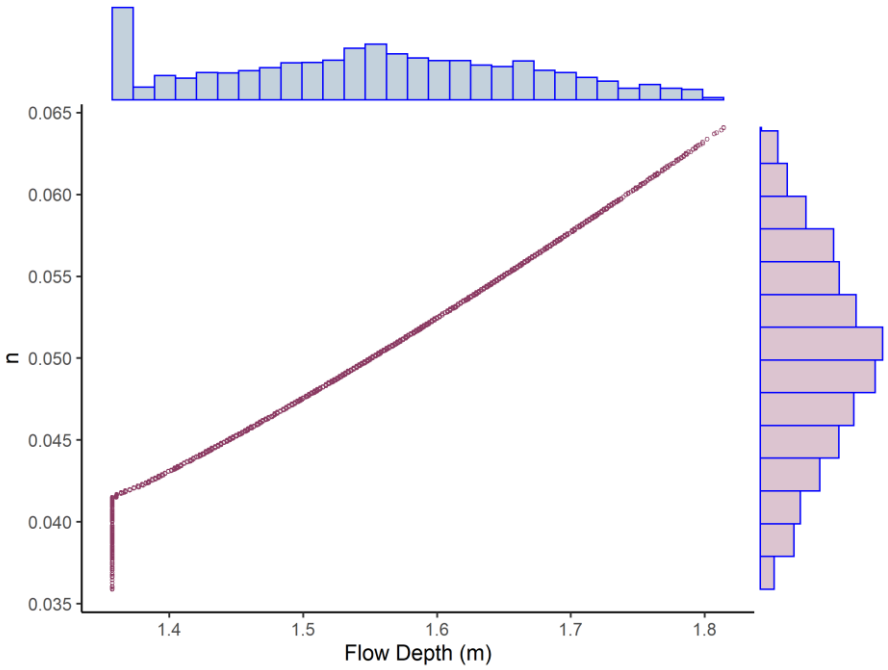

Figure C.8. Marginal Distribution of Output Flow Depth (m) vs Manning's Roughness Coefficient for Cross-Section 3019.

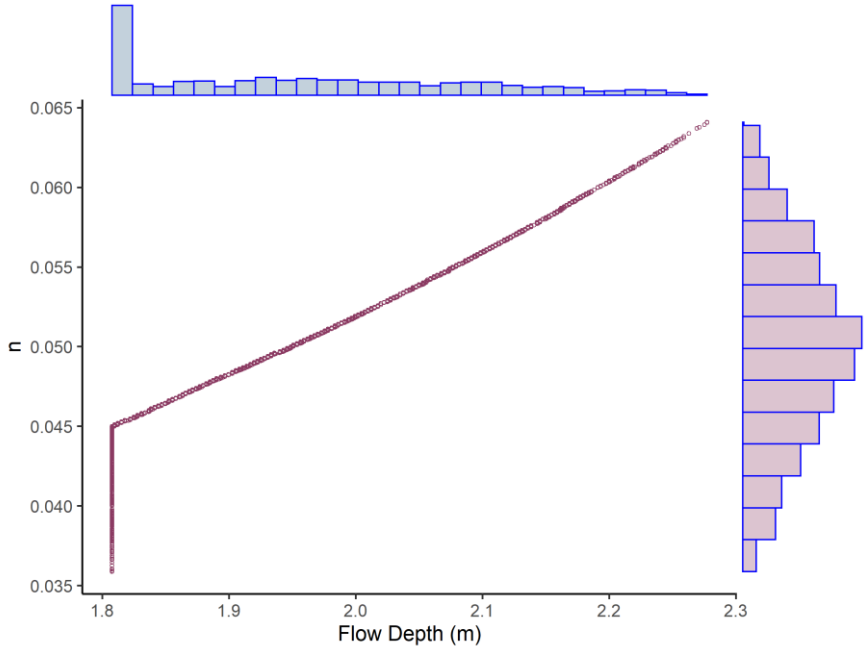

Figure C.9. Marginal Distribution of Output Flow Depth (m) vs Manning's Roughness Coefficient for Cross-Section 6477.

D. HISTOGRAMS OF OUTPUT FLOW DEPTHS AT CROSS-SECTIONS FOR COMBINED UNCERTAINTIES

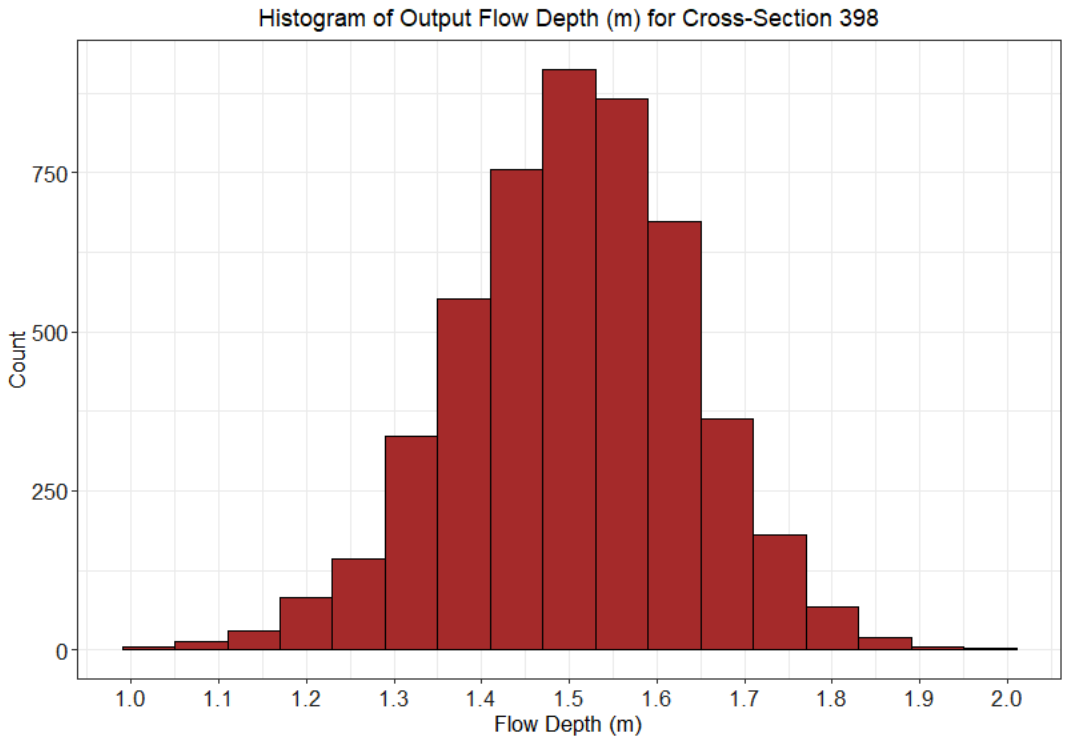

Figure D.1. Histogram of Combined Uncertainties Output Flow Depth (m) for Cross-Section 398.

Figure D. 2. Histogram of Combined Uncertainties Output Flow Depth (m) for Cross-Section 684.

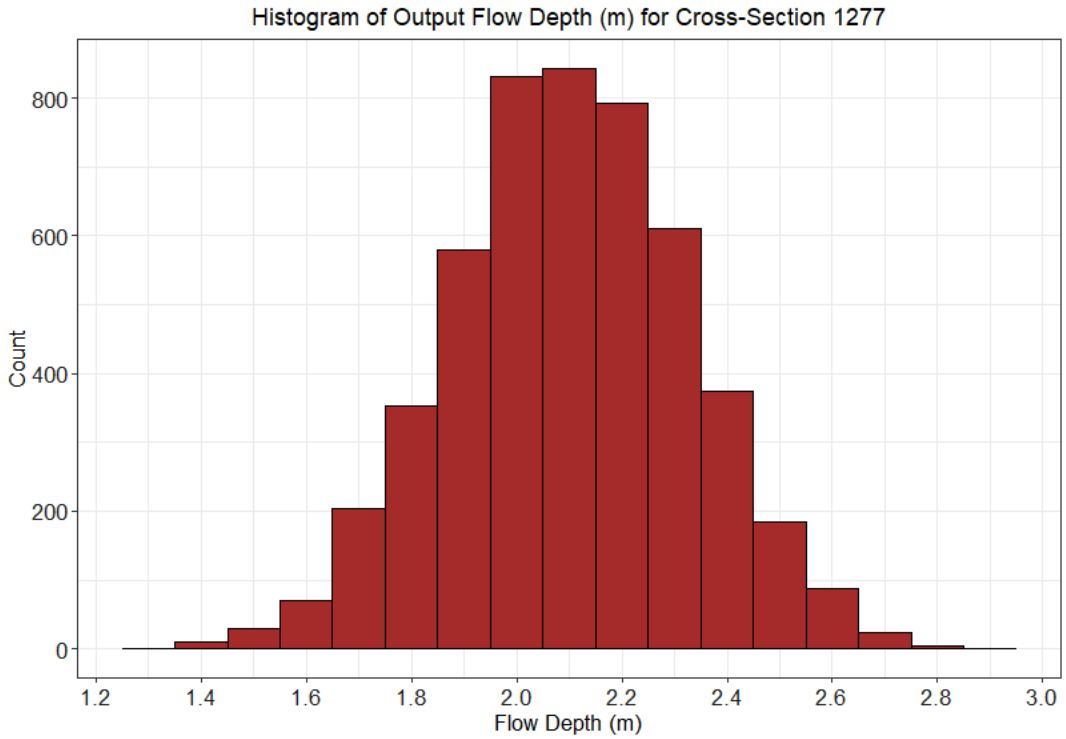

Figure D.3. Histogram of Combined Uncertainties Output Flow Depth (m) for Cross-Section 1277.

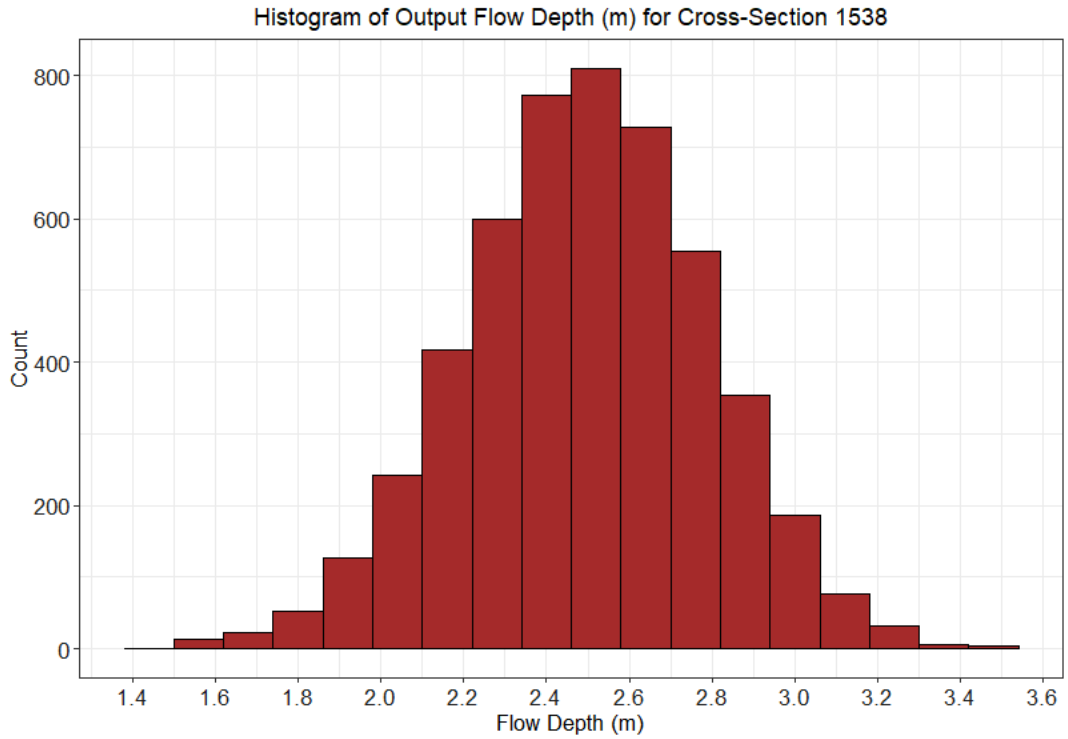

Figure D.4. Histogram of Combined Uncertainties Output Flow Depth (m) for Cross-Section 1538.

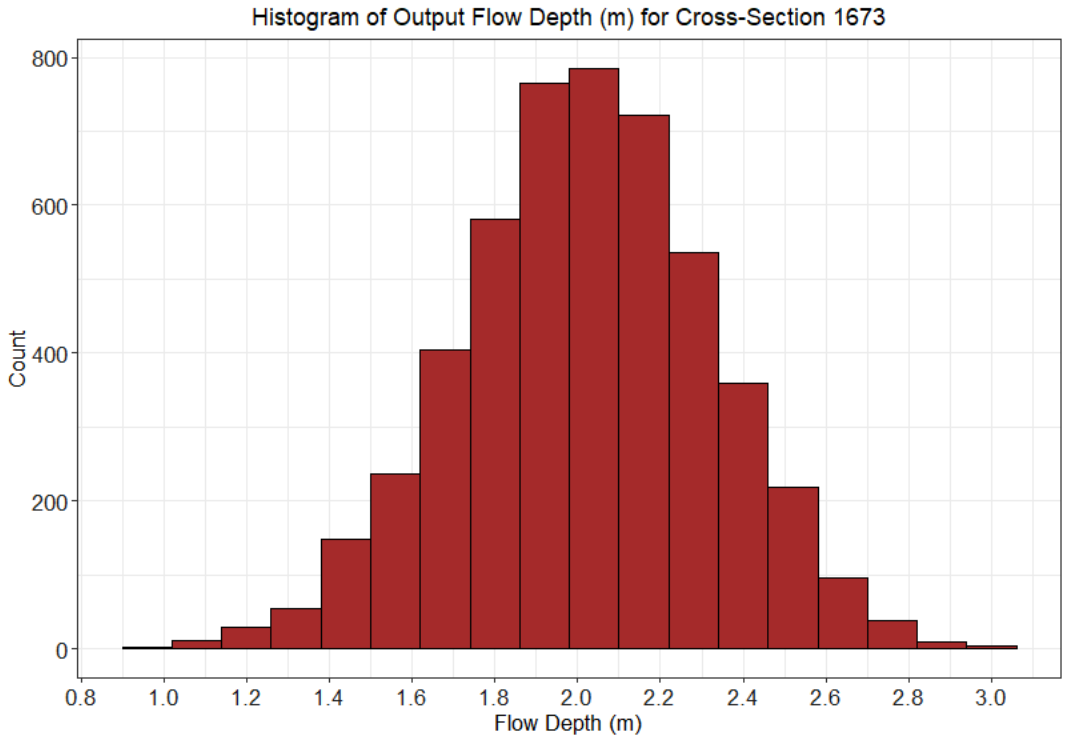

Figure D.5. Histogram of Combined Uncertainties Output Flow Depth (m) for Cross-Section 1673.

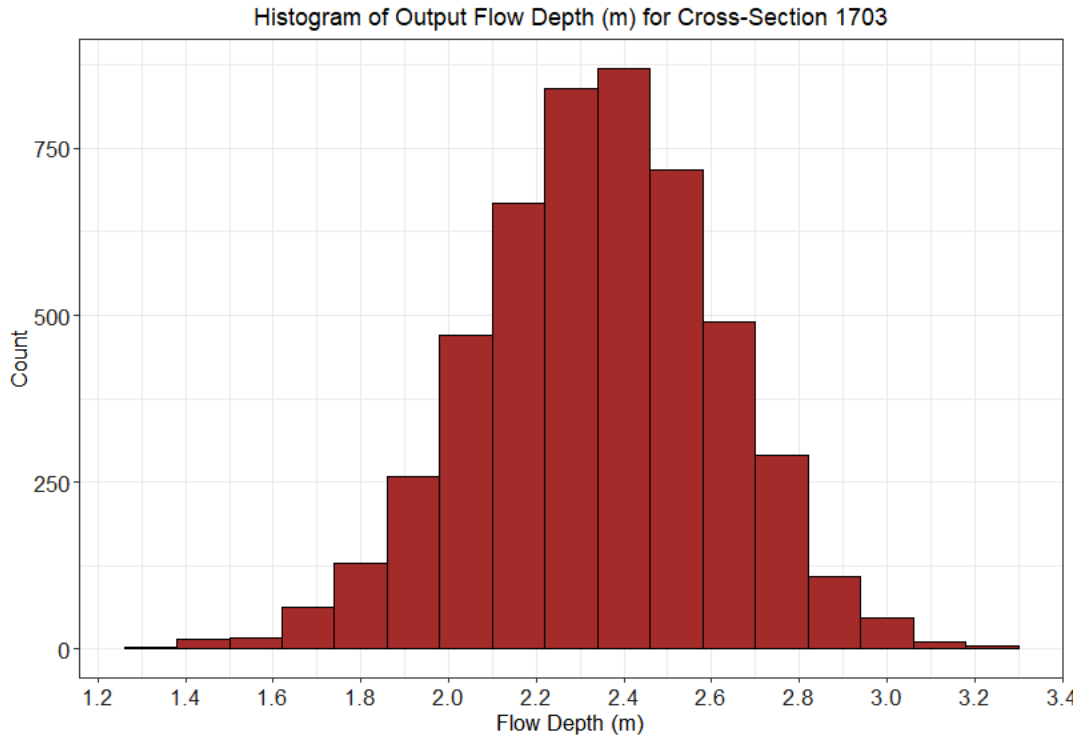

Figure D.6. Histogram of Combined Uncertainties Output Flow Depth (m) for Cross-Section 1703.

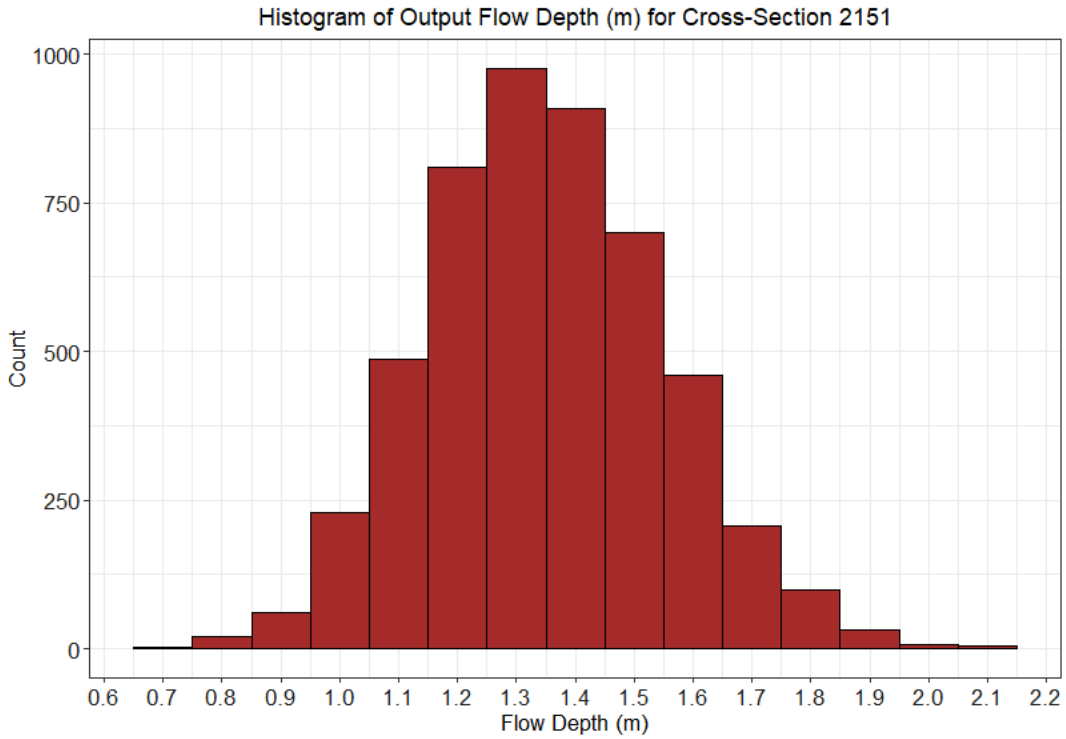

Figure D.7. Histogram of Combined Uncertainties Output Flow Depth (m) for Cross-Section 2151.

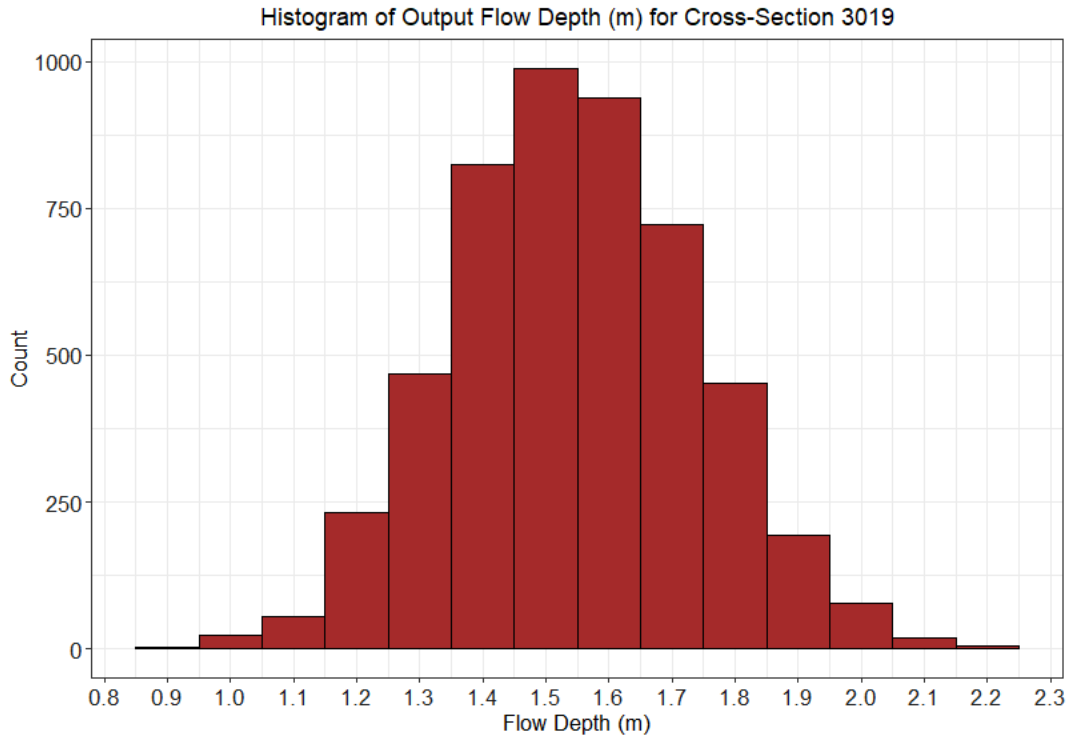

Figure D.8. Histogram of Combined Uncertainties Output Flow Depth (m) for Cross-Section 3019.

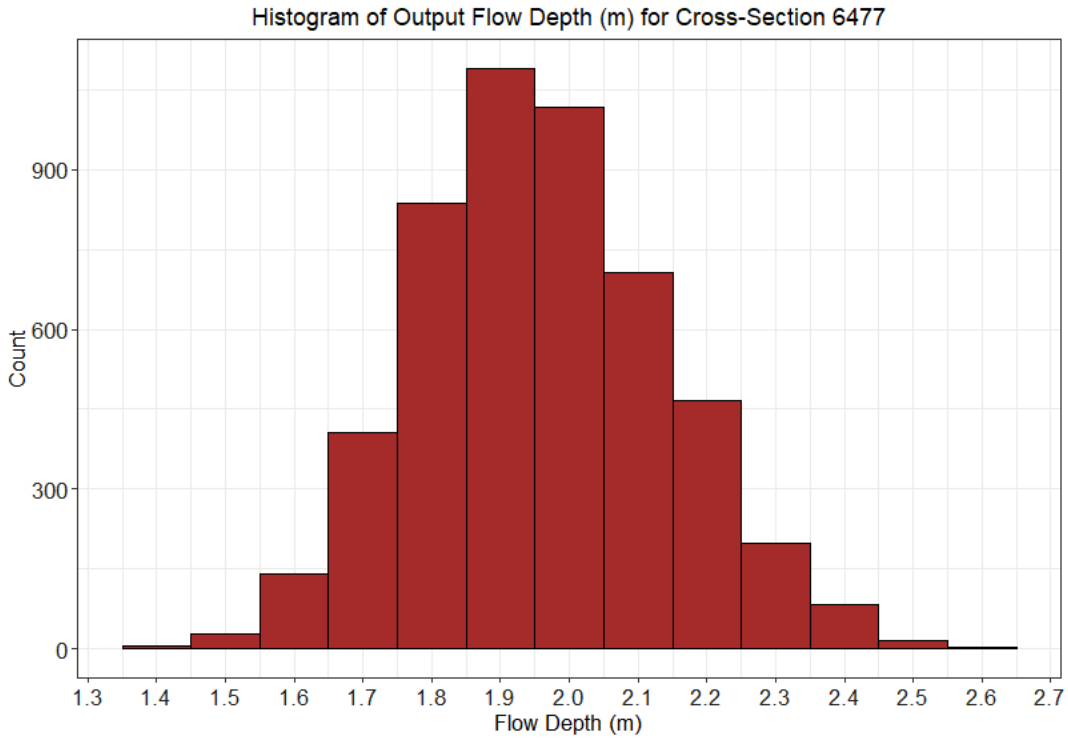

Figure D.9. Histogram of Combined Uncertainties Output Flow Depth (m) for Cross-Section 6477.

E. TRIANGULAR MANNING'S ROUGHNESS COEFFICIENT DISTRIBUTION DETERMINATION

After convenient coefficient of variation is selected (12.5% as explained in this study), mean value of Manning's roughness coefficient should be determined accordingly. This value has to be evaluated with the proper methods or fields studies for the study area/basin. In this study, mean value of the Manning's roughness coefficient is determined as 0.05 from the field study. Next step is to determine the lower and upper limits of these Manning's roughness coefficients by using Equation 4.3 and 4.4 as depicted below.

$$C.o.V = \Omega_y = \frac{1}{\sqrt{6}}\frac{(x_u - x_l)}{x_u + x_l} \rightarrow 0.125 * \sqrt{6} = \frac{(x_u - x_l)}{x_u + x_l} = 0.306$$

$$\frac{1}{2}(x_l + x_u) = 0.05$$

When these two equations are solved, x_l = 0.036 and x_u = 0.064 are concluded.